CRABforOERE

Construction and short-term assessment of demonstration CRM-pavements

Deliverable D6

September 2021

Universität Kassel, Germany

Institut français des sciences et technologies des transports, de l'aménagement et des réseaux (IFSTTAR), France

Nottingham Transportation Engineering Centre (NTEC), UK

Università degli Studi di Palermo Italy

Statens väg- & transportforskningsinstitut (VTI), Sweden

Università Politecnica delle Marche (UPdM), Italy

Project Nr. 867466

Project acronym: CRABforOERE

Project title:

Cold Recycled Asphalt Bases for Optimised Energy & Resource Efficient Pavements

Deliverable D6 – Construction and short-term assessment of demonstration CRM-pavements

Due date of deliverable: 31.03.2020

Actual submission date: 29.09.2020

Start date of project: 01.09.2018 End date of project: 31.08.2021

Authors of this deliverable:

Andrea Graziani, Chiara Mignini, Università Politecnica delle Marche (UPdM), Italy

Konrad Mollenhauer, Marius Winter; Universität Kassel, Germany

Davide Lo Presti; Università degli Studi di Palermo, Italy and Nottingham Transportation Engineering Centre (NTEC), UK

Gaspare Giancontieri; University of Palermo, Italy

Vincent Gaudefroy, Institut français des sciences et technologies des transports, de l'aménagement et des réseaux (IFSTTAR), France

Henrik Bjurström, Björn Kalman; Statens väg- & transportforskningsinstitut (VTI), Sweden

Version: draft 01

Table of content

1 Introduction

1.1 Background

Cold recycled material (CRM) mixtures are characterised by an evolutive behaviour caused by water-related phenomena like evaporation, emulsion breaking and cement hydration. Therefore, a curing period is necessary for their physical and mechanical properties to evolve from the ‘‘fresh” to the ‘‘hardened” state (Godenzoni et al., 2018; Graziani et al., 2018; Miljković & Radenberg, 2014; Pouliot et al., 2003). The curing process is normally characterised by a reduction of water content and by an increase in stiffness and strength. Although the process can take months or years before being completed, the short-term evolution of the material properties is essential to decide when the pavement can be opened to traffic. The long-term value of stiffness and strength, as well as their short-term rate of evolution, are affected by numerous factors, including:

- material composition (dosage of bituminous and cementitious binders, initial water content);
- construction features (layer thickness, compaction level, pavement drainage);
- environmental conditions (temperature, humidity, wind, rainfall).

All these factors are extremely variable and therefore their simulation in the laboratory for predicting the possible evolution of material properties in the field is challenging. National specifications require different curing protocols, but these protocols are used for the characterisation and acceptance of the CRM mixtures, rather than for predicting their field performance (Cardone et al., 2015; Doyle et al., 2013; Graziani et al., 2016; Y. Kim et al., 2011).

In the common practice, the water content of CRM mixtures is considered a good estimator of the curing process because water affects the rate and the effectiveness of emulsion breaking and the cement hydration, and consequently the development of the mechanical properties (Godenzoni et al., 2017). Some road agencies also suggest curing the CRM layer until reaching a certain water content (generally lower than 2%) before covering the layer with the hot mix asphalt (HMA) overlay (Woods et al., 2012).

1.2 Objective and methodology

The objective of this deliverable report as the main output of CRABforOERE work package 6 (WP6) was to demonstrate the applicability of the cold central-plant recycling technique and characterise the short-term and mid-term development of the CRM layer properties, with particular attention on the influence of climate conditions on the curing process.

The original work plan of WP6 included the construction of three pavement sections incorporating a CRM base or binder layer, in different European climatic regions. The demonstration sites should had been provided by National Road Authorities. Unfortunately, also due to the outbreak of the COVID-19 pandemic, it was possible to finalize only the Italian demonstration site. The CRM-pavement test section was built in the Republic of San Marino were the Azienda Autonoma di Stato per i Lavori Pubblici[1] (AASLP) decided to support the CRABforOERE project, in collaboration with the University of the Republic of San Marino (UniRSM).

[1] State-owned Enterprise for Public Works (https://www.aaslp.sm/)

The pavement test section included a 10 cm binder layer that was built using a CRM mixture. During construction, temperature and moisture sensors were installed within the layer. In addition, a testing plan was implemented, including laboratory and field testing, aimed at characterising the physical and mechanical properties of the CRM layer, and their evolution during the first year of service life.

The present deliverable report is organised as follows. Section 2 contains a general description of the Italian demonstration site, giving and overview of the pavement maintenance project, along with the description of the employed materials and the installed sensors. Section 3 describes the construction of the pavement and the installation of the sensors and Section 4 describes the testing plan developed as part of the WP6 activities. The results of the laboratory and field testing activities, as well as the sensors measurements are described in Section 5.

2 Planning of the demonstration site

2.1 Project overview

The Italian demonstration site was built in the Republic of San Marino from the 6th to the 8th of July 2020, The pavement section is located along via XXV Marzo (Figure 1), a four-lane, dual-carriageway facility, which is the main connector between the San Marino historic centre and Rimini, on the Adriatic coast. The annual average daily traffic (AADT) is 4000 veh/day, with 10% of heavy vehicles. The pavement test section was included in the AASLP pavement maintenance plan for the year 2020, The existing pavement consisted in an asphalt concrete layer (wearing and binder courses) with a total thickness of 12 cm, on unbound granular base and foundation layers. Detailed information on the subgrade is not available.

a)

b)

Figure 1. Italian demonstration site: a) via XXV Marzo, Republic of San Marino, b) pavement condition before maintenance

The pavement test section was characterised by different distresses, and therefore the maintenance plan considered two subsections (Figure 2):

- **Subsection 1** (right lane, about 400 m^2 from km 5,200 to km 5,300) showed a series of interconnecting cracks in the asphalt layers caused by traffic loading (high-severity fatigue cracking), combined with localised depressions due to permanent deformations in the granular base (Figure 3a);
- **Subsection 2** (right lane, about 400 m^2 from km 5,300 to km 5,400) showed medium-severity fatigue cracking (Figure 3b).

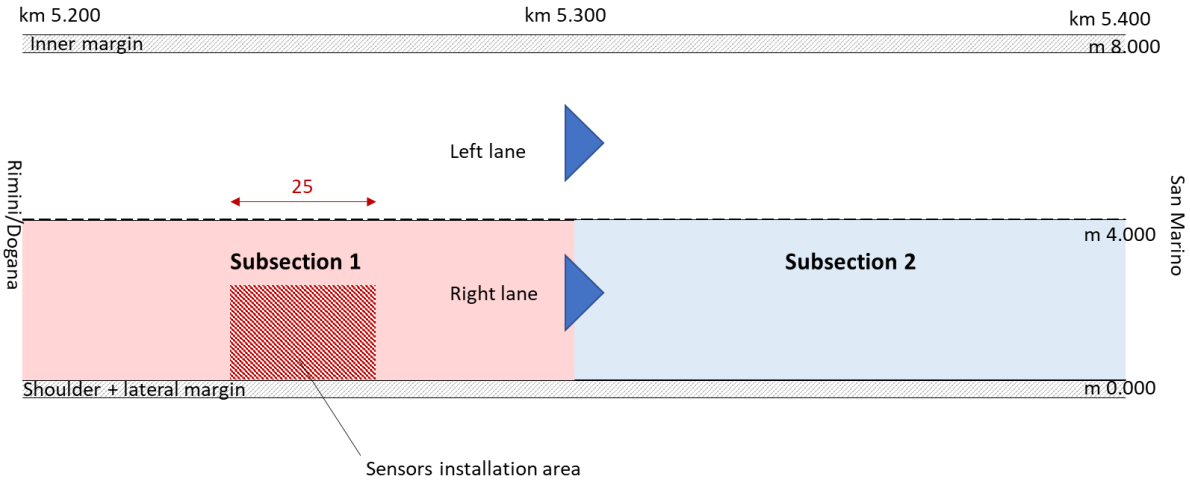

Figure 2. Plan view of the subsections

a) b)

Figure 3. Pavement conditions before the maintenance: a) subsection 1, b) subsection 2

Following the project-level assessment, the maintenance activities were identified according to the AASLP guidelines. They can be summarized as follows (Figure 4):

- **Subsection 1**
  - milling of the existing pavement to the depth of 29 cm;
  - construction of a new base layer with a thickness of 15 cm using a cement treated recycled material (CTRM) mixture;

- application of a prime coat (bituminous emulsion with dosage of 1,0 kg/m^2 of residual bitumen and saturation with mineral filler);
- **construction of a new binder layer with a thickness of 10 cm using a cold recycled material (CRM) mixture**;
- application of a tack coat (bituminous emulsion with dosage of 0,45 kg/m^2 of residual bitumen and saturation with mineral filler);
- construction of a new wearing course with a thickness of 4 cm using an asphalt concrete (AC) mixture produced with modified bitumen.

- **Subsection 2**
  - milling of the existing pavement to the depth of 14 cm;
  - application of a prime coat (bituminous emulsion with dosage of 1,0 kg/m^2 of residual bitumen and saturation with mineral filler);
  - **construction of a new binder layer with a thickness of 10 cm using a cold recycled material (CRM) mixture**;
  - application of a tack coat (bituminous emulsion with dosage of 0,45 kg/m^2 of residual bitumen and saturation with mineral filler);
  - construction of a new wearing course with a thickness of 4 cm an AC produced with modified bitumen.

It is highlighted that the CRM mixture is enclosed within two practically impermeable bituminous membranes (the tack coat and the prime coat).

The sensors for monitoring the evolution of temperature and water content were installed in Subsection 1 (Figure 2), whereas the other sampling and field testing activities were carried out on both Subsection 1 and Subsection 2.

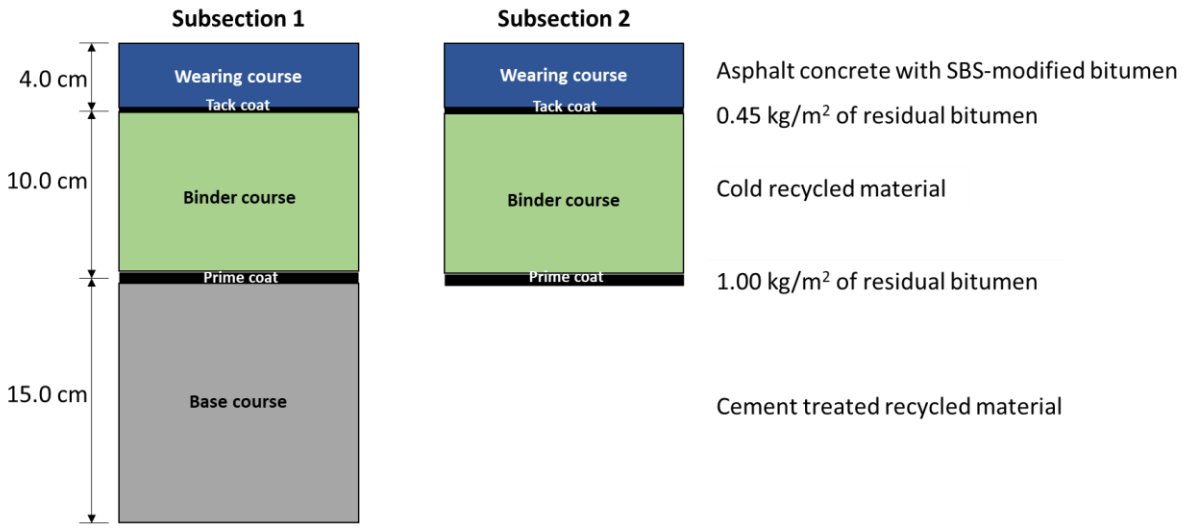

Figure 4. Structural design for Subsections 1 and 2

Figure 5 and Figure 6 compare the layer thicknesses of the test section (Figure 4) with those of the pavements investigated within the WP2 activities (Bjurström et al., 2020). In the WP6 demonstration site the CRM mixture was used in the binder layer, whereas in the other pavements it was always used in the base or subbase layers. Considering the variability in the

traffic levels of the considered pavements, the layers thicknesses of the WP6 demonstration site can be considered comparable to those of the Italian pavements (Figure 5). In addition, considering only the total thickness of the bound layers, the demonstration site follows the common trend identified for the pavements investigated within WP2 (Figure 6).

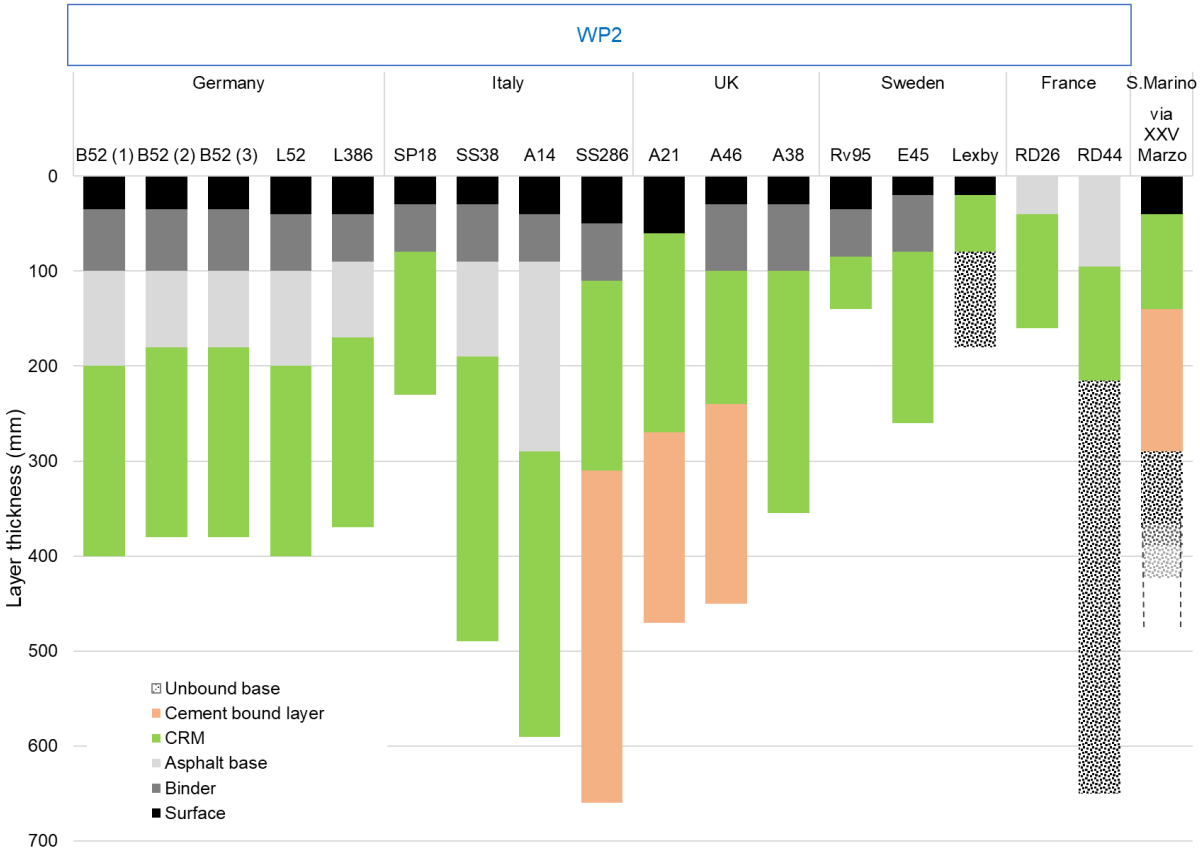

Figure 5. Comparison between the layer thickness of the demonstration site and the 17 pavements investigated within the WP2 (Bjurström et al., 2020)

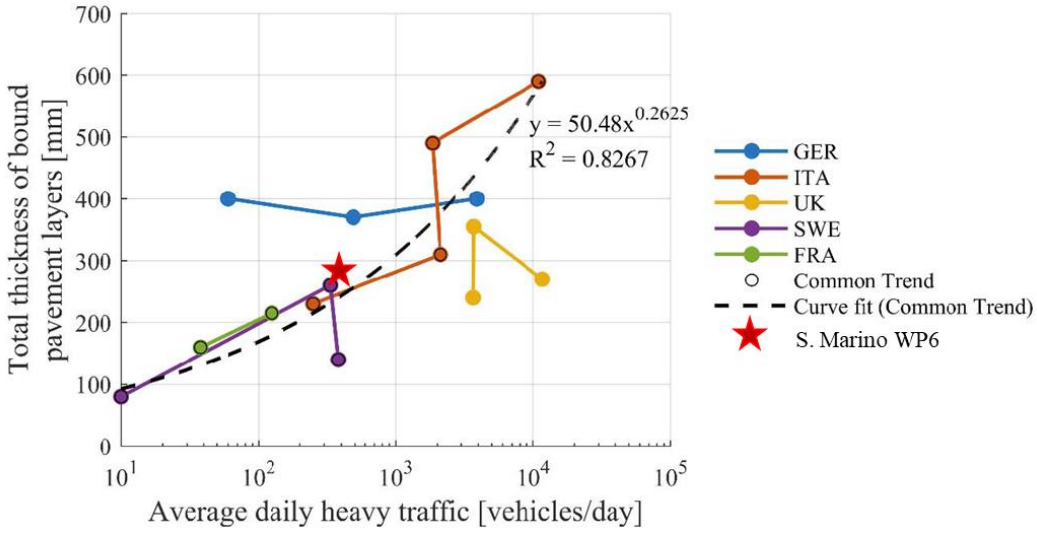

Figure 6. Total thickness of bound layers plotted against the average number of daily heavy vehicles: comparison between the WP6 demonstration site and the pavements investigated within WP2 (Bjurström et al., 2020)

Figure 7 compares the layer thicknesses of the WP6 demonstration site with those obtained within the WP5, where national pavement design procedures for different model pavements were compared (Mollenhauer et al., 2020). The traffic and subbase conditions of the demonstration site are similar to those of the model pavement 2 characterised by:

- AADT on 1 lane: 4500 vehicles/day, proportion of heavy vehicles: 3%
- traffic increase: 2 %/year
- subbase with medium bearing capacity: E_{V2} = 50 MN/m², CBR = 10%

The total thickness of the WP6 demonstration site is comparable to those derived from the UK, Sweden and France national pavement design procedures. However, it must be highlighted that the adopted materials are different, and that in the WP6 demonstration site the CRM was used for the construction of the binder layer rather than for the base course.

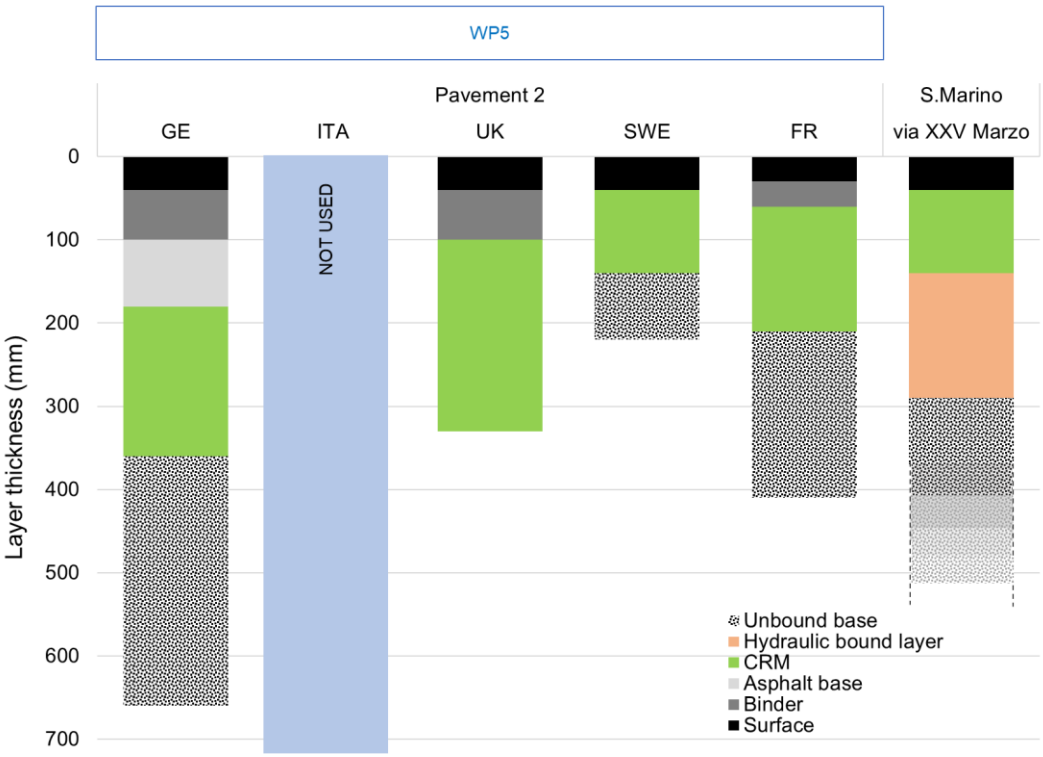

Figure 7. Comparison between the layer thickness of the WP6 demonstration site with those obtained for the model pavement 2 within the WP5 (Mollenhauer et al., 2020)

2.2 Materials

2.2.1 Construction specifications

The materials used were defined according the AASLP construction specification (Azienda Autonoma per i Lavori di Stato, 2020), which are summarised in Annex A, whereas Annex B reports the information documents provided by the suppliers.

2.2.2 Mix granulate

The RA aggregate was stockpiled at the CRM production plant owned by the company Società Cooperativa Braccianti Riminese, located in San Leo (Rimini). This RA aggregate was previously investigated within the WP3, identified with the code “ITA_1”. Before stockpiling, the RA source was subjected to crushing and sieving operations (Figure 8).

For a better control of the mixture gradation, two RA aggregate fractions are available at the production plant, RA 0/10 and RA 8/20, Figure 9 shows the grading distributions of the RA aggregate fractions (“black curve”) and their extracted aggregate (“white curve”).

A natural fine aggregate was added to correct the RA aggregate gradation and fit the design grading envelope of the CRM mixture. The sand (0/1) had a maximum grain diameter of 1 mm (Figure 9). The added filler was a finely ground limestone dust. Table 1 summarises the main physical properties of the aggregates.

a) b)

Figure 8. CRM production plant: a) stockpiled RA, b) aggregate selection process

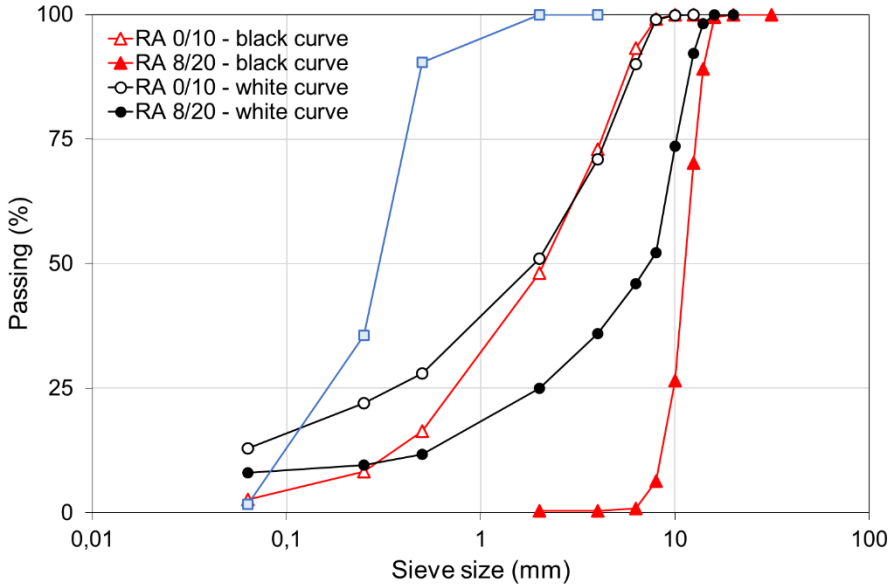

Figure 9. Grading distributions of the RA aggregate fractions

Table 1. Main properties of the aggregates

Property	Standard	RA 0/10	RA 8/20	Sand	Filler
Density (kg/m^3)	EN 1097-6	2475	2510	2680	2700
Water absorption (%)	EN 1097-6	1,7	2,0	8,5	
Soluble binder content* (%)	EN 12697-1	4,89	3,38		

* by aggregate mass

2.2.3 Binders

The bitumen emulsion, provided by Valli Zabban SpA, was a slow setting, overstabilised emulsion, specifically designed for cold recycling. The emulsion was designated C60BP10 according to EN 13808. The emulsion was obtained by mixing neat bitumen and SBR latex, its residual bitumen content was 60%. Table 2 reports the main properties of the emulsion.

The cement was a Portland-limestone CEM II/A-LL 32.5R according to EN 197-1. Its particle density was 3000 kg/m^3.

Table 2. Main properties of the emulsion

Property	Standard	Minimum value	Maximum value
Emulsion			
Binder content (%)	EN 1428	60	
Viscosity at 40 °C / efflux time at 40 °C (s)	EN 12846-1	15	70
pH value	EN 12850	2	4
Mixing stability with cement (%)	EN 12848		2
Settling after 7 days (%)	EN 12847		10
Residual bitumen			
Penetration at 25 °C (mm/10)	EN 1426	50	70
Softening point (°C)	EN 1427	55	
Fraas Breaking Point (°C)	EN 12593	-10	
Elastic recovery at 25 °C (%)	EN 13398	55	

2.2.4 CRM mixture

The mix design of the CRM mixture for binder course was established in a previous study (Ferrotti et al., 2020). The grading distribution was close to the maximum density grading distribution and was obtained by mixing 92% of RA aggregate (48% of RA 0/10 and 44% of RA 8/20), 4% of sand and 4% of filler (Figure 10).

The dosage of bitumen emulsion was 4,5% (2,7% of residual bitumen), the dosage of cement was 2,0% and the total water content was 5,0% by aggregate mass (including water brought in by emulsion).

Figure 11 compares the dosages of residual bitumen and cement adopted in the demonstration site with those found for the mixtures investigated within WP2 (Bjurström et al., 2020) and WP4.

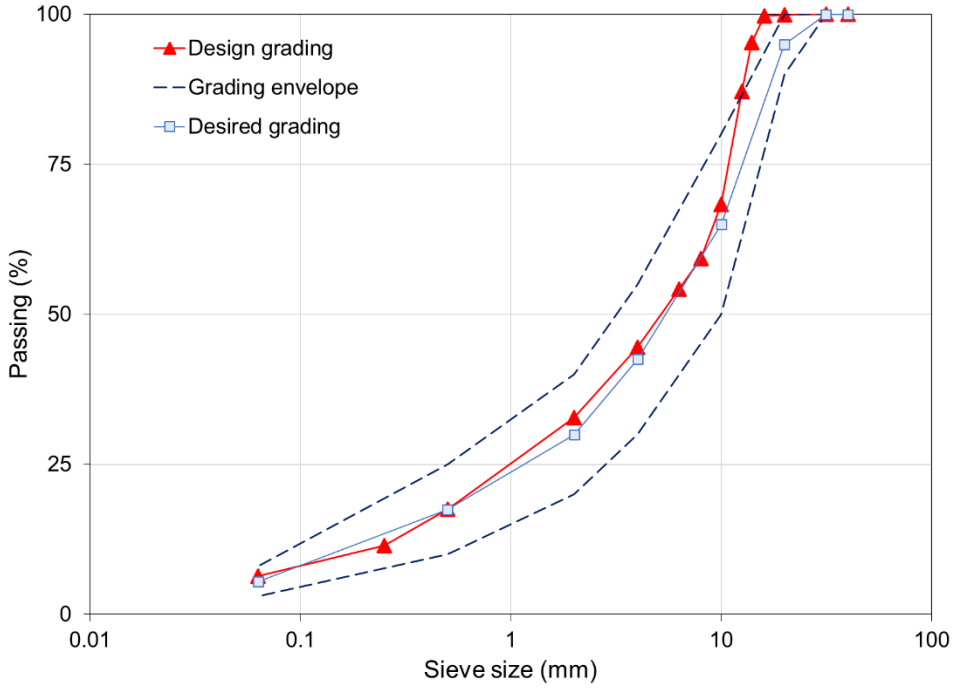

Figure 10.Grading distribution of the CRM aggregate blend

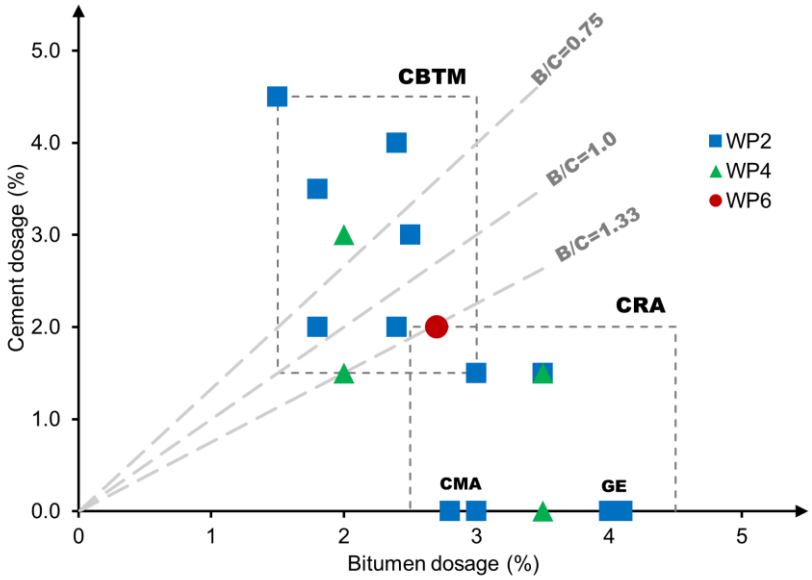

Figure 11. Identification of CRM mixtures families: comparison between the mixtures investigated within WP2 (Bjurström et al., 2020)*, WP4 and WP6*

2.2.5 AC mixture

The mix design of the asphalt concrete wearing course was obtained following the AASLP construction specifications (Azienda Autonoma per i Lavori di Stato, 2020). Figure 12a depicts the grading distribution of the AC mixture, which comprised 40% of natural basalt coarse

aggregate. The mixture was produced using an SBS-modified bitumen, with a dosage of 5,55% by aggregate mass.

2.2.6 Cement-treated recycled material

The cement-treated recycled material (CTRM) base employed in Subsection 1 was produced using 30% of RA aggregate and 70% of recycled aggregate (C&D products). Figure 12b depicts the grading distribution of the CTRM base. The cement dosage was 3,0% by aggregate mass and the optimal water content was 4,96% by aggregate mass.

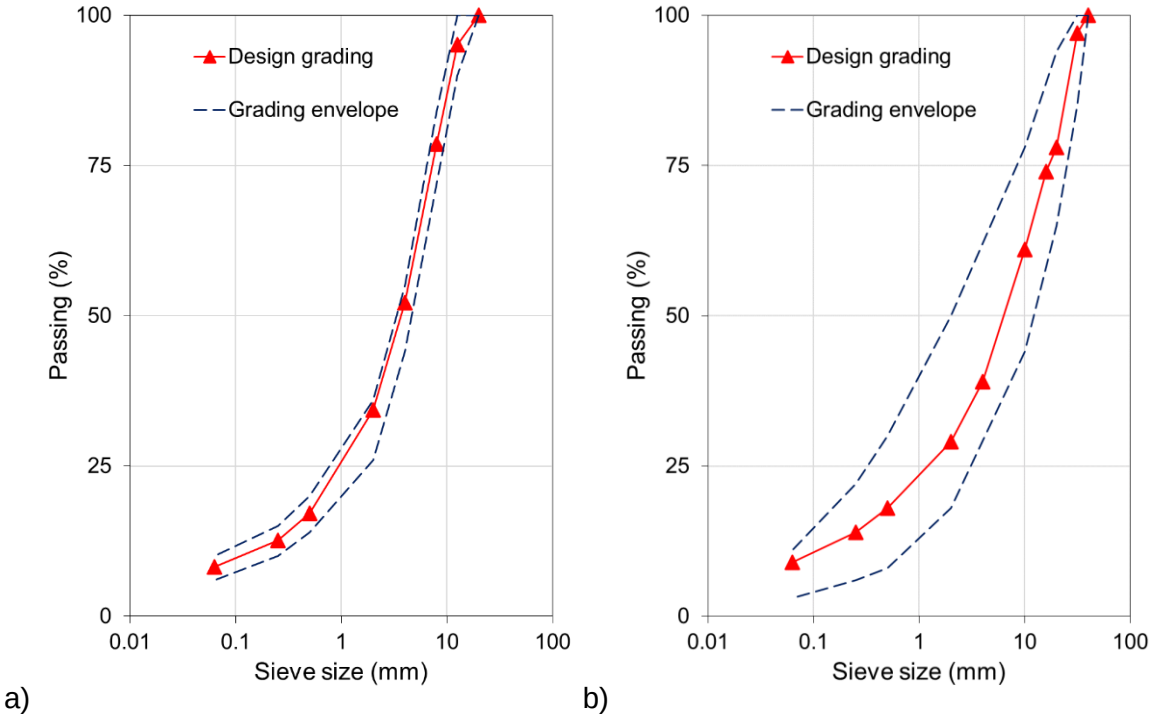

Figure 12. Grading distributions and grading envelopes: a) asphalt concrete, b) cement-treated recycled material

2.3 Description of the sensors

The sensors installed in the demonstration site provide information on the evolution of the temperature and the volumetric water content, which can be related to the development of the curing process. At the end of the project, the installed equipment, which include the sensors and the datalogger device, will be managed by UNIVPM.

2.3.1 Moisture sensors

The TEROS 12 is a dielectric capacitance sensor that measures the volumetric water content (VWC), the temperature and the electrical conductivity (EC) using three stainless steel needles (Figure 13). The sensor determines the dielectric permittivity of the medium by measuring the charge time of a capacitor, using the medium as a dielectric. At low frequencies (below 50 MHz), dielectric sensors polarize the water and the salts making them sensitive to salinity in the medium. The dielectric measurement frequency of TEROS 12 sensor is 70 MHz,

therefore, the salinity influence is reduced. Like most moisture sensors available on the market, it was originally designed to be installed in soils (Meter Group, 2021).

The sensors measure the VWC between needle 1 and needle 2 and EC between needle 2 and needle 3. Temperature is measured with an embedded thermistor in needle 2. The ferrite core positioned 7,6 cm away from the sensor head is utilized to isolate the sensor from any interferences in the system. This mitigates any potential noise from the system on the measured sensor data. Table 3 summarises the sensors specifications, whereas Figure 14 depicts the volume of influence for the measurement of the VWC, which is about 1 dm^3.

Table 3. TEROS 12 specifications

Property	Specifications
Volumetric water content NOTE: The VWC range is dependent on the media the sensor is calibrated to. A custom calibration will accommodate the necessary ranges for most substrates.	**Range** Mineral soil calibration: 0,00–0,70 m^3/m^3 Soilless media calibration: 0,0–1,0 m^3/m^3 Apparent dielectric permittivity (ε_a): 1 (air) to 80 (water) **Resolution** 0,001 m^3/m^3 **Accuracy** Generic calibration: ±0,03 m^3/m^3 (±3.00% VWC) typical in mineral soils that have solution EC <8 dS/m Medium specific calibration: ±0,01–0,02 m^3/m^3 (±1–2% VWC) in any porous medium Apparent dielectric permittivity (ε_a): 1–40 (soil range) , ±1 ε_a (unitless) 40–80, 15% of measurement
Temperature	**Range** −40 to 60 °C **Resolution** 0,1 °C **Accuracy** ±0,5 °C from −40 to 0 °C ±0,3 °C from 0 to +60 °C
Bulk electrical conductivity	**Range** 0 to 20 dS/m (bulk) **Resolution** 0,001 dS/m **Accuracy** +/- (5% +0,01 dS/m) from 0 to 10 dS/m +/- 8% from 10 to 20 dS/m

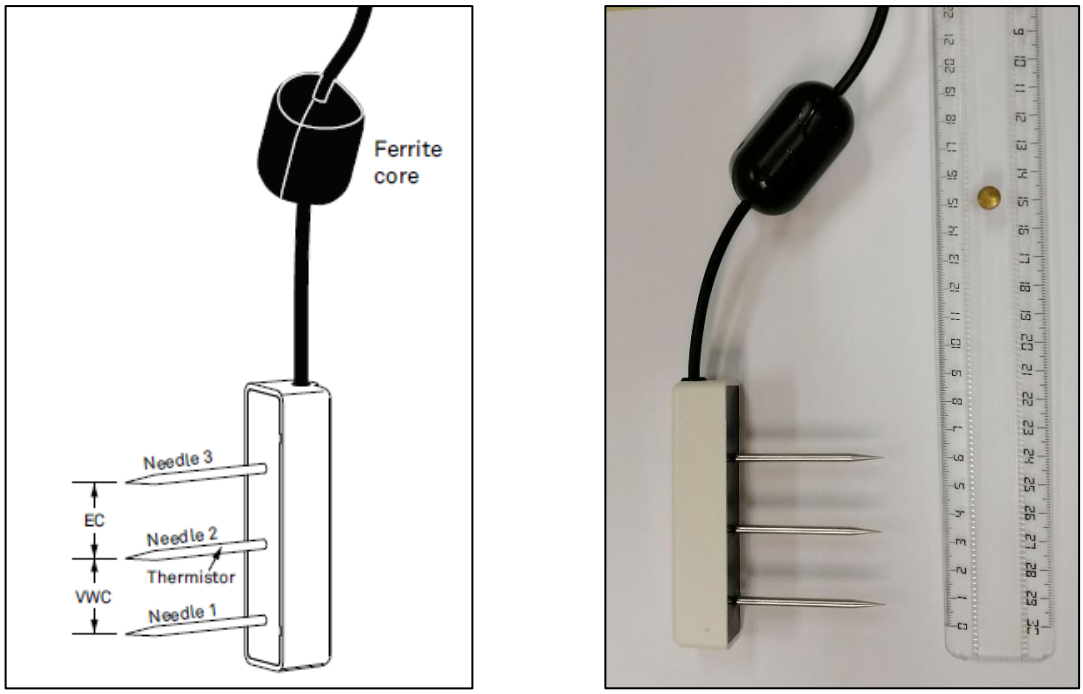

Figure 13. The TEROS 12 Sensor

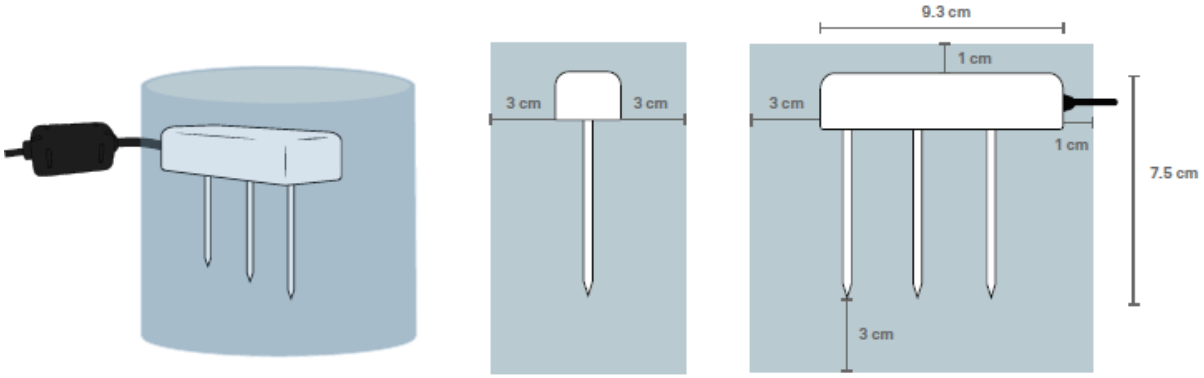

Figure 14. Volume of influence for VWC measurement

2.3.2 Data logger

The ZL6 is a self-contained, plug-and-play data logger for field research. It is housed in a weather-resistant enclosure, making it suitable for long-term outdoor operation (Figure 15a). The logger includes built-in circuitry to charge nickel-metal hydride (NiMH) batteries using energy from two integrated solar panels. Up to 6 sensors can be connected using 3,5 mm stereo plug connectors (Figure 15 and Figure 16). The logger has integrated GPS, temperature and barometric pressure measurement

Collected data are transmitted to the ZENTRA Cloud web service via cellular communication. The ZENTRA Utility software is used configure the sensor interface and download the data from the cloud.

Figure 15. The ZL6 datalogger: a) enclosure; b) Six TEROS 12 sensors connected

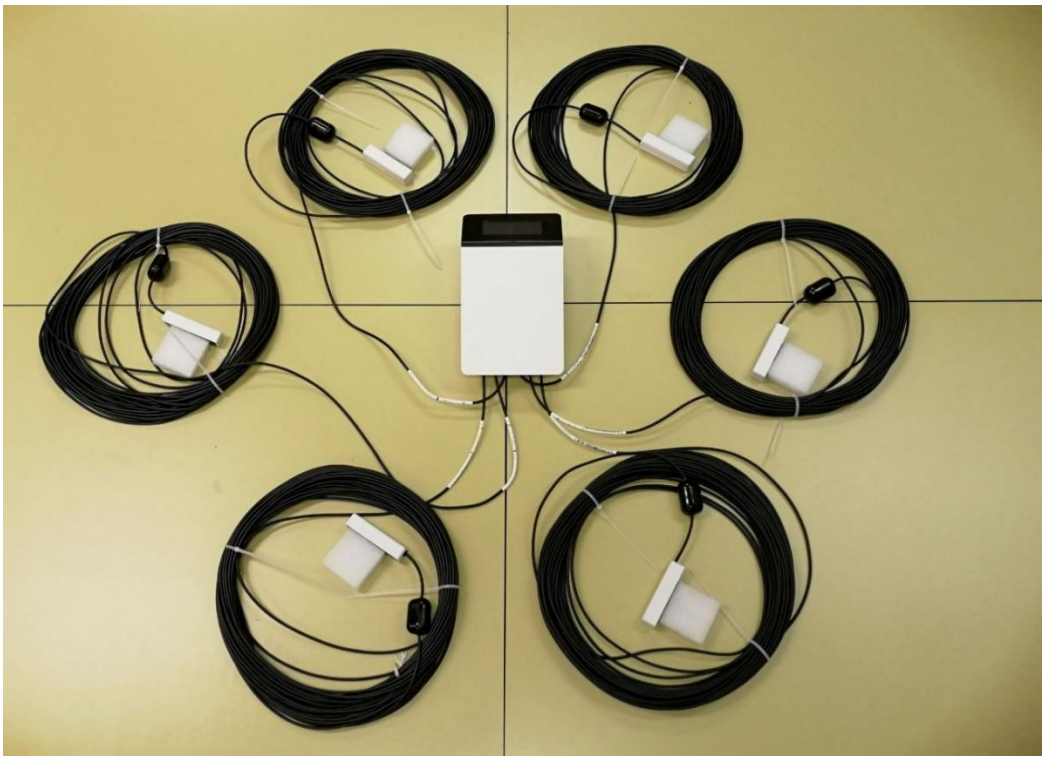

Figure 16. Six TEROS 12 Sensors connected to the ZL6 datalogger

3 Construction of the demonstration site

3.1 Construction of the pavement

The present section contains a step-by-step description of the construction activities.

06/07/2020 – day 1

8:30-10:30

Cold milling of the existing pavement to the depth of 29 cm (Subsection 1). Milling was carried out in two passes: the first pass was 4 cm, the second pass was 25 cm

06/07/2020 – day 1

10:30-12:30

Cold milling of the existing pavement to the depth of 14 cm (Subsection 2). Milling was carried out in two passes: the first pass was 4 cm, the second pass was 10 cm

06/07/2020 – day 1

11:00-12:00

Cleaning and preparing the connection to the manhole (installed at the roadside the week before) for collecting and housing of the sensors' cables

07/07/2020 – day 2

7:00

Light falling weight deflectometer (LFWD) tests on the existing subbase.

07/07/2020 – day 2

09:00-10:00

Laydown of the CTRM base layer (15 cm) in Subsection 1.

07/07/2020 – day 2

9:30-10:30

Compaction of the CTRM base layer using the steel roller.

07/07/2020 – day 2

9:30-10:30

Compaction of the CTRM base layer using the pneumatic roller.

07/07/2020 – day 2

11:00 – 12:00

Application of the prime coat in Subsections 1 and 2.

07/07/2020 – day 2

13:00-15:00

Laydown of the CRM binder layer in Subsections 1 and 2.

07/07/2020 – day 2

14:00 – 15:00

Preparation for the installation of sensors (Subsection 1).

07/07/2020 – day 2

14:30-16:30

Compaction of the CRM binder layer using the steel roller.

07/07/2020 – day 2

14:30-16:30

Compaction of the CRM binder layer using the pneumatic roller.

07/07/2020 – day 2

16:30

CRM binder layer compacted.

07/07/2020 – day 2

16:00

LFWD tests on the compacted CRM binder layer.

07/07/2020 – day 2

16:30-18:30

Installation of the sensors (details in Section 3.2)

08/07/2020 – day 3

7:30

LFWD tests on the CRM binder layer after about 18 hours from its construction

08/07/2020 – day 3

8:30-9:30

Tack coat application about 18 hours after the CRM construction.

08/07/2020 – day 3

10:30-11:30

Laydown of the AC wearing course in Subsections 1 and 2.

08/07/2020 – day 3

11:00-12:30

Compaction of the AC wearing course using the steel roller.

08/07/2020 – day 3

12:30

Pavement construction completed.

3.2 Installation of the sensors

Six THEROS 12 sensors were installed within Subsection 1. Figure 17 and Figure 18 show the layout and the cross section of the installation site. Sensors were placed in the centre of the right lane at mid-depth of the CRM binder layer. The datalogger was fixed on a support at the roadside.

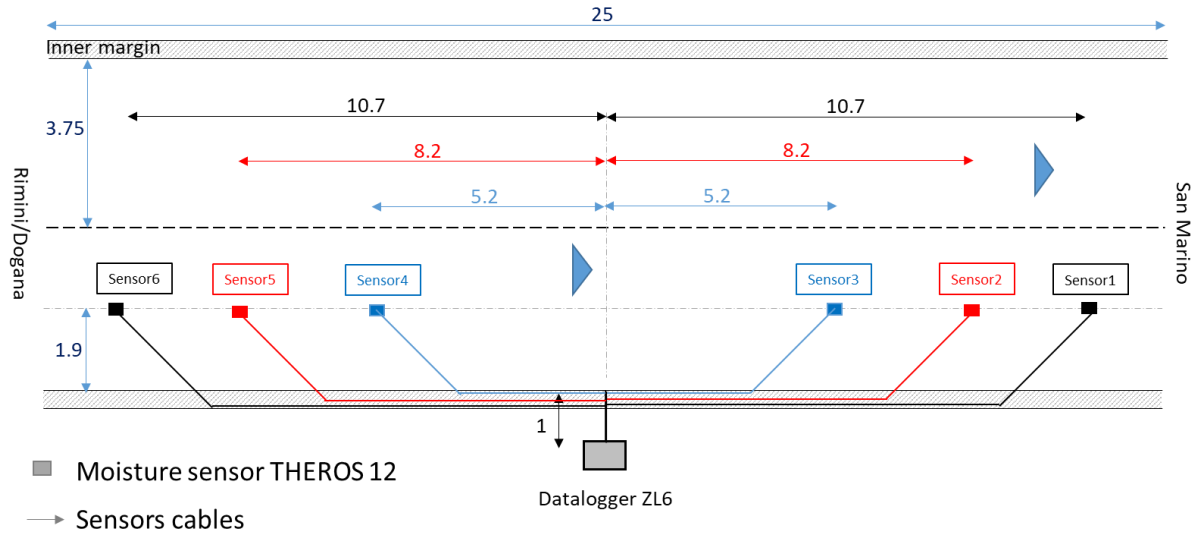

Figure 17. Plan view of the test section with sensors layout

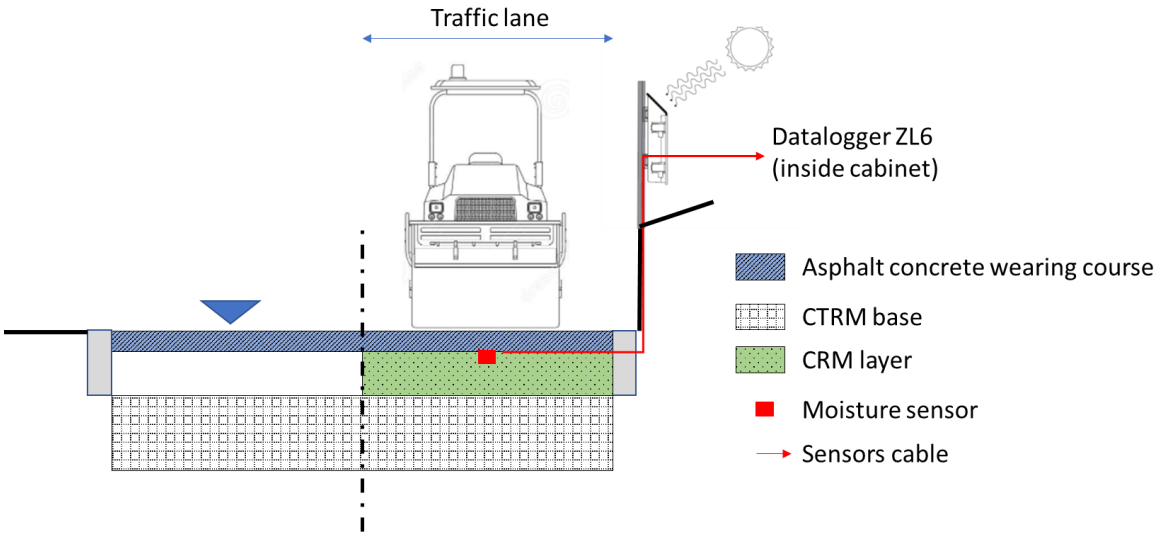

Figure 18. Cross section view of the test section with sensors position

Before installation, sensors were calibrated in the laboratory to convert the raw electrical measurement in volumetric and gravimetric water content (GWC) (Annex C). Figure 19 outlines the main phases of sensors installation whereas Figure 20 and Figure 21 show the corresponding field activities.

Before installation, parallelepiped-shaped wood tablets with 3 nails placed in the needles position were prepared. The wood tablets were 40x9 cm with a thickness of 3 cm (Figure 20a). Moreover, the sensors cables were protected with flexible metallic tubes to prevent damaging during installation (Figure 20b). The installation procedure was as follows:

A. The installation started immediately after laydown of the CRM binder layer, before its compaction.

B. Small trenches were excavated into the uncompacted CRM binder layer and the wood tablets were positioned where the sensors were to be installed (Figure 20c-d). Steel bars were placed in trenches created in the position defined for cables (Figure 20e).

C. The CRM binder layer was compacted to its final density.

D. During the compaction, the wood tablets and the steel bars created a housing for placing the sensors and their cables (Figure 20f).

E. The wood tablets and steel bars were removed from the compacted CRM layer. This operation was carried out with extreme care to limit the disturbance of the surrounding material. The flat bottom of the trench was further regularised.

F. The sensors were installed (Figure 21a).

G. The cables were laid inside the trenches (Figure 21b).

H. The sensor trench was filled with a cold recycled mortar obtained by sieving the CRM mixture used for the layer on the 4 mm sieve. The fill was compacted by hand, using a portable Marshall hammer. Extreme care was needed in this phase, in order to avoid damage to the sensors (Figure 21c). The cables trenches were filled using a cementitious mortar (Figure 21d). Finally, the sensors were connected to the data logger (Figure 21e-f).

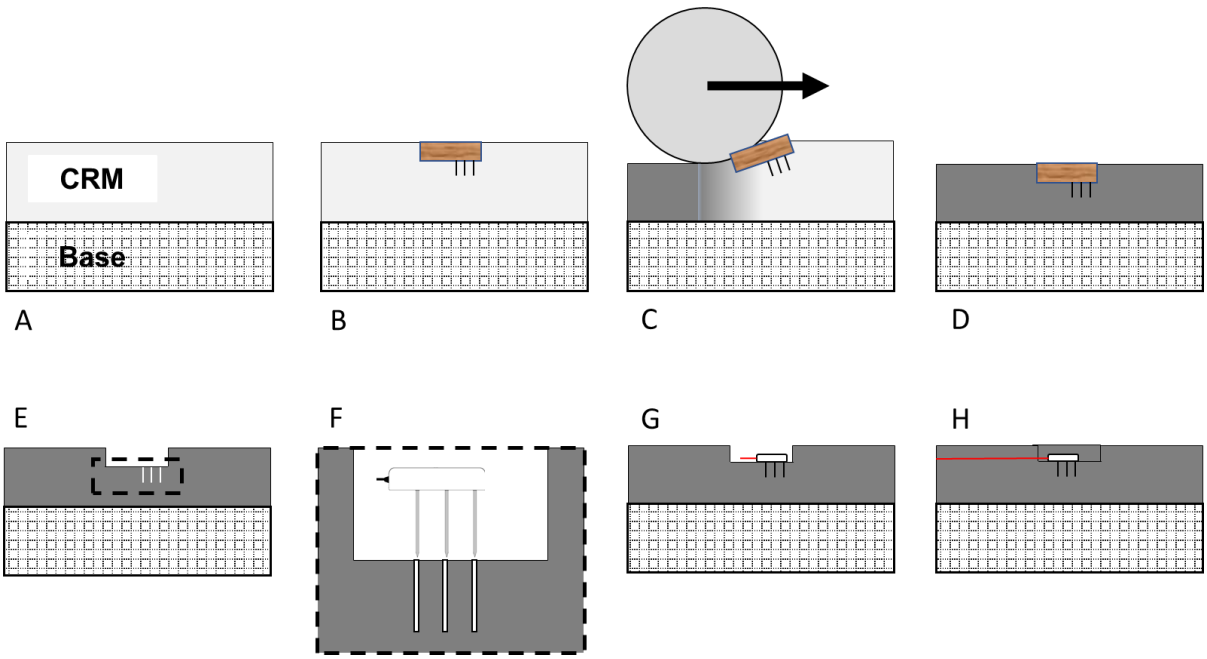

Figure 19. Phases of sensors installation

a) 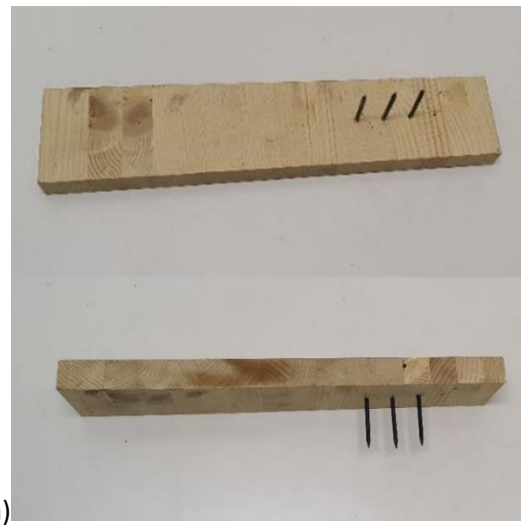

b) 

c) 

d) 

e) 

f) 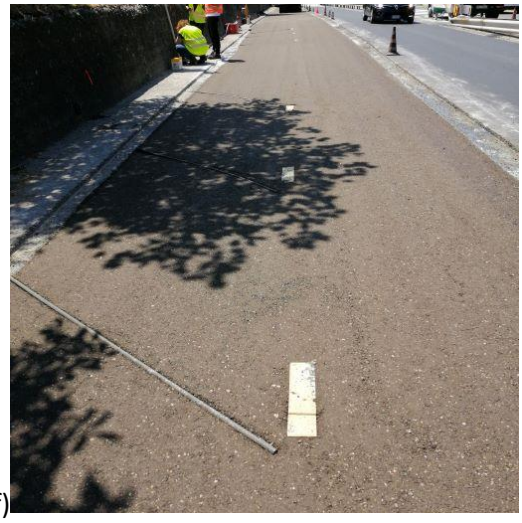

Figure 20. Sensors installation (phases A to D): a) wooden tablets before installation, b) cables covered with flexible metallic tubes before installation, c) positioning of the steel bars d) to f) positioning of the tablets

a) 

b) 

c) 

d) 

e) 

f) 

Figure 21.Sensors installation (phases F to J): a) sensors installed, b) sensors and cables, c) sensor covered by cold recycled mortar, d) cables blocked with cementitious mortar, e) data logger installation, f) sensors connected to the data logger.

4 Testing plan

The testing plan consisted in:

- laboratory testing on the CRM mixture sampled during the construction activities and compacted in the field using a gyratory compactor, and on cores extracted after construction;
- monitoring of pavement moisture and temperature during the first year of service life;
- field testing carried out during the construction activities (light falling weight deflectometer, LFWD) and after construction (falling weight deflectometer, FWD).

4.1 Laboratory testing

During construction, loose samples of the CRM mixture were collected and compacted on site for quality control, following the AASLP specifications (Azienda Autonoma per i Lavori di Stato, 2020). Additional specimens were compacted specifically for the laboratory evaluation of the curing process. Specimens were compacted using a gyratory compactor with a 150 mm mould, 600 kPa pressure, 30 rpm speed and 1,25° gyration angle. In particular:

- 19 specimens weighing 2800 g were compacted with 100 gyrations, 9 specimens were used for acceptance testing and 10 specimens for evaluating the curing process.
- 1 specimen weighing 4500 g was compacted with 180 gyrations and was used for the complex modulus measurement.

A total of twelve cores were extracted by AASLP from the in-service pavement:

- 8 cores were extracted 22 days after construction (Figure 22), during the first FWD measuring campaign;
- 4 cores were extracted 302 days after construction (Figure 23), during the second FWD measuring campaign.

All the cores were extracted from the middle of the right lane, outside the traffic wheelpaths. Table 4 reports the thickness of the layers measured from the cores. It must be highlighted that the reported thickness of the CRM binder layer may be underestimated because only in a few cases undamaged cores including the cement stabilised base were extracted (cores 1.3 and 2.3). In the other cases the core was broken during extraction within the CRM layer (core 1.1, 1,4) or at the interlayer bond to the sublayer (1.2, 1.3, 1.5 to 1.8, 2.1 to 2.4). For cores 1.1 and 1.4 the the lower portion of the CRM layer could not be extracted.

Table 5 summarises the experimental program on specimens and cores.

The specimens from the cores extracted after 22 days were tested for stiffness 6 days after curing (in total 28 days after construction) as well as after 85 days and 308 days of laboratory curing at 25 °C.

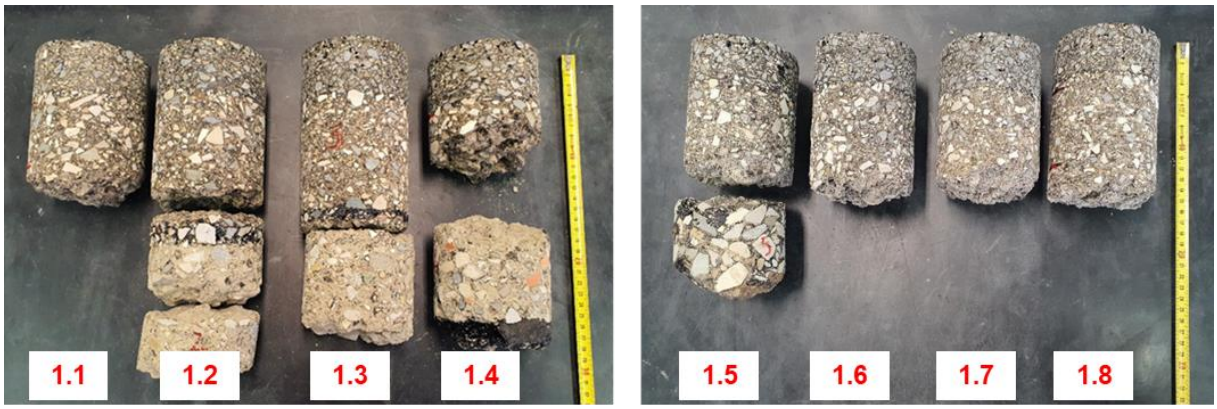

Figure 22. Cores collected after 22 curing days

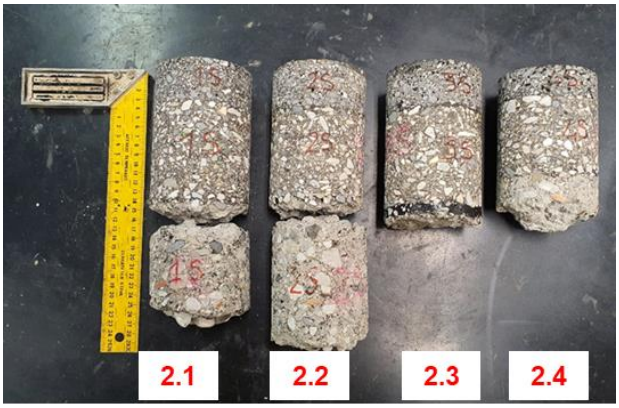

Figure 23. Cores collected after 302 curing days

Table 4. Thickness of the pavement layers

Core ID	Subsection	Asphalt concrete wearing course (mm)	CRM binder course (mm)	Location (m)*
1.1	1	42,5	76,8	+30
1.2	1	44,1	83,1	+49
1.3	1	46,6	97,6	+62
1.4	1	48,2	n.a.	+79
1.5	2	39,5	69,4	+120
1.6	2	41,7	79,7	+134
1.7	2	44,4	70,2	+140
1.8	2	39,7	90,9	+160
2.1	1	41,6	95,8	+20

2.2	1	42,7	84,7	+45
2.3	2	44,1	93,6	+102
2.4	2	29,7	72,3	+134
Average		42,0	83,1	
Standard deviation		4,6	10,3	

*from km 5,200

Table 5. Summary of the laboratory testing plan on CRM

Specimen	Curing conditions	Curing time (days)	Test	n° specimens
Gyratory specimens	40 °C Oven	3	ITS	6
	40 °C Oven (sealed)	3	ITS	3
	10 °C climatic chamber	1, 1,25, 2, 3, 7, 14, 28, 85	Moisture loss	4
		3, 7, 14, 28, 85	Stiffness (IT-CY)	2
			Volumetric properties	4
	25 °C climatic chamber	3, 7, 14, 28, 85	Stiffness (IT-CY)	2
			Volumetric properties	2
		310	Complex modulus	1
	40 °C oven	1, 1,25, 2, 3, 7, 14, 28, 85	Moisture loss	4
		3, 7, 14, 28, 85	Stiffness (IT-CY)	2
			Volumetric properties	4
Cores@22 days	25 °C climatic chamber		Volumetric properties	4 (ρ_{bsea}) + 3 (ρ_{bdry})
		22 days on site +6, 63, 286 days in laboratory	Stiffness (IT-CY)	7
Cores@302days	25 °C climatic chamber		Volumetric properties	4 (ρ_{bdry})
		308	Stiffness (IT-CY)	4

4.1.1 Acceptance testing

The acceptance testing consisted in the measurement of the indirect tensile strength (ITS) at 25 °C, after 3 days of curing at 40 °C. The ITS test was carried out on 6 gyratory specimens: 3 were cured in unsealed conditions and 3 in sealed conditions. The ITS was measured according EN 12697-23.

4.1.2 Volumetric properties

The bulk density of the gyratory specimens (herein coded “Lab”) was evaluated after long-term curing (> 10 months) according to EN 12697-6 procedure D (by dimensions). Similarly, the bulk density of the cores was evaluated after long-term curing (> 10 months) according to:

- EN 12697-6 procedure A (dry specimen) on 3 cores collected after 22 days (coded 1.1, 1.3 and 1.6) and the 4 cores collected after 302 days (from 2.1 to 2.4);
- EN 12697-6 procedure C (sealed specimen) on 4 cores collected after 22 days (coded 1.2, 1.5, 1.7 and 1.8).

The maximum density of the CRM mixture was determined according to EN 12697-5 procedure A (volumetric), and the air voids of the specimen were calculated following the EN 12697-8.

4.1.3 Evolution of the physical and mechanical properties

The curing process was characterised by measuring and modelling the evolution of the moisture loss (DW) and the stiffness modulus (E) measured applying pulse indirect tension to cylindrical specimens (EN 12697-26 Annex C).

The gyratory specimens were cured at 3 temperatures, 10 °C (4 specimens), 25 °C (2 specimens) and 40 °C (4 specimens). DW was measured on the specimens cured at 10 °C and 40 °C by weighing the specimens:

$$DW = \frac{M_0 - M_i}{M_0} \cdot 100 \quad (1)$$

where M_0 is the specimen mass after 1 day of curing at ambient temperature, M_i is the specimen mass after *i* curing days.

Among the specimens considered for measuring DW, six (2 specimens for each curing temperature) were also tested for evaluating the evolution of the stiffness, that was measured according to EN 12697-26 Annex C (IT-CY). The testing temperature was 25 °C and the target horizontal strain was 2×10^{-6} mm/mm. The stiffness modulus was also measured on 11 cores. One of the cores collected after 22 days (coded 1.4) was excluded as the thickness of the CRM layer was too small for being tested.

The evolution of material properties was modelled using an asymptotic function, obtained as a modified version of the Michaelis-Menten model (Mignini et al., 2018):

$$y(t) = y_i + (y_a - y_i)\frac{t - t_i}{(h_y - t_i) + (t - t_i)} \quad (2)$$

where $y(t)$ is the property under investigation (DW or E), y_i is its value at the time t_i and y_a is its long-term asymptotic value. The time t_i represents the early-stage of curing, and here it was considered the time at which was obtained the first measurement of the property. The parameter h_y represents the time to reach the value $(y_a - y_i)/2$ by $y(t)$. The model parameters y_i, y_a and h_y were estimated using non-linear least-squares minimization.

4.1.4 Complex modulus of the CRM mixture

One specimen was considered for evaluating the stiffness and the temperature-frequency dependence of the CRM mixture by measuring the complex modulus $E^*(\omega)$.

$$E^*(\omega) = \frac{\sigma_0}{\varepsilon_0}\exp[j\varphi(\omega)] = E_0(\omega)\exp[j\varphi(\omega)] = E_1 + jE_2 \quad (3)$$

where $E_0(\omega)$ is the stiffness modulus, $\varphi(\omega)$ is the phase angle and E_1 and E_2 are the storage and loss moduli, $\omega = 2\pi f$ is the angular frequency (f is the testing frequency in Hz).

The test was carried out after long-term curing (> 10 months) at 25 °C, on a cylindric specimen with diameter of 75 mm and height of 110 mm, obtained by coring and cutting the original gyratory sample. $E^*(\omega)$ was measured by means of cyclic axial tension/compression tests using an AMPT PRO system (EN 12697-D) Three LVDT, placed 120° apart measured the axial strain in the middle part of the specimen, with a measuring base of 70 mm. The sequence of testing temperatures was 5, 15, 25, 35, 45 and 55 °C. The testing frequencies were 10, 5, 1, 0,5 and 0,1 Hz. Tests were carried out in control stress mode and the applied sinusoidal stress amplitude σ_0 was adjusted to obtain the steady state strain amplitude ε_0 of 30 10^{-6} mm/mm.

Based on the time-temperature superposition principle (TTSP) principle, the master curves of the stiffness modulus were obtained considering the reference temperature $T_{ref} = 25$ °C and shifting the data measured at the other temperatures parallel to the log-frequency axis:

$$f_r = f \cdot a_{Tref}(T) \quad (4)$$

where f is the testing frequency, f_r is the reduced frequency and $a_{Tref}(T)$ is the shift factor required to obtain the superposition between the data measured at different temperatures T and at T_{ref}. The shift factors were calculated using the closed form shifting algorithm, based on the minimization of the area between two adjacent isothermal segments (Gergesova et al., 2011). The master curves of the phase angle were obtained applying the shift factors calculated for the stiffness modulus.

The temperature-dependency of the shift factors was modelled with the Williams–Landel–Ferry (WLF) equation (Ferry, 1980):

$$\log\left(a_{T_{ref}}\right) = -\frac{C_1(T - T_{ref})}{C_2 + T - T_{ref}} \quad (5)$$

where C_1, C_2 are constants obtained by least squares fitting.

The complex modulus data were fitted with the 2S2P1D-HY model, a modified version of the 2S2P1D rheological model introduced for CRM (Graziani et al., 2020):

$$E^*(\omega) = \left[E_e + \frac{E_g - E_e}{1 + d \cdot (j\omega\tau)^{-k} + (j\omega\tau)^{-h} + (j\omega\beta\tau)^{-1}}\right]\exp(j\,\varphi_{HY}) \quad (6)$$

where E_e and E_g are the equilibrium and glassy values of the stiffness modulus, d, h k and β are dimensionless parameters controlling the shape of the model, τ is a characteristic time whose value depends on the selected reference temperature. The term $\exp(j\,\varphi_{HY})$ is a correction which adds a constant (i. e. temperature- and frequency-independent) phase angle φ_{HY}, describing non viscous dissipation mechanisms, such as internal friction phenomena and the presence of cementitious bonds.

4.1.5 Stiffness of the AC mixture

Five cores (coded 1.1, 1.3, 1.6, 2.1 and 2.3) were used for evaluating the stiffness of the asphalt concrete wearing course, and its temperature dependence. The test was carried out according to EN 12697-26, Annex F (CIT-CY) using a servo-pneumatic press. The testing frequencies were 10 and 1 Hz, and the testing temperatures were 5, 15, 25 and 35 °C.

The master curve of the stiffness modulus was obtained following the same procedure described above. In this case, since the phase angle values were not measured, the five-parameters Richards model was used to fit the experimental data:

$$\log E(\omega) = \delta + \frac{\alpha}{[1 + \exp(\xi + \gamma \log \omega)]^{\frac{1}{\lambda}}} \quad (7)$$

where δ is the lower asymptote, corresponding to the logarithm of E_e, $\delta + \alpha$ is the upper asymptote, corresponding to the logarithm of E_g, ξ, γ and λ are shape parameters.

4.2 Monitoring of pavement moisture and temperature

The sensors measurements were recorded for one year after the construction of the demonstration site. The data logger automatically uploaded the measured data to a cloud server (**Fehler! Verweisquelle konnte nicht gefunden werden.**). The cloud server also allows the management of the measurement and communication settings, e.g., measurement interval and server upload frequency (**Fehler! Verweisquelle konnte nicht gefunden werden.**). The selected measurement intervals were:

- 5 minutes, from 7th July 2020 (18:05) to 9th July 2020 (18:15)
- 15 minutes, from 9th July 2020 (18:15) to 21st July 2020 (8:30)
- 30 minutes, from to 21st July 2020 (8:30)

The rainfall data (accumulated rainfall every 30 minutes) measured by the San Marino weather station managed by the *Agenzia Prevenzione Ambiente Energia Emilia-Romagna* (ARPAE) were also collected.

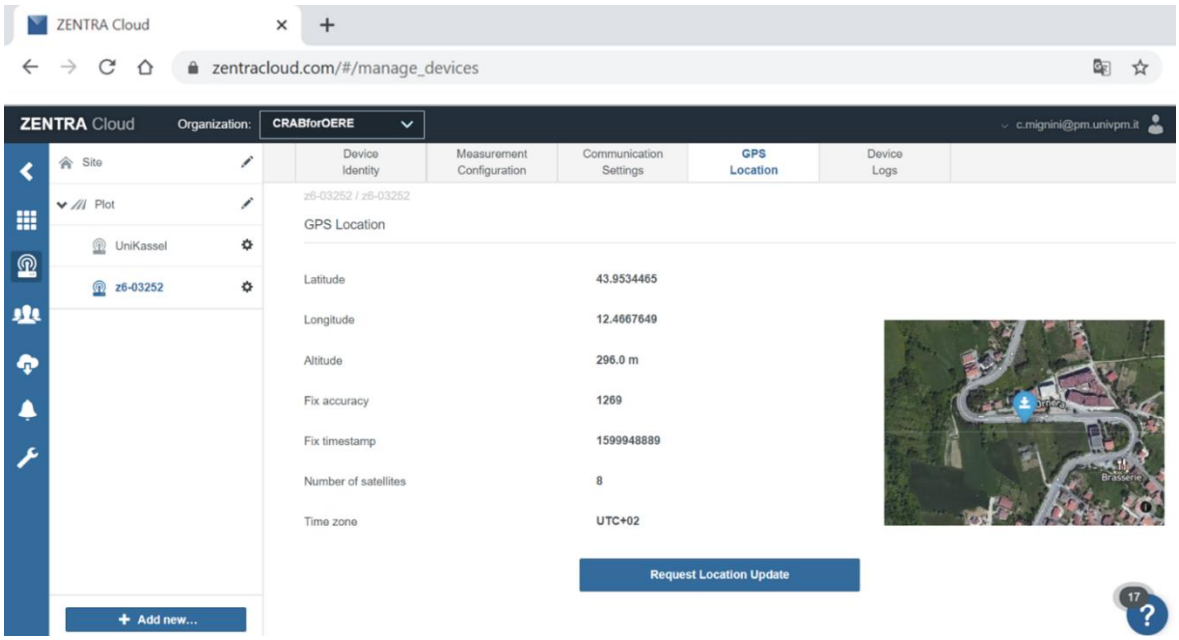

Figure 24. Cloud service, device information

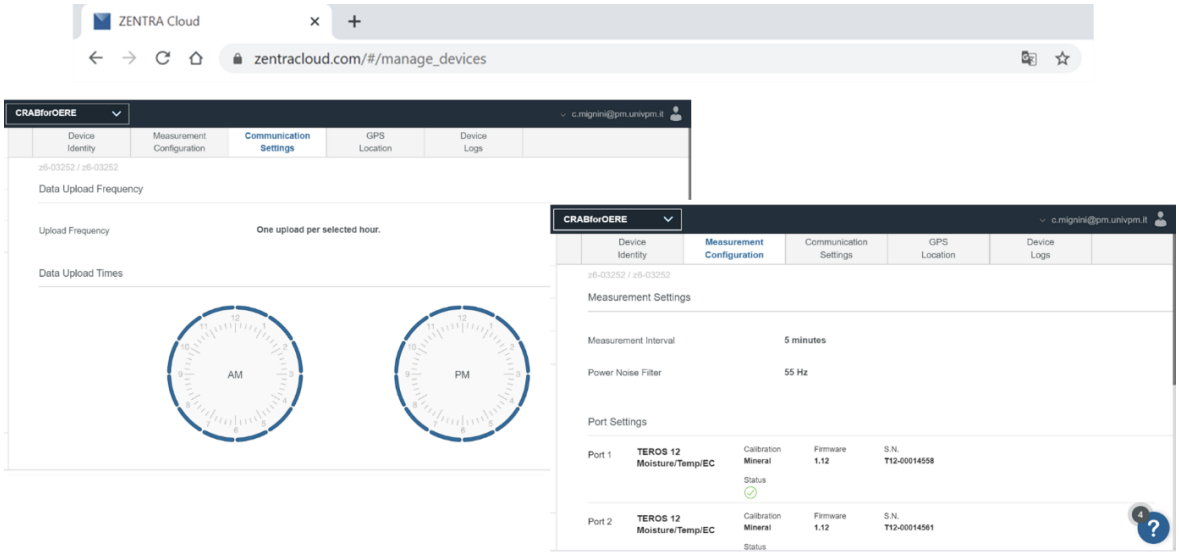

Figure 25. Cloud service: communication setting and measurement configuration

4.3 Field testing

4.3.1 Light Falling Weight Deflectometer

Light Falling Weight Deflectometer (LFWD) tests (Figure 26a) were carried out during the construction of the demonstration site on:

- Subbase of subsection 1, after milling to the depth of 29 cm;
- CTRM base layer of subsection 1, right after compaction;
- CRM binder layer right after compaction of subsections 1 and 2 (layer temperature about 40 °C);

- CRM binder layer after about 18 hours of curing of the subsections 1 and 2 (the layer temperature was about 25 °C).

4.3.2 Falling Weight Deflectometer

Falling Weight Deflectometer (FWD) tests were carried out after 22, 305 and 371 days from the CRM layer construction by Nievelt Labor GmbH. Four test runs were carried out within the same working day in order to cover a wide range of pavement temperatures (Figure 26b-c). In particular, the runs were carried out:

- in the early morning, when the temperature was about the minimum of the day;
- in the early afternoon, when the temperature was about the maximum of the day;
- in the mid-morning, when temperature was about halfway between the maximum and the minimum of the day.

Each run consisted in 12 measuring points along the right wheel path, 6 within Subsection 1 and 6 within Subsection 2.

The diameter of the loading plate was 300 mm, the peak load was 80 kN and the deflections were measured by eight sensors positioned at 0, 200, 300, 600, 900, 1200, 1500 and 1800 mm from the centre of the loading plate. Three drops were performed in each position.

From the measured deflections the following deflection indices were calculated:

- Surface Curvature Index (SCI) – difference between the deflection measured in the centre of the loading plate (D_0) and the deflection measure at an offset of 300 mm (D_{300});

$$SCI = D_0 - D_{300} \quad (8)$$

- Base Damage Index (BDI) – difference between the deflections measured at 300 mm (D_{300}) and 600 mm (D_{600});

$$BDI = D_{300} - D_{600} \quad (9)$$

- Base Curvature Index (BCI) – difference of deflections measured in the distance 600 mm (D_{600}) and 900 mm (D_{900}).

$$BCI = D_{600} - D_{900} \quad (10)$$

The backcalculation of the layers' moduli was carried out considering a 3-layer structure:

- Layer 1: wearing course + CRM binder course (total thickness = 14 cm)
- Layer 2: Base course (total thickness = 15 cm)
- Layer 3: Subgrade (half-space)

It is highlighted that in Subsection 1 we have the new cement-treated base course, whereas in Subsection 2 we have the existing unbounded base.

During the FWD tests, cores were extracted for measuring the mechanical properties and the voids content of the CRM layer (Figure 26d).

Table 6 summarises the information about the FWD test campaign and coring.

a)

b)

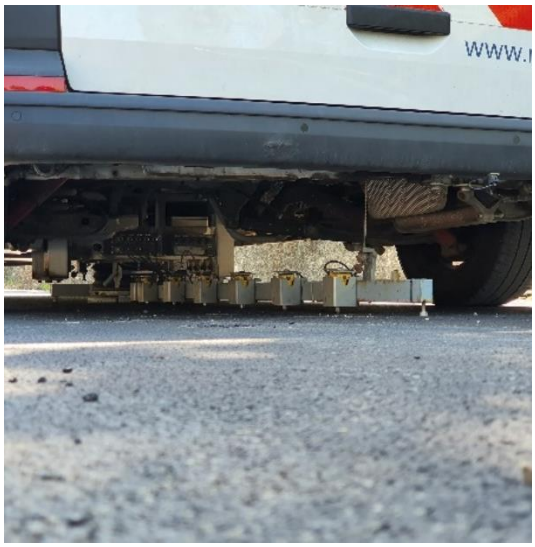

c)

d)

Figure 26. Field testing: a) LFWD, b) FWD, c) detail of the FWD equipment, d) coring

Table 6. Summary of the FWD test campaign and coring

Data	Curing (days)	FWD runs	FWD points	Cores
28/07/2020	22	4	12	8
05/05/2021	302	4	12	4
13/07/2021	371	4	12	-

5 Results

5.1 Laboratory testing

5.1.1 Materials acceptance

Figure 27 shows the results of the CRM acceptance testing carried out according to the AASLP specifications (Azienda Autonoma per i Lavori di Stato, 2020). The unsealed specimens reached an ITS at 25 °C of 0,60 MPa after a curing period of 72 hours at 40 °C. The value is well above the limit required by the specification (0,40 MPa). The average ITS of the sealed specimens also satisfied the specification limit. The average dry density of the specimens was 2061 kg/m^3.

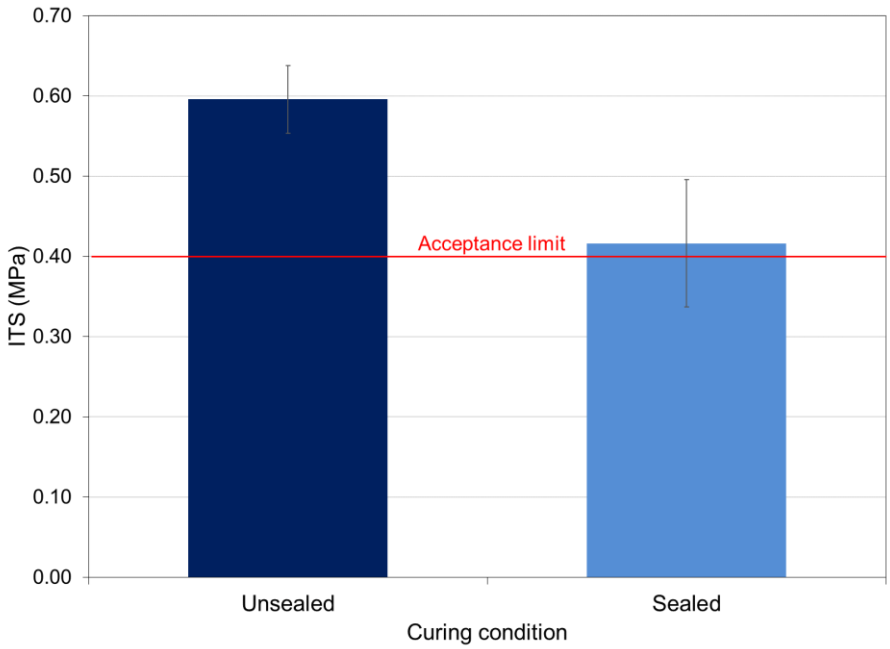

Figure 27. CRM acceptance results

5.1.2 Volumetric properties

The maximum density of the CRM mixture was 2504 kg/m^3. The gyratory specimens (compacted with 100 gyrations) had an average bulk density of 2158 kg/m^3 (standard deviation of 9,4 kg/m^3) resulting 13,8% (0,4%) air voids. Table 7 summarises the bulk density and voids values measured on the cores. As it can be observed Subsection 2 was characterised by higher voids 17,3% (1,02%) with respect to Subsection 1 16,1% (0,81%). A similar range of voids (from 14,1% to 17,0%, with an average value of 15,5%) was measured during the field trial that was carried out in 2018 at the mixing plant (Ferrotti et al., 2020) where the same mixture was used for the binder layer and the laydown and compaction procedures were optimised.

The results of the volumetric characterisation can be summarised as follows:

- The target air voids value in the field for the adopted CRM mixture is between 15,5% and 16,0%;

- The air voids value of the gyratory specimens overestimated the field value because the gyration number requested by the specifications (100) overestimates the actual compaction energy applied in the field with the available rollers;
- The higher voids value measured in Subsection 2 was probably related to the lower stiffness of the underlying base layer, which led to a non-optimal compaction.

Table 7. Volumetric properties of the cores

Core ID	Subsection	Bulk density EN 12695-6 – A (kg/m^3)	Bulk density EN 12695-6 – C (kg/m^3)	Voids (%)
1.1	1	2117		15,4
1.2	1		2076	17,1
1.3	1	2081		16,9
2.1	1	2122		15,2
2.2	1	2087		16,7
Average (st. dev.) for subsection 1				**16,1 (0,81)**
1.5	2		2072	17,3
1.6	2	2047		18,2
1.7	2		2049	18,2
1.8	2		2052	18,1
2.3	2	2099		16,1
2.4	2	2109		15,7
Average (st. dev.) for Subsection 2				**17,3 (1,02)**

5.1.3 Evolution of the physical and mechanical properties

Figure 28 shows the evolution of the moisture loss of the gyratory specimens in unsealed condition (free evaporation). The lines depict the fitted curing model, whose parameters are reported in Table 8. All the specimens showed a faster moisture loss during the first curing days, then the evaporation rate decreased.

After the first curing day the moisture loss was similar for the specimens cured at 10 °C and 40 °C (y_i). Then, the specimens cured at the higher temperature showed a higher water evaporation rate. Specimens cured at 40 °C lost 2,5% and 3,5% of moisture during the first 3 and 28 curing days, respectively. The moisture loss of specimens cured at 10 °C was 2,0% and 3,0% at the same curing times. The two groups of specimens had different asymptotic values (y_a), which was 3,0% and 3,65% for specimen cured at 10 °C and 40 °C, respectively. This difference related to a different relative humidity (RH) level of the climatic chamber (curing at 10 °C) and the oven (curing at 40 °C).

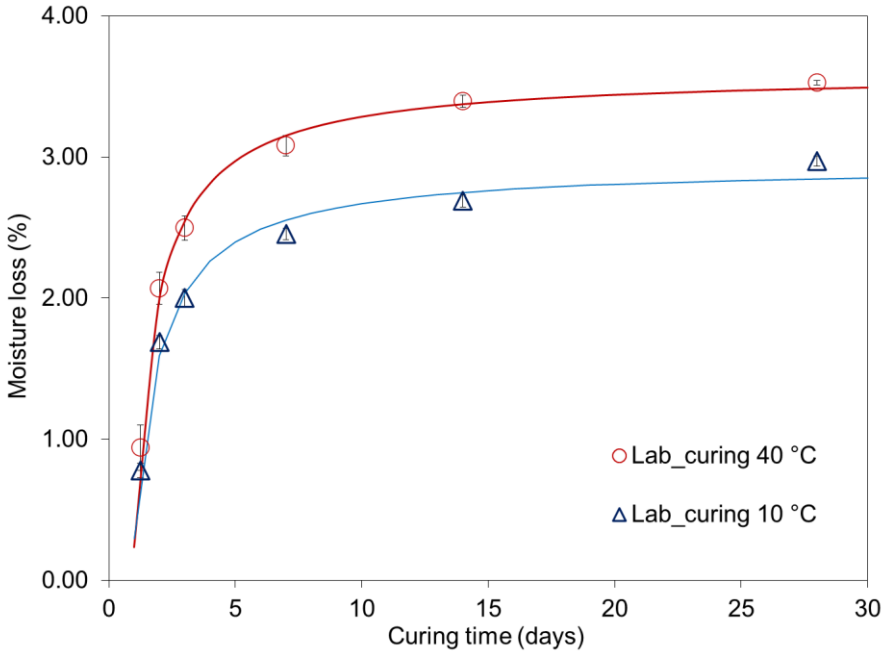

Figure 28. Evolution of the moisture loss of the specimens as a function of the curing temperature

Figure 29 shows the evolution of the stiffness modulus of the gyratory specimens and cores. The model fitting parameters are listed in Table 8. All the gyratory specimens had a similar evolution, with a major increase in stiffness in the first curing days. After 3 days E was always higher than 3000 MPa regardless of the curing temperature. The specimens cured at 40 °C had always the highest stiffness, reaching 4172 MPa after 3 days and 6385 MPa after 28 days. The curing process continued after 28 days of curing at 40 °C: E increased about 22% from 28 to 85 days. It must be pointed out that the increase in stiffness may be ascribed to both curing and possible bitumen ageing. The stiffness of the specimens cured at 10 °C was always the lowest. After 28 days, the average E was 5894 and 4996 MPa when the curing temperatures were 25 and 10 °C, respectively. The increase in the curing temperature led to an increase in the rate of evolution of E. The asymptotic values of E (y_a) reflected the hierarchy already identified through the experimental measurements.

The cores of the group sampled 22 days after construction showed a lower stiffness than the gyratory specimens. After 28 days (22 days of in-field curing and 7 days of laboratory-curing at ambient temperature) the cores extracted from Subsection 1 and Subsection 2 had average E of 3323 MPa and 2789 MPa, respectively. Afterwards E increased and, after 308 days (22 days of in field curing and 286 days of laboratory curing at ambient temperature), its average value for the two subsections was 4825 MPa and 4431 MPa, respectively.

The average stiffness of the cores sampled 305 days after construction was 4013 MPa after 308 curing days (305 days of in field curing and 3 days of laboratory curing at ambient temperature). Although the curing conditions were different, this value is comparable to that of the cores sampled after 22 days and cured in laboratory up to the same specimen age . This confirms that the curing temperature affects mainly the initial curing rate, whereas its effect on the long-term value is negligible.

Table 8. Regression parameters for the curing model for water content (DW) and stiffness (E)

	Curing temperature	Initial value y_i	Asymptotic value y_a	h_y	t_i	R^2
DW	(°C)	(%)	(%)	(days)	(days)	
Gyratory specimens	10	0,80	3,00	2,6	1	0,99
Gyratory specimens	40	0,95	3,65	2,4	1	0,99
E	(°C)	(MPa)	(MPa)	(days)	(days)	
Gyratory specimens	10	3311	6653	15,2	3	0,91
Gyratory specimens	25	3791	7710	17,6	3	0,92
Gyratory specimens	40	4114	8151	9,8	3	0,91
Cores 22days_section 1	22d in Field, then 25 °C	3323	4971	55	28	0,40
Cores 22days_section 1		2789	4616	59	28	0,40

The difference in stiffness between the gyratory specimens and the field cores may be explained by the different compaction levels (compare section 5.1.2). The average voids of the gyratory specimens (13,8%) was lower than the voids of the cores in both subsections (Table 7). Ferrotti et al. (2020) observed that the stiffness could be directly related to the air voids regardless of the curing conditions. In particular, testing a material having the same composition as the one considered in the present investigation, they found that a 1% increase in air voids led to a reduction of E of about 900 MPa. Therefore, the stiffness of the cores can be corrected as follows:

$$E_{corrected} = E + 900 \cdot \Delta Vm \quad (11)$$

where ΔVm is the difference between the voids of the cores and gyratory specimens. As shown in Figure 29, by applying this correction to the E of the cores a value comparable to those obtained on the gyratory specimen would be obtained.

In the first 22 field curing days (thus before the coring), the average temperature measured by the sensors in the CRM binder layer was 33 °C, the minimum and the maximum ones were 17,7°C and 67,2°C (the latter was measured during the AC laydown), respectively. Therefore, it appears that the laboratory curing at 25 °C well simulated the field process, even though the RH conditions were very different. The gyratory specimens were cured in unsealed conditions, at an RH of (70±5) %. In contrast, the field curing likely occurred at RH close to 100% in sealed conditions, as the CRM was placed between two waterproof layers of emulsion (prime coat and tack coat).

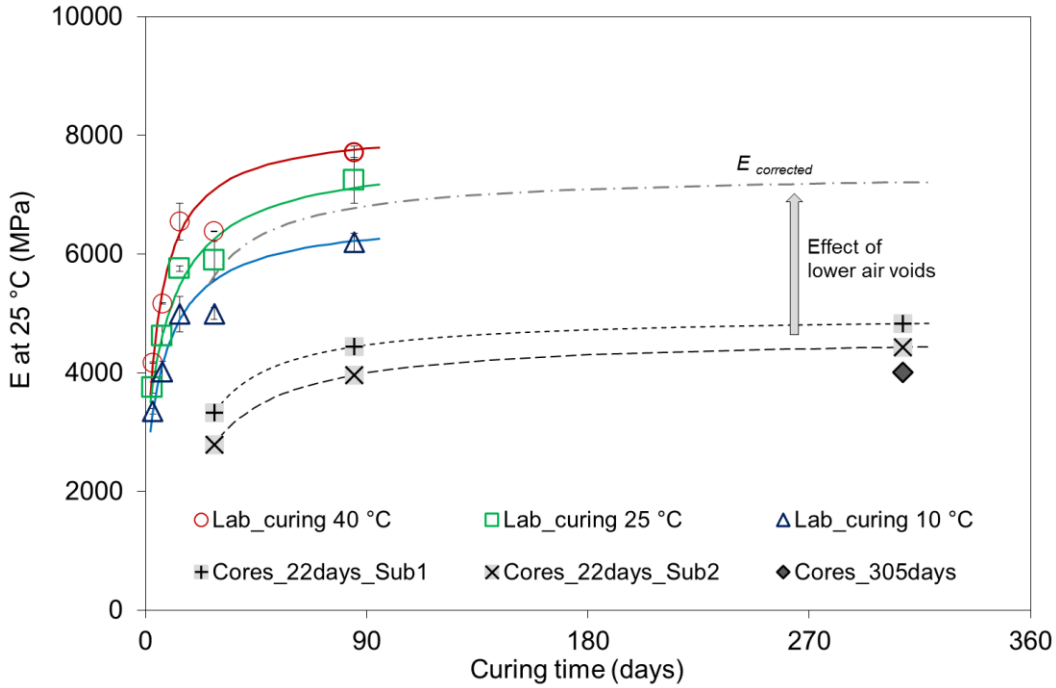

Figure 29. Evolution of the stiffness modulus of the specimens (cured at 10, 25 and 40 °C) and the cores (field curing)

5.1.4 Complex modulus of the CRM mixture

The specimen used for characterising the temperature-frequency dependence of the CRM mixture had a voids content of 9,7%. Figure 30 shows the complex modulus results in the Black ($\log E_0$ vs φ) and Cole-Cole (E_2 vs E_1) diagrams. The maximum stiffness was 10680 MPa measured at 5 °C and 10 Hz, the minimum stiffness was 1262 MPa, measured at 55 °C and 0,1 Hz. Compared to hot mixtures, the thermal sensitivity of the CRM mixture was reduced due to the presence of cementitious bonds. The minimum and maximum values of the phase angle were 5,14° (measured at 5 °C and 10 Hz) and 16,53° (measured at 55 °C and 10 Hz). These phase angle values are lower than typical values measured on AC mixtures (Kim, 2009) because of the lower frequency and thermal sensitivity of CRM mixtures, whose dissipation behaviour is affected by the presence of the aged bitumen from the RA and by the cementitious bonds.

The (E_0, φ) and (E_1, E_2) pairs describe single curves in the Black and Cole-Cole diagrams, respectively. This confirmed the validity of the TTSP and allowed the construction of the master curves depicted in Figure 31a and b, through the horizontal shifting of the isothermal data using the shift factors reported in Figure 31c.

Table 9 shows the parameters of the WLF and 2S2P1D-HY models. The parameters h, k, δ and β of the 2S2P1D-HY model represent the linear viscoelastic behaviour of the mixture, which is linked to its bituminous component. In the case of CRM, this includes both the fresh bitumen brought by the emulsion and aged bitumen coating the RA aggregate. In particular, h and k must be comprised between 0 and 1, with lower values representing a more elastic behaviour and higher values representing a more viscous behaviour. For the tested specimen the values of h and k were similar to those obtained for other CRM mixtures (Graziani et al., 2020; Raschia et al., 2021) but significantly lower than those commonly obtained for conventional hot and hot-recycled asphalt mixtures (Mangiafico et al., 2016; Olard & Di Benedetto, 2003).

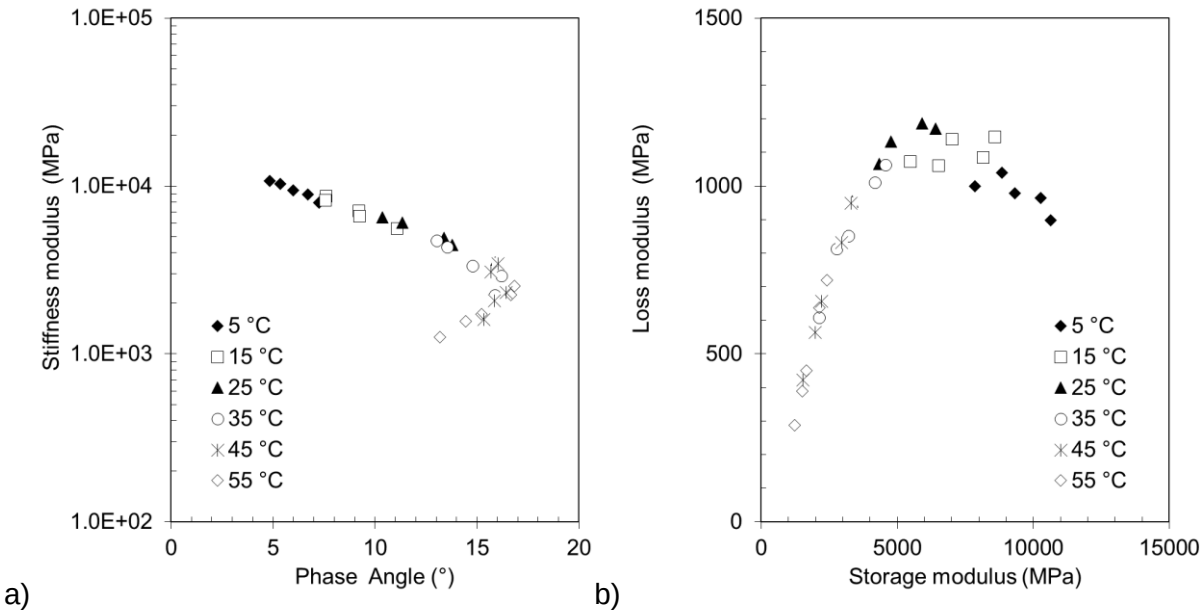

a) b)

Figure 30. Complex modulus results: a) Black diagram, b) Cole-Cole diagram

Table 9. 2S2P1D-HY and WLF models parameters for the CRM master curve (T_{ref} = 25 °C)

E_g (MPa)	E_e (MPa)	k (-)	h (-)	δ (-)	β (-)	$Log\ \tau$ (-)	φ_{HY} (°)	C_1 (°)	C_2 (-)
15342	912	0,132	0,357	1,657	1995	0,200	0,961	15,8	132,4

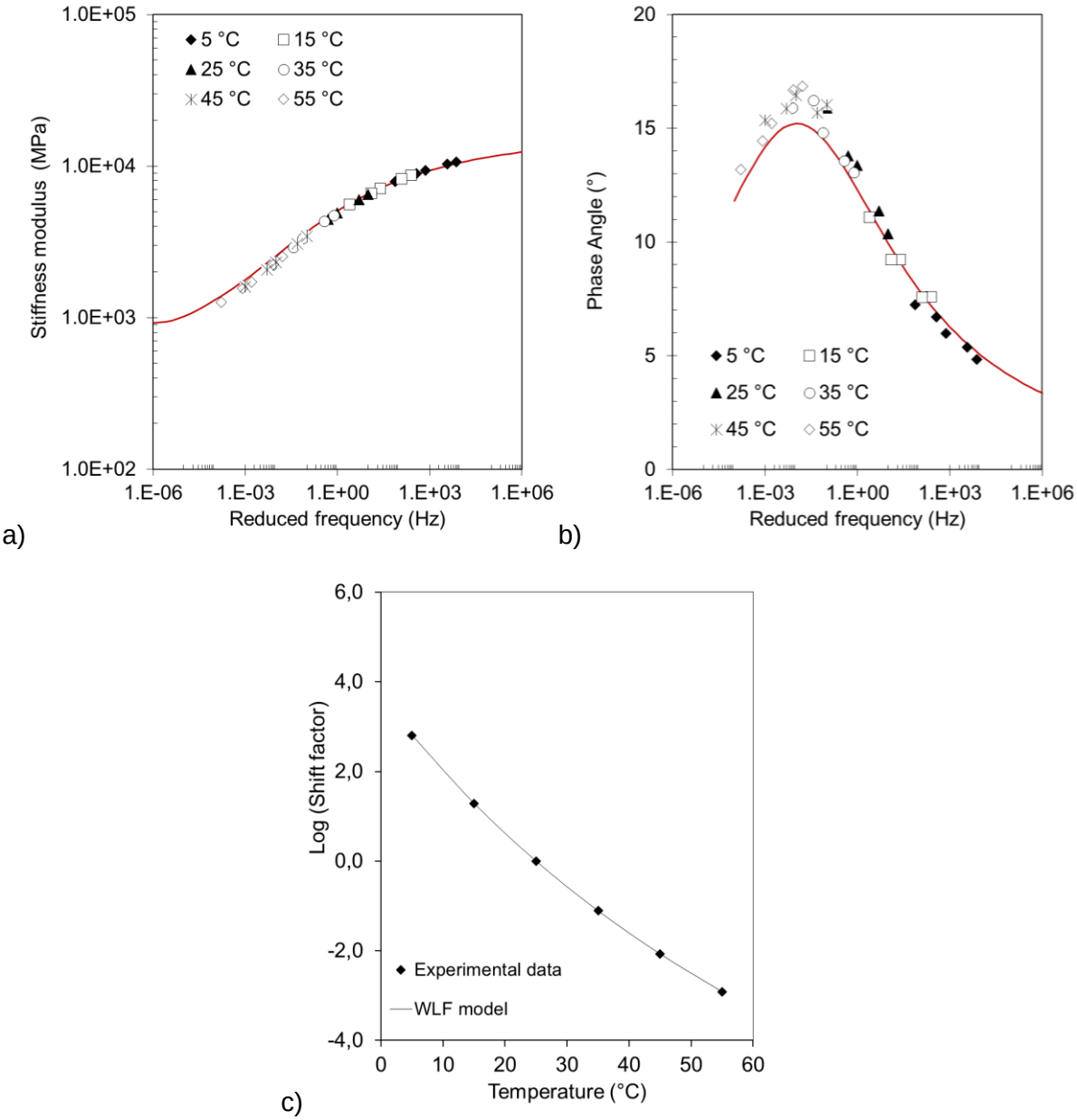

Figure 31. CRM master curve at 25 °C: a) stiffness modulus, b) phase angle and c) shift factors

5.1.5 Stiffness of the AC mixture

Figure 32a shows the stiffness modulus of the AC wearing course measured on the extracted cores in indirect tensile configuration. The experimental data (isochronal curves) have been fitted with a parabolic model (Figure 32b).

The master curve obtained by applying the TTSP is reported in Figure 32c and the shift factors are reported in Figure 32d. Table 10 shows the parameters of the WLF and Richards models.

Figure 32c also shows the master curve the CRM mixture obtained in tension-compression on the gyratory-compacted specimen (Figure 31a) and the stiffness modulus of the CRM binder course. The latter were measured on the extracted cores in indirect tensile configuration and using an impulse loading (IT-CY), they are reported at the frequency of 2 Hz.

As can be observed, the stiffness measured on the cores of the AC wearing course and CRM

binder course are comparable. The stiffness values measured on the gyratory specimens are higher, but they were measured on a specimen with lower air voids. As expected, the AC wearing course shows a higher temperature sensitivity as shown by the larger range of variation of the shift factors.

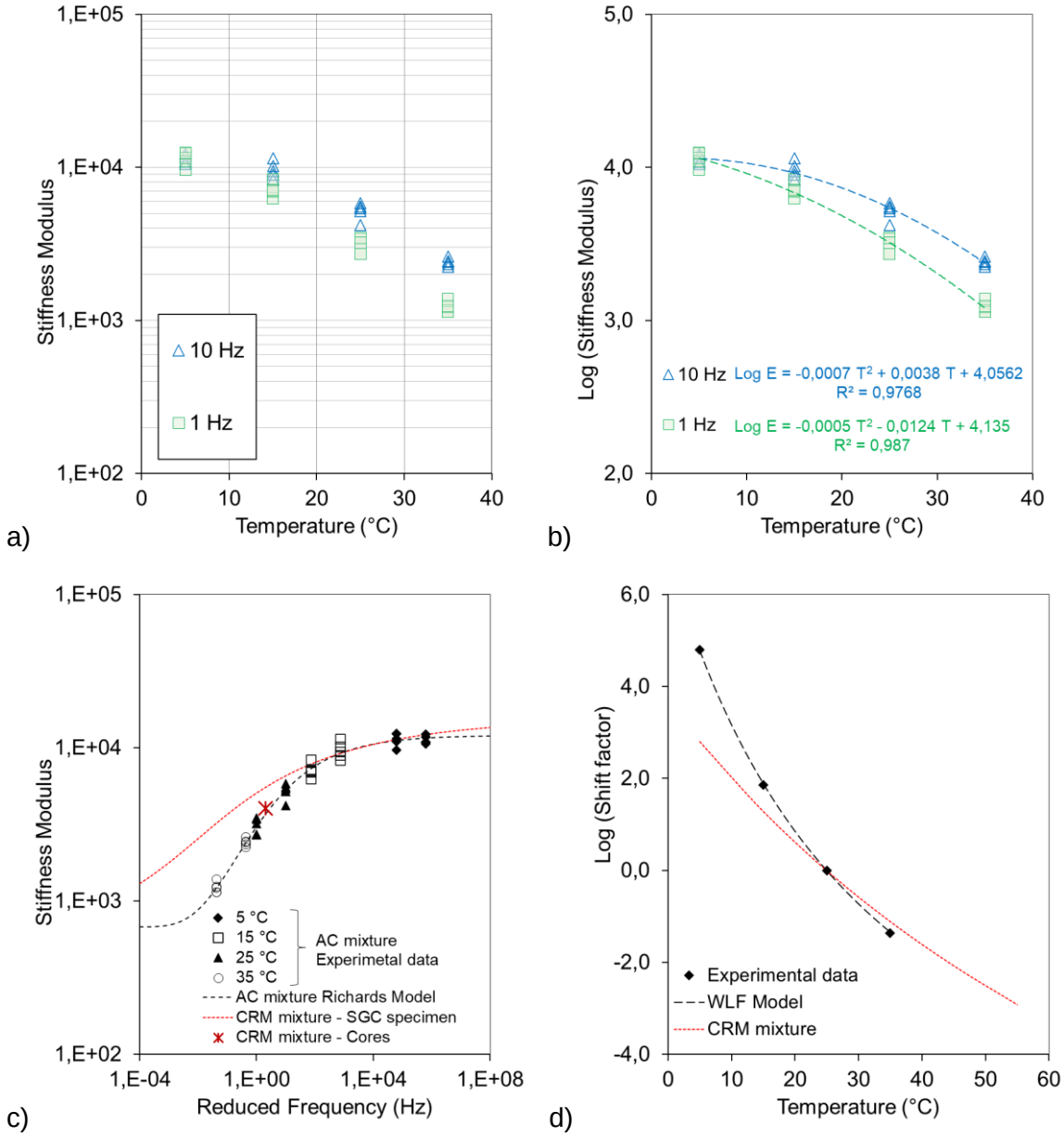

Figure 32. Stiffness modulus of the AC wearing course a) Measured data (isochronal representation), b) Parabolic regression of Log E Vs Temperature, c) Master curve at 25 °C, d) Shift factors.

Table 10. Richards and WLF models parameters for the AC master curve (T_{ref} = 25 °C)

E_g (MPa)	E_e (MPa)	ξ (-)	γ (-)	λ (-)	C_1 (°)	C_2 (-)
12087	680	0,132	0,357	1,657	9,1	58,0

5.2 Monitoring of pavement moisture and temperature

Figure 33 and Figure 34 show the temperature and VWC raw data measured by the sensors in the first 3 days after the CRM layer construction, from 7th July 2020 to 10th July 2020, In the first 18 curing hours the temperature of the CRM binder layer varied from a maximum of 35 °C to a minimum of 18 °C, and water evaporation was free from the top surface. The sensors recorded values of VWC ranging between 0,093 and 0,112 m^3/m^3 (Figure 34). Then, sealed curing started because the tack coat was applied. The time corresponding to the laydown of the AC wearing course can be easily located because the sensors registered a sudden increase in the temperature of the CRM binder layer (Figure 33) up to a maximum value of 67,2 °C. During the AC laydown, the VWC increased reaching VWC values up to 0,122 m^3/m^3. The VWC remained quite constant in the following hours, with some slight fluctuation.

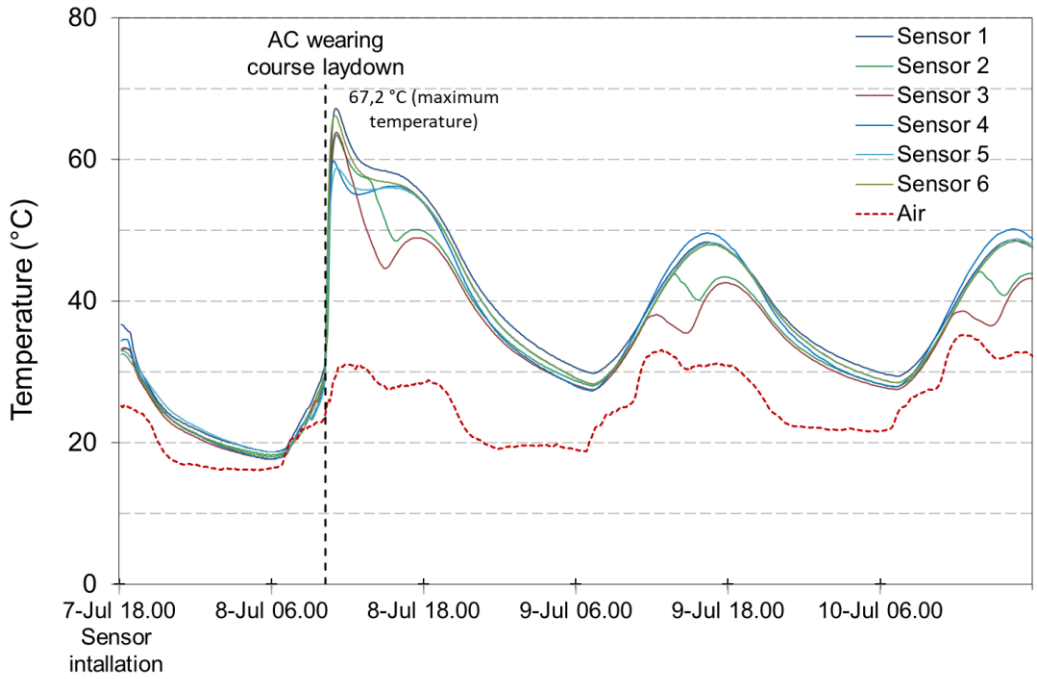

Figure 33. Temperature measured by the TEROS 12 sensors in the first 3 days

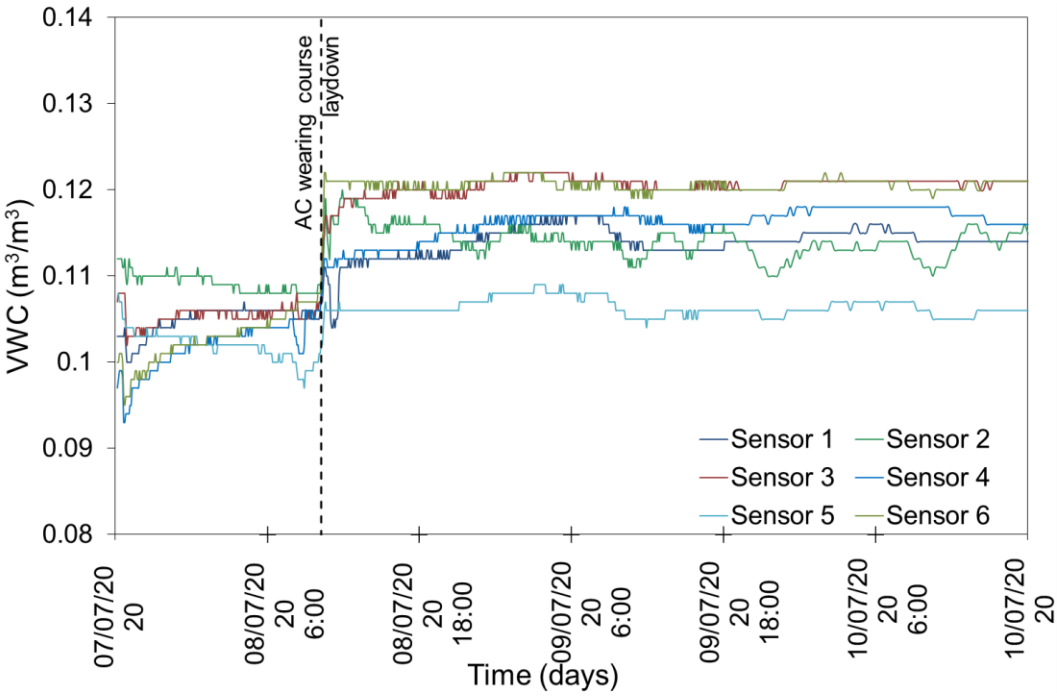

Figure 34. VWC measured by the TEROS 12 sensors in the first 3 days

Figure 33 also shows that in the middle of the day sensors 2 and 3 measured a temporary decrease in temperature. This is highlighted in Figure 35 where the temperature measured by sensor 3 and 6, from 5th to 9th August 2020, are reported. In the first two cloudy and rainy days, the temperature variations were similar. In the next two sunny days sensor 3 showed a temporary decrease of temperature for about two hours. This phenomenon is linked to the shadow occurring on the pavement in the position where the sensor was installed (Figure 20f). This is a "local" effect, whereas most of the pavement test section is not affected by the shadow.

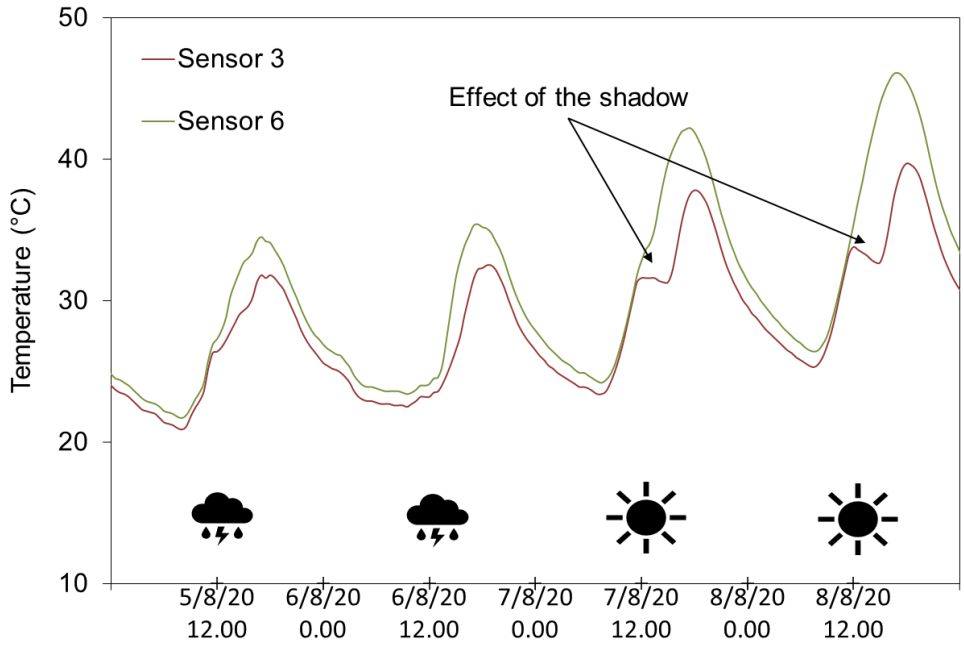

Figure 35. Temperature measured from 5th to 9th August 2020 by sensors 3 and 6

Figure 36 shows the temperature measured by the sensors in the first curing year, from 7th July 2020 to 7th July 2021 (raw data, daily, and monthly averages). The air temperature was generally lower than those measured within the CRM binder layer, except for the winter months, from November 2020 to March 2021, when the two temperatures were practically the same. The temperature showed fluctuations linked to the daily hours. The maximum and minimum measured air temperatures were, respectively:

- 38,7 °C, recorded on 7th July 2021 at 13:00;
- -3,2 °C, recorded on 13th February 2021 at 20:30,

As regards the CRM binder layer, excluding the temperatures measured during the laydown the of the AC wearing course, the maximum and minimum temperatures were:

- 53,1 °C registered by sensor 4 on 29th July 2020 at 16:30;
- -0,7 °C recorded by sensor 2 on 13th January 2021 at 6:30,

Stronger daily excursions were registered in the summer months, when also the maximum daily temperatures were recorded. On the contrary, during winter the excursions were reduced, and the minimum daily temperatures were recorded.

Figure 37 shows the frequency distribution of the average daily temperatures during the year. The median value was 16,7 °C, whereas 67% of the days had an average daily temperature below 25 °C.

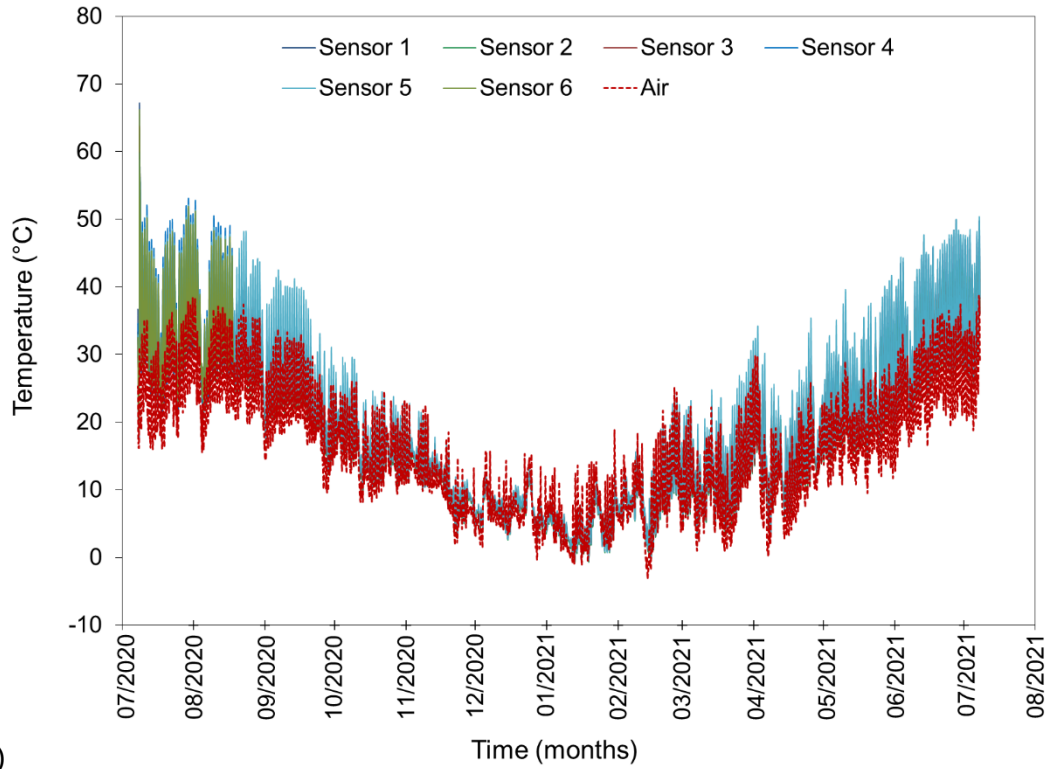

a)

b)

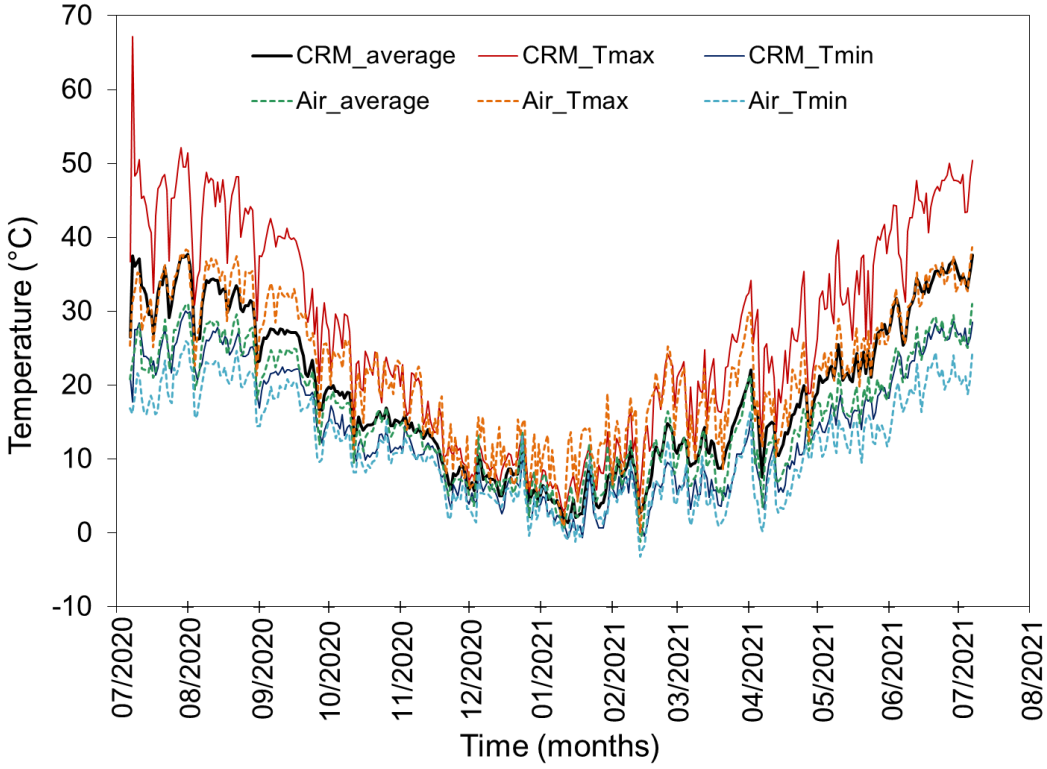

c)

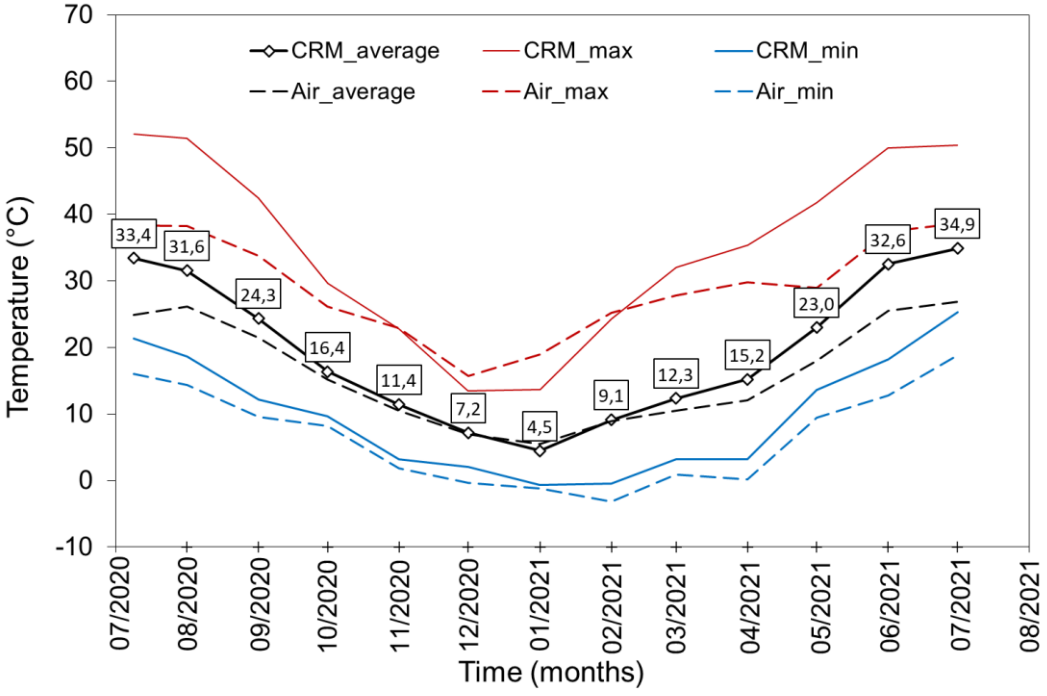

Figure 36. Temperature measurements: a) raw data; b) daily average; c) monthly average

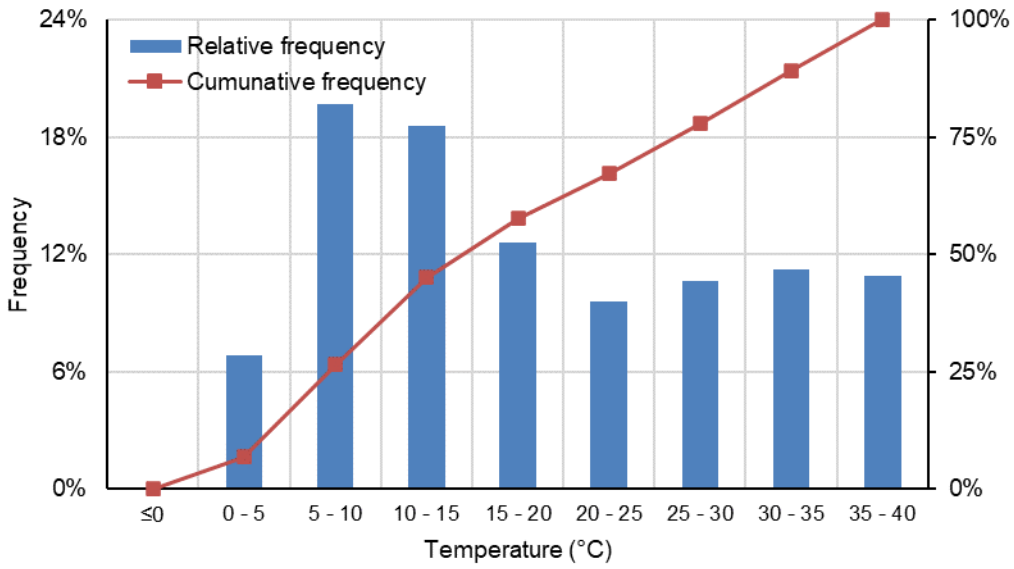

Figure 37. Statistical distribution of the average daily temperatures within CRM layer

Figure 38 depicts the VWC reading of the sensors (raw data) in the first curing year and the accumulated rainfall for 30 minutes intervals registered by the San Marino weather station. Figure 39 shows a detail of the data, considering the first eight weeks after construction and reporting only the measurements of sensors 4, 5 and 6. As it can be observed, the VWC readings were generally characterised by daily fluctuations, and some of the sensors measured huge peaks, directly related to rainfall events. On 18 August 2020, during one of those rainfall events, the sensors 4 and 6 stopped working.

The daily fluctuations are related to the temperature sensitivity of the sensors, with higher temperatures leading to higher values of VWC. The VWC peaks corresponding to rainfall events cannot be due to a direct effect of the rainfall on the actual moisture content of the CRM mixture because the CRM binder layer was sealed by two bituminous interlayers and because the peaks were not registered by all the sensors. More likely, the presence of those peaks was due the infiltration of water from the roadside through the trenches excavated for the cables of the sensors or directly through the corrugated tubes that were used to protect the cables. Therefore, similar to the effect of the shade on the temperature, those VWC peaks are considered a “local” effect that cannot be extended to the whole pavement.

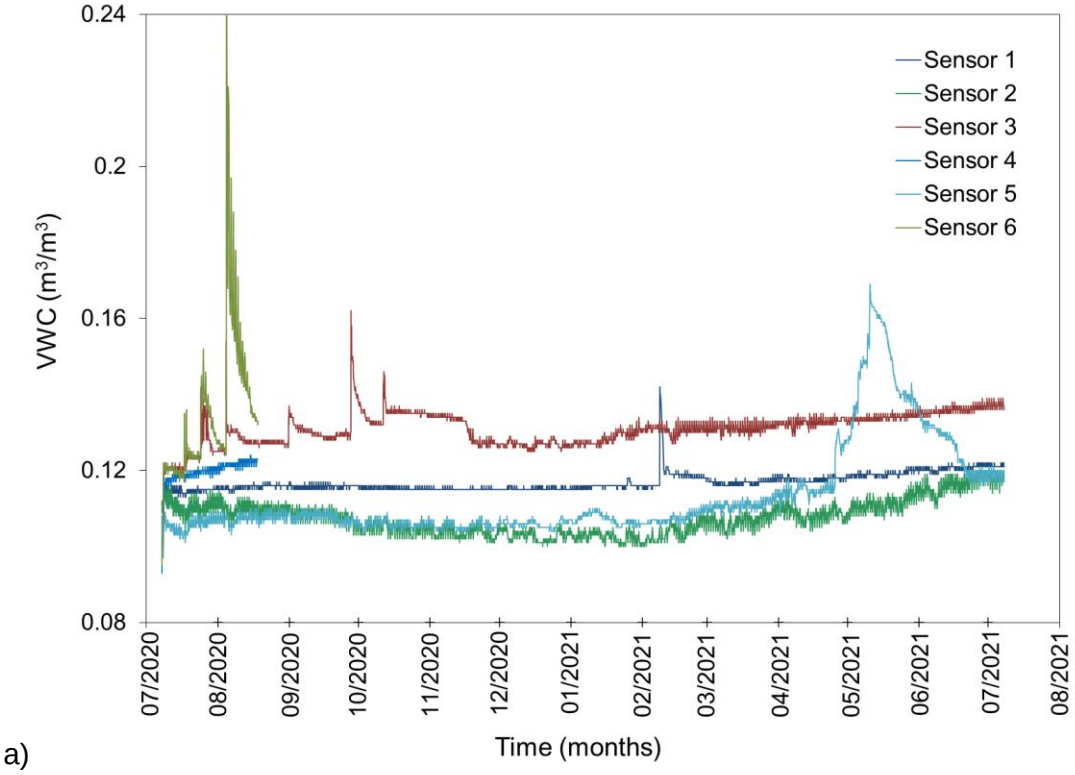

a)

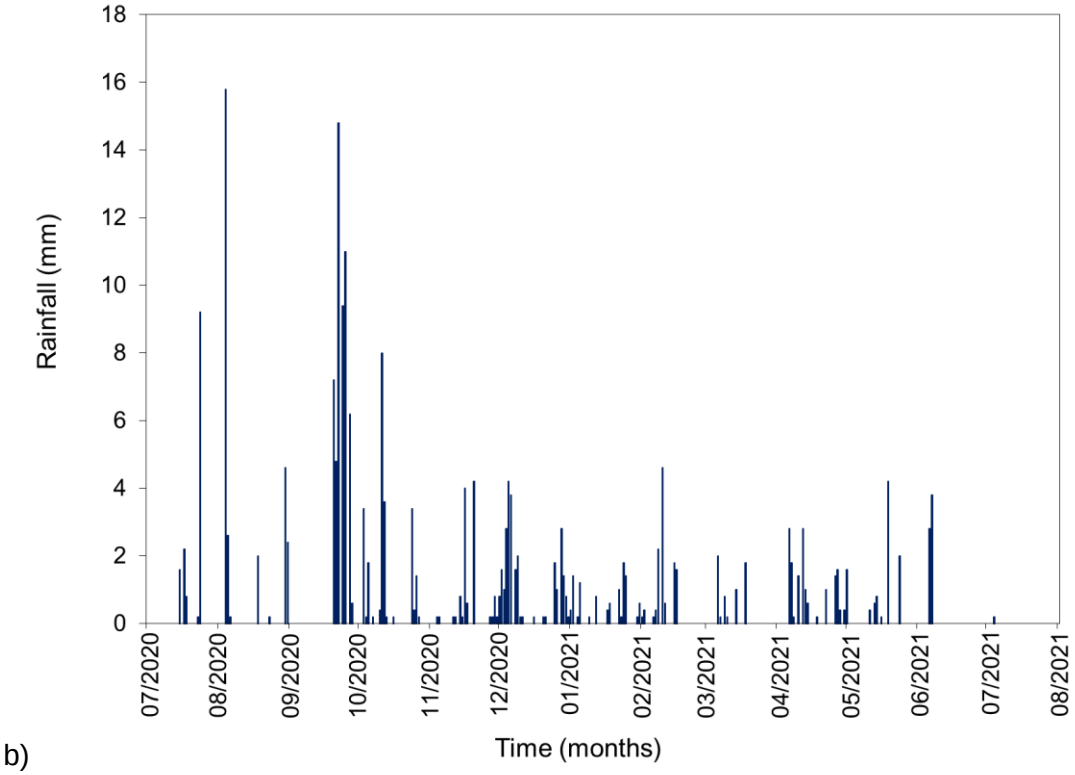

b)

Figure 38. 1 year raw data of the a) VWC of the CRM binder layer b) accumulated rainfall for 30 minutes

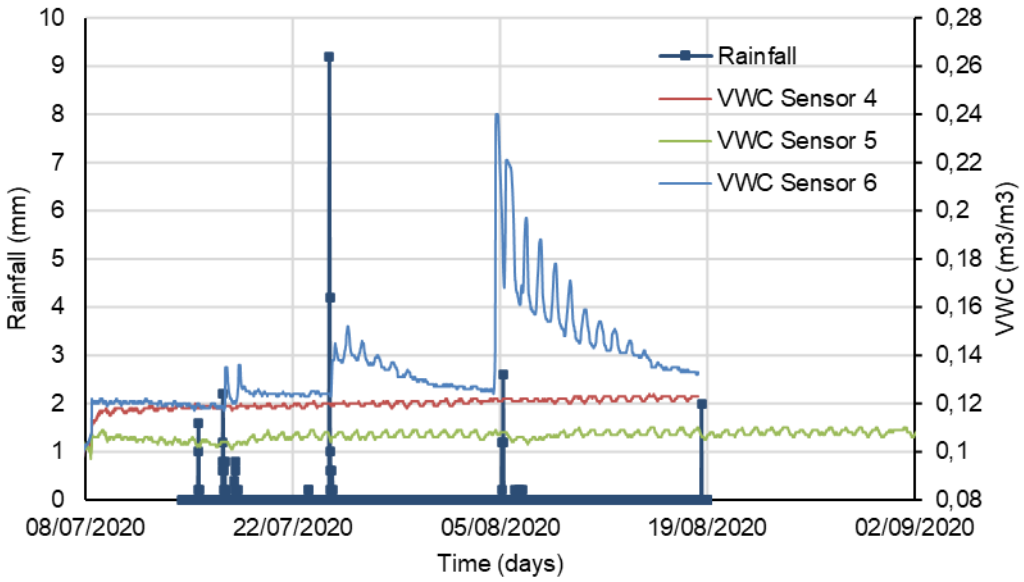

Figure 39. VWC and accumulated rainfall for 30 minutes in the first eight weeks

The gravimetric water content (GWC) of the CRM binder layer was calculated by using the calibration curves obtained in the laboratory (Annex C). To eliminate the daily fluctuations of VWC (due to the daily temperature excursion) the average daily values were calculated. Only sensors 1, 2 and 5 were considered (sensors 4 and 6 were excluded because they stopped working and the measurements of sensor 3 were excluded because it was strongly affected by the presence of peaks due to the water infiltration). Therefore, the average daily values of the VWC measured by the sensors were converted to the actual VWC of the CRM mixture using the calibration equation:

$$VWC_{CRM} = 0{,}0156 \exp[15{,}364 \cdot VWC_{sensors}]$$

Finally, the average GWC of the CRM binder layer was obtained as follows:

$$GWC_{CRM} = \frac{VWC_{CRM}}{\rho_b}$$

where ρ_b is the bulk density of the CRM binder layer. This final conversion was performed using the maximum (2122 kg/m^3) and the minimum (2081 kg/m^3) bulk densities measured on the cores extracted from Subsection 1 (Table 7). The resulting trends of the average GWC are shown in Figure 40.

During the measurement year, the average GWC gradually increased from about 4,0% to about 4,5%. Such long-scale variation of the water content probably reflects the gradual transition towards equilibrium conditions with the moisture of the soil surrounding the pavement. This hypothesis could be validated by the future joint measurements of temperature and GWC.

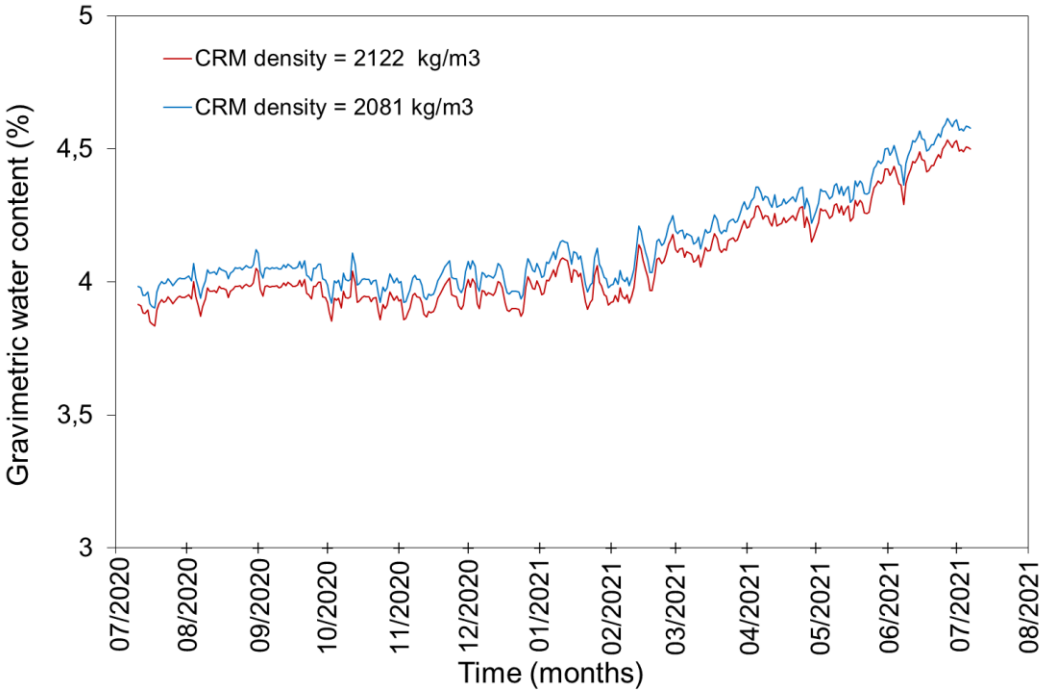

Figure 40. Average daily GWC

5.3 Field testing

5.3.1 Light Falling Weight Deflectometer

Figure 41 shows the values of the LFWD modulus measured during pavement construction on the subgrade (64 MPa), the CTRM base course right after construction (79 MPa) and the CRM binder course, right after construction (137 MPa) and after 18 hours of curing, right before the tack coat application (218 MPa). The increase in stiffness of the CRM layer is an effect of both curing and temperature. In fact, during the first measurement (7th July 16:00 – 16:30) the average layer temperature as measured by the TEROS 12 sensors was 33,8 °C, whereas during the second measurement (8th July 7:30 – 8:00) the average layer temperature was 24,1 °C.

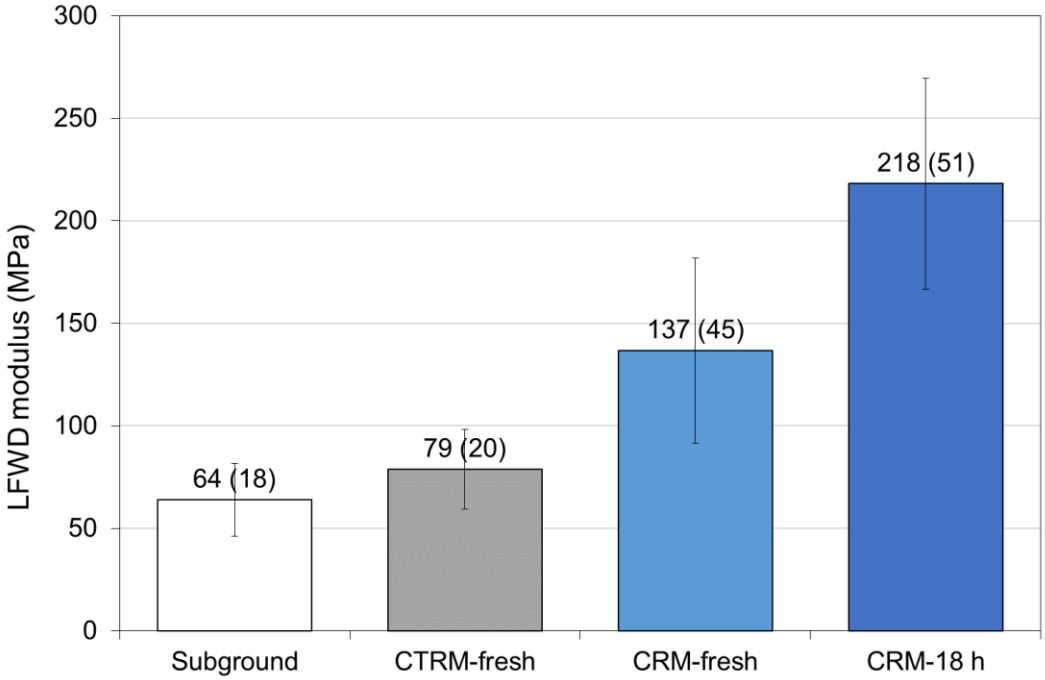

Figure 41. Average value (standard deviation) of the LFWD modulus measured during construction

5.3.2 Falling Weight Deflectometer

Figure 42 shows the temperature of the CRM binder layer (as measured by Sensor 5) during the FWD testing runs carried out on 29th July 2020, 5th May 2021, and 13th July 2021. The average air and pavement temperature values during each testing run are summarised in Table 11.

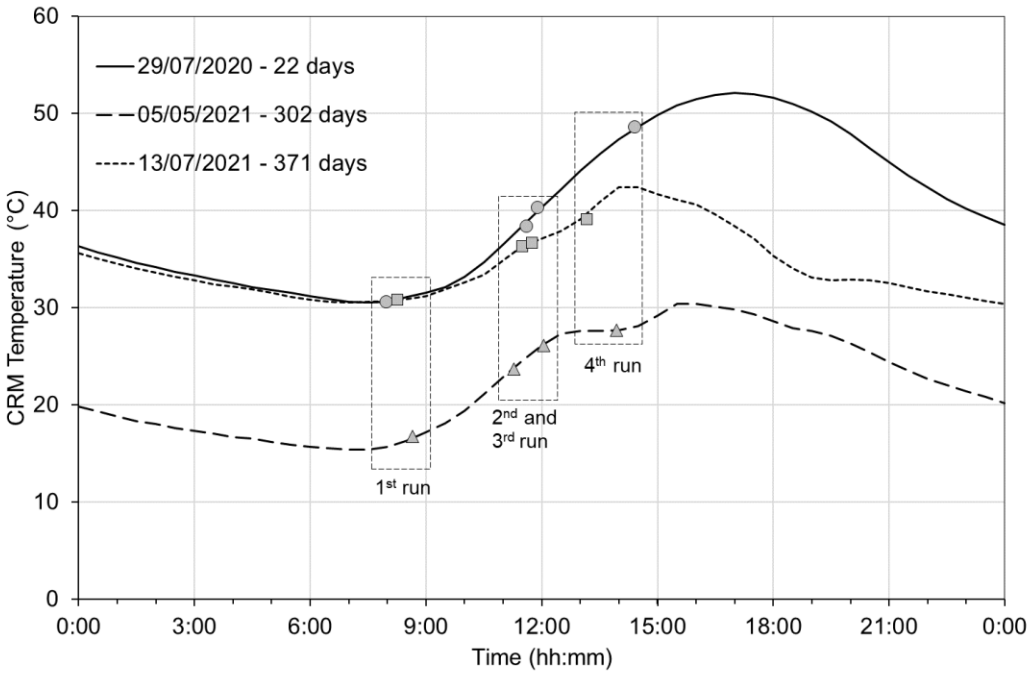

Figure 42. Temperature measurement obtained with Sensor 5 during the FWD measurement

Table 11. Times and temperatures of the FWD measurements

Date	Curing	Times of the measurement runs		Average temperature	
		START	END	Air	CRM layer
	(days)	(hh:mm)	(hh:mm)	(°C)	(°C)
28/07/2020	22	7:50	8:06	25,8	30,5
		11:31	11:42	33,9	38,6
		11:49	11:58	36,3	40,6
		14:18	14:30	35,9	49,0
05/05/2021	302	8:34	8:45	15,05	16,6
		11:12	11:22	19,3	23,2
		11:58	12:09	21,3	25,7
		13:51	14:01	19,9	27,0
13/07/2021	371	8:10	8:20	26,4	30,8
		11:25	11:35	31,6	36,1
		11:40	11:49	31,75	36,4
		13:05	13:15	33,2	38,7

One reason for performing multiple testing runs in each day was to obtain overlapping temperature ranges among the three FWD testing campaigns that were carried out in different seasons. As it can be observed, the temperature ranges during the measurements performed in July 2020 and July 2021 partially overlapped (between 20 and 39 °C). Therefore, those results can be compared without performing temperature corrections. Such a comparison allows evaluating the effect of the 1-year curing period on the pavement response.

Another reason for performing multiple FWD runs in each day was to evaluate the impact of temperature on the pavement response. In this regard, it can be observed that the stiffness measurements carried out in the laboratory (Figure 29), as well as the literature data (Figures 11 and 12 in Ferrotti et al. (2020)) suggest that the increase in stiffness of the CRM binder layer from 302 to 371 curing days can be considered very low. Therefore, the joint analysis of the FWD measurements performed in May 2021 and July 2021 will allow evaluating the impact of a wide temperature range (from 15 °C to 40 °C) on the pavement deflections.

Surface deflections

Figure 43 shows, as an example[2], the central deflections (D_0), the deflections measured at an offset of 1800 mm (D_{1800}) and the SCI values measured during the first FWD campaign (28/07/2020, 22 days after construction). The effect of temperature on D_0 and SCI is evident, especially when comparing the first (30,5 °C) and the last (49,0 °C) testing runs. Both values appear to be higher in Subsection 2 with respect to Subsection 1. A different pavement response between the two subsections was expected because in Subsection 1 a new cement-treated base was built, whereas in Subsection 2 the existing granular base was left in place.

On the other hand, the value of D_{1800} appears to be temperature-independent and shows a slightly decreasing trend when moving from Subsection 1 to Subsection 2. This confirms that D_{1800} is mainly related to the subgrade stiffness, which is probably slightly higher in Subsection 2.

[2] All the measured deflections, the calculated deflection indices and the back-calculated moduli are reported in the Annex D.

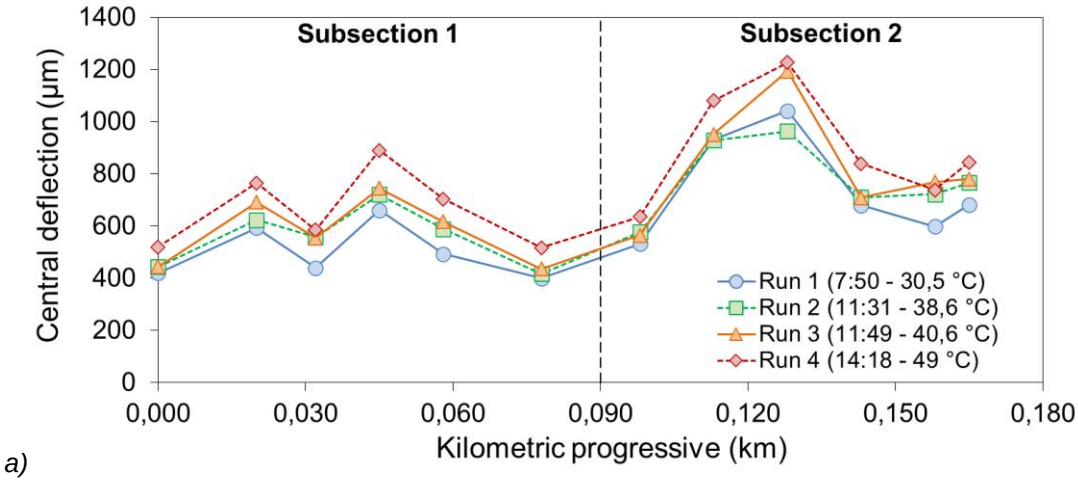

a)

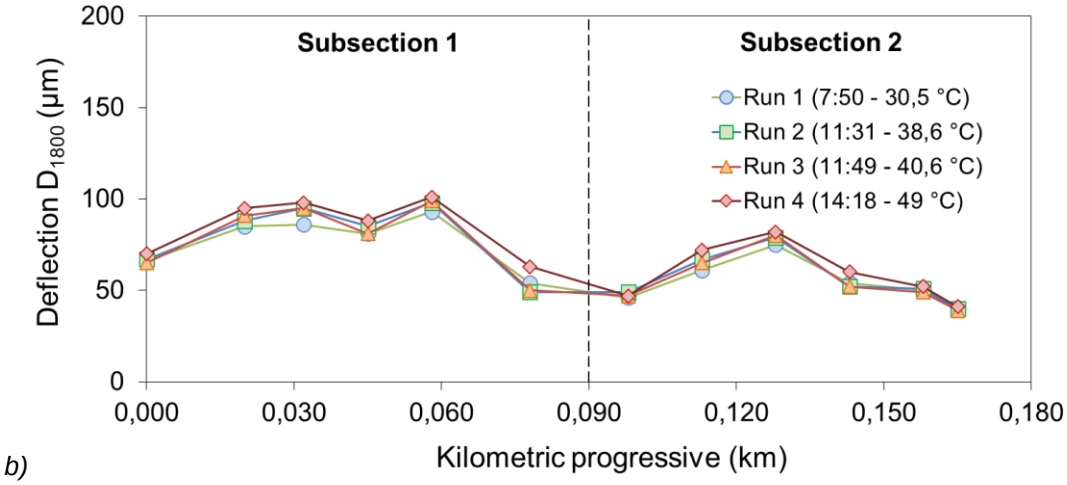

b)

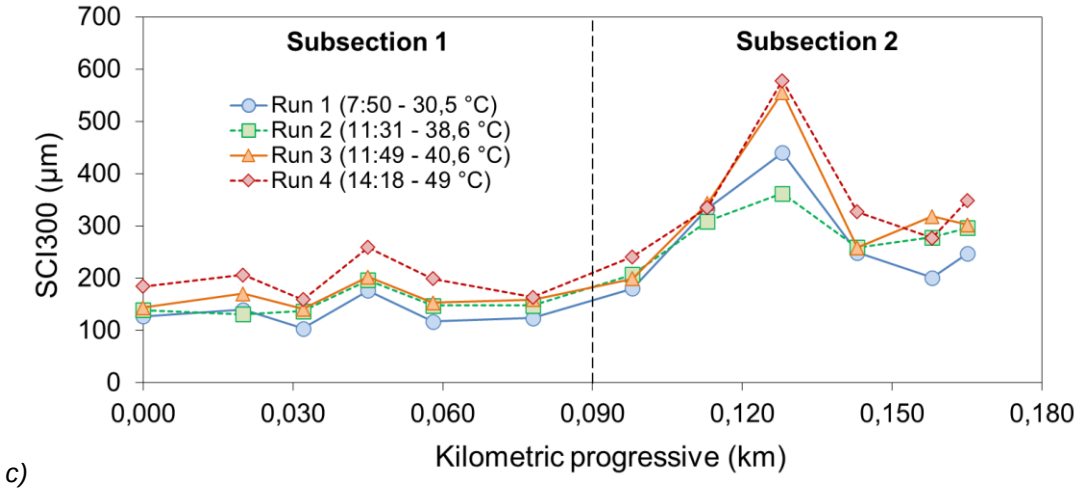

c)

Figure 43. FWD deflections after 22 days of curing (28/07/2020): a) Central deflection; b) deflections at an offset of 1800 mm; c) SCI.

The effect of temperature is better highlighted in Figure 43, which shows the average values of D_0 in Subsection 1 and Subsection 2, for the FWD testing run carried out after 302 and 371 curing days. As it can be observed, in both subsections there is a gradual increase of D_0 with the increase in temperature.

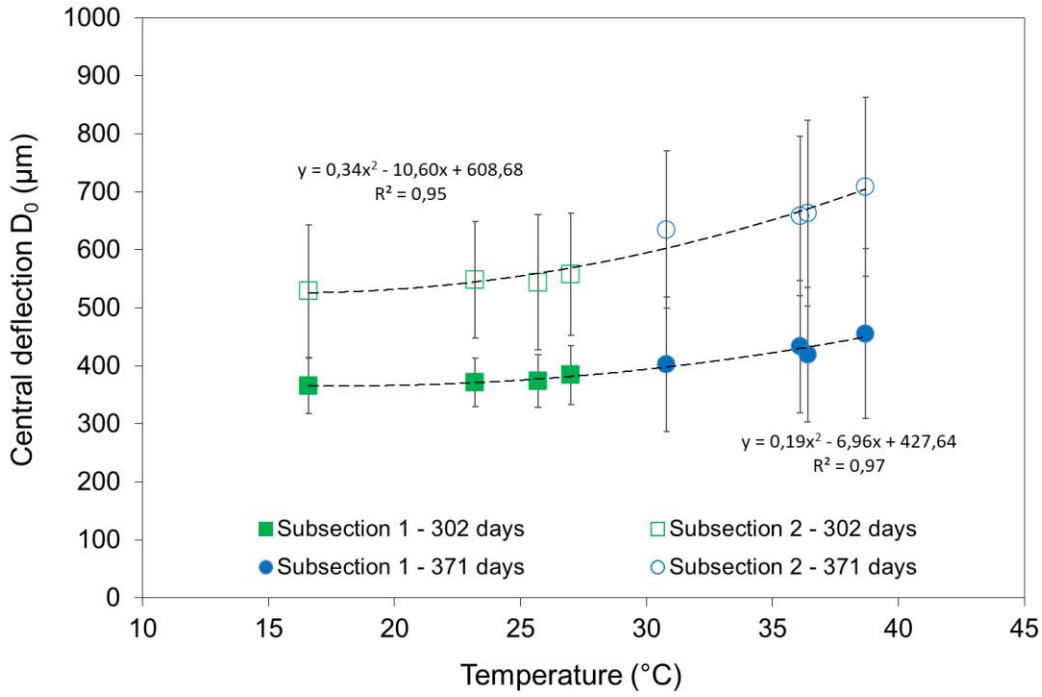

Figure 44. FWD central deflections after 302 and 371 days of curing (average values and standard deviations in Subsections 1 and 2).

The effect of curing is highlighted in Figure 45 that, considering D_0, D_{1800} and SCI, shows the ratio between the values measured in the second and third FWD testing campaigns (302 and 371 days of curing) with the corresponding values measured during the first campaign (22 days of curing). To minimize the effect of temperature, testing runs characterized by similar temperatures were selected: 30,5, 27,0 and 30,8 °C, for the first, second and third campaigns, respectively. As it can be observed, after 302 and 371 days of curing, the average reduction of D_0 was 23% and 25%, respectively, whereas the average reduction of SCI was 33% and 31%, respectively. On the other hand, the values of D_{1800}, remained practically constant. The reduction of D_0 and SCI can be related to an increase in stiffness of the CRM binder layer due to the curing process, and possibly also to the aging of the bituminous binder. The data also confirm that the effect of curing was practically the same after 302 and after 371 days of curing.

The combined effect of curing and testing temperature is also highlighted in Figure 46 that shows the average values of D_0 in Subsection 1 and Subsection 2, for the FWD testing runs carried out after 22 and 371 curing days. Comparing the deflections in the overlapping temperature range (30 °C – 39 °C), one year of curing led to an average D_0 reduction of 29% and 28%, for Subsection 1 and Subsection 2, respectively.

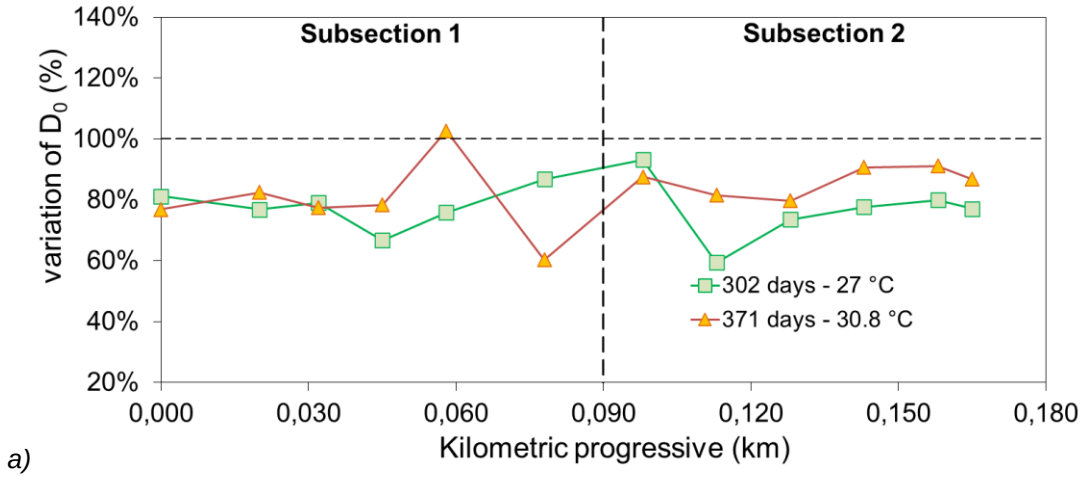

a)

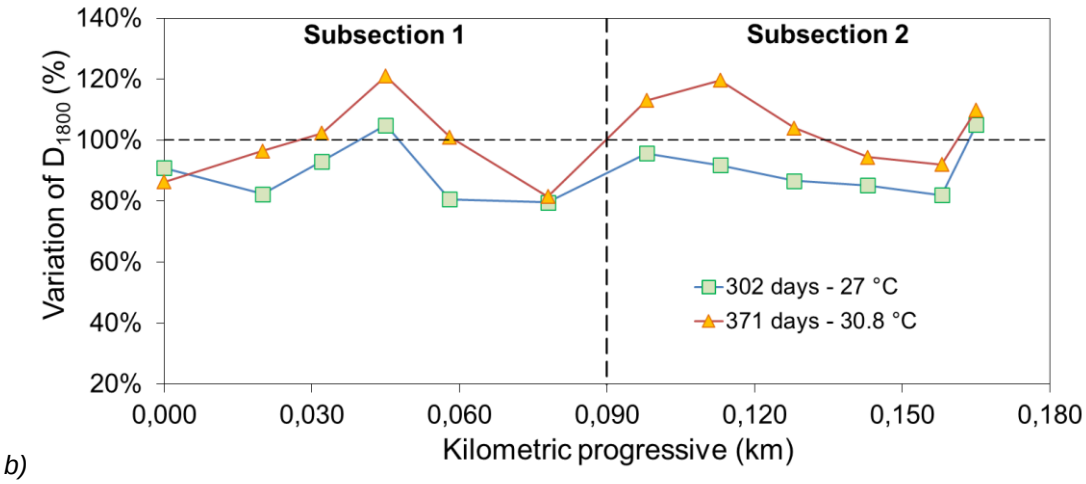

b)

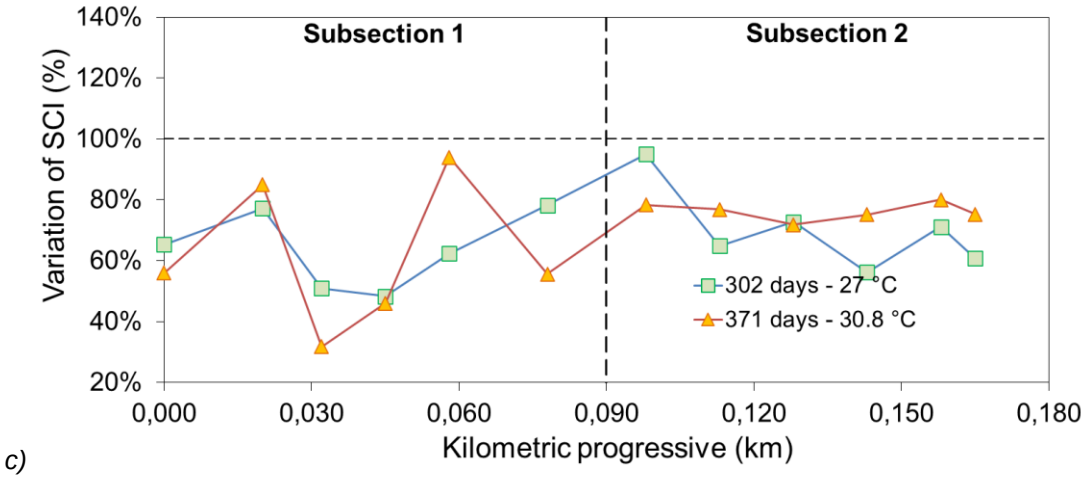

c)

Figure 45. Variation of the FWD deflections in second and third testing campaigns with respect to the first testing campaign: a) Central deflection; b) Deflection at an offset of 1800 mm; c) SCI.

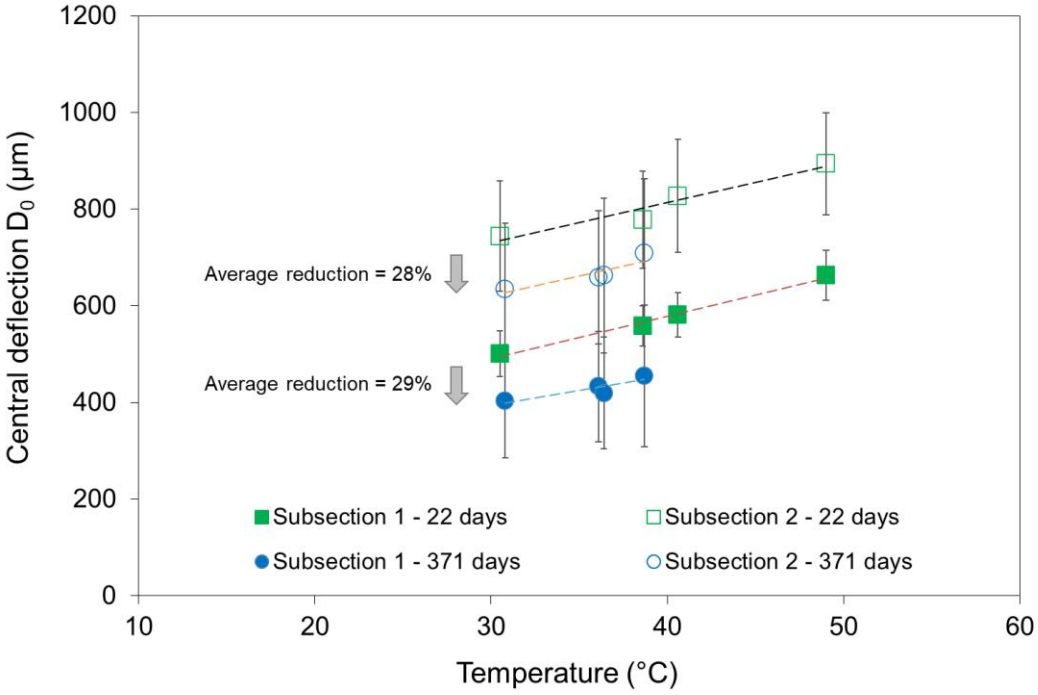

Figure 46. FWD central deflections after 22 and 371 days of curing (average values and standard deviations in Subsections 1 and 2).

Figure 47 shows the deflection basins measured during the first FWD campaign (28/07/2020, 22 days after construction). The basins from Subsection 1 are represented by continuous lines whereas the basins from Subsection 2 are represented by dashed lines. As it can be observed, the latter are characterized by a higher curvature especially between 0 and 600 mm, which highlights a lower stiffness of the upper pavement layers. The lower bearing capacity of the granular base, resulting in a reduced support during compaction, may have also affected the volumetric properties of the CRM binder layer leading to higher voids in Subsection 2, as highlighted in Table 7.

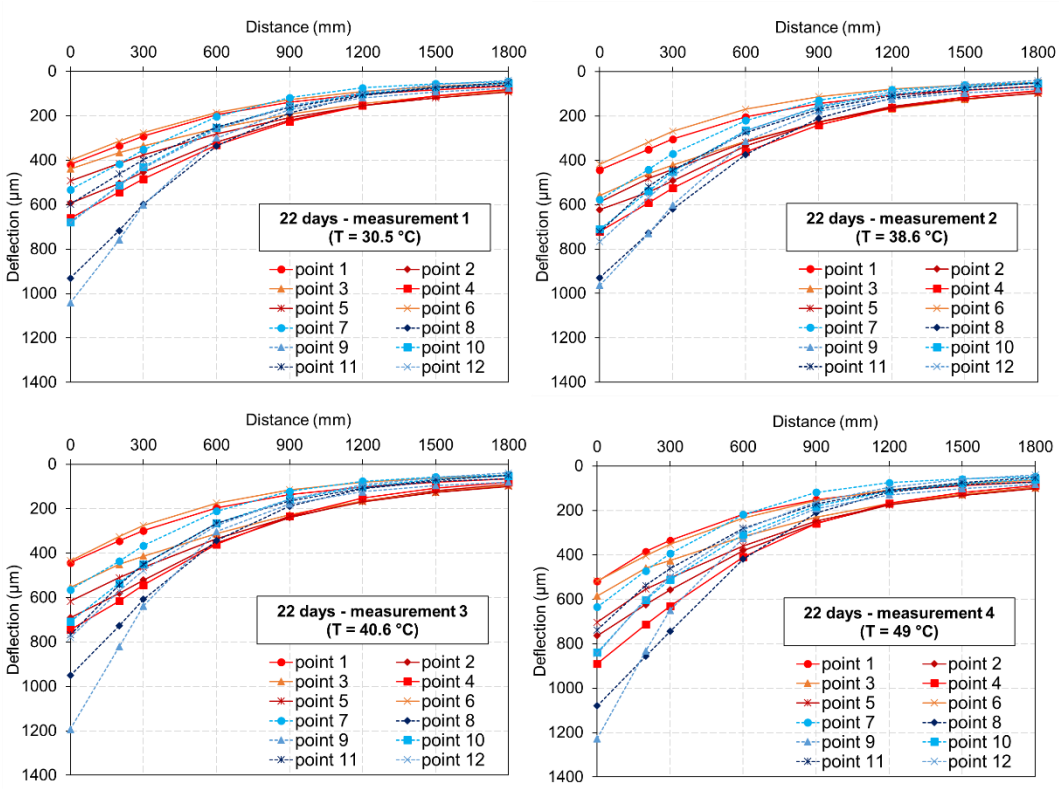

Figure 47. FWD deflection basins measured after 22 days of curing (28/07/2020)

Layer moduli

Table 12 summarises the back-calculated moduli of the three pavement layers:

- E1 = modulus of the AC wearing course + CRM binder layer (140 mm);
- E2 = modulus of the base layer (200 mm);
- E3 = modulus of the subgrade (half-space).

The average values and standard deviations were calculated separately for Subsection 1 and Subsection 2, and for each testing run.

Figure 47 and Figure 48 show the average values of the backcalculated moduli, E_1 and E_2 as a function of the temperature measured by the sensors. As expected, the temperature had a clear effect on E_1, and the values in Subsection 1 were always higher than the values in Subsection 2, especially at lower temperatures. This is probably due to the different air voids content of the two subsections. On the other hand, the temperature had only a minor effect on E_2. In particular, the average value in Subsection 1 (new cement-treated base) and Subsection 2 (old granular base), calculated on all measurement runs, was 2789 MPa and 1017 MPa, respectively.

Table 12. Back-calculated moduli: average value and standard deviation in each subsection

Run	Temp	E_1 (MPa)		E_2 (MPa)		E_{SUB} (MPa)	
		Average	St.dev.	Average	St.dev.	Average	St.dev.
23/07/2020 – Subsection 1							
1	30,5	3435	433	2450	557	124	54
2	38,6	2276	290	2562	569	110	70
3	40,6	2227	253	2434	602	105	65
4	49,0	1351	268	2458	540	86	54
23/07/2020 – Subsection 2							
1	30,5	2771	761	640	339	77	22
2	38,6	2052	273	694	327	72	22
3	40,6	1966	357	704	363	70	22
4	49,0	1304	243	737	324	67	21
05/05/2021 – Subsection 1							
1	16,6	6031	1133	3162	883	154	47
2	23,2	5897	342	2812	813	162	54
3	25,7	5084	469	3291	543	158	50
4	27,0	6000	1110	3020	707	138	39
05/05/2021 – Subsection 2							
1	16,6	3526	1473	1382	862	107	34
2	23,2	3286	1286	1447	813	95	36
3	25,7	3318	1067	1325	705	104	43
4	27,0	3247	1192	1293	574	97	40
13/07/2021 – Subsection 1							
1	30,8	3807	538	2680	673	206	126
2	36,1	3252	524	2381	382	191	138
3	36,4	3266	455	2888	729	160	69
4	38,7	2525	419	3333	1791	148	62
13/07/2021 – Subsection 2							
1	30,8	3079	638	916	481	82	24
2	36,1	2649	816	1008	646	83	32
3	36,4	2692	357	981	664	83	30
4	38,7	1909	250	1080	626	78	22

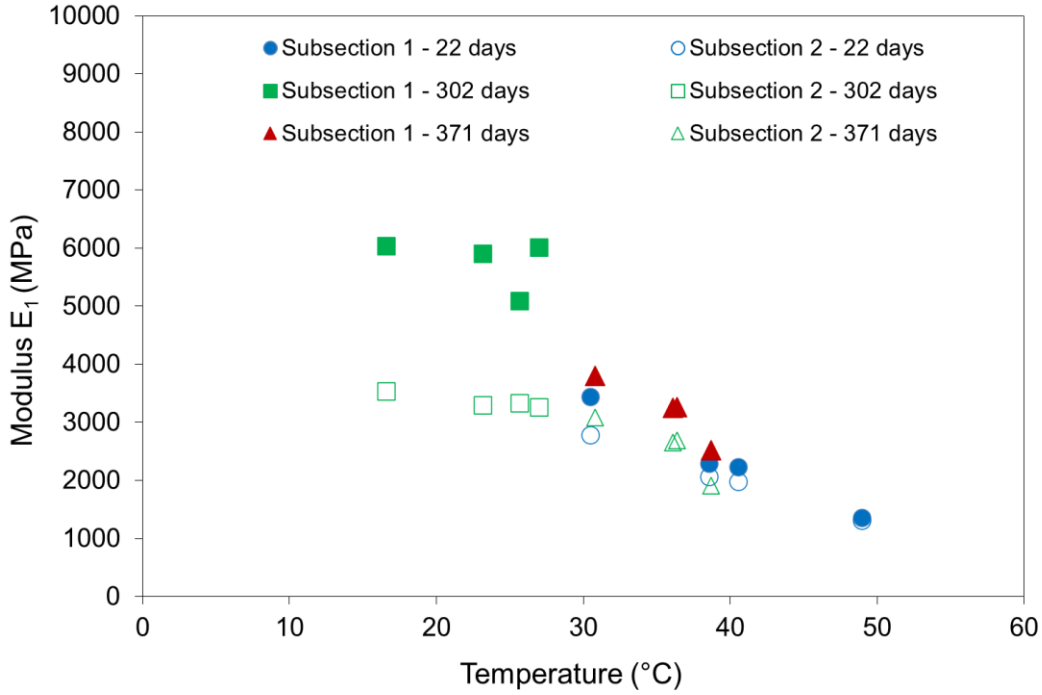

Figure 48. Back-calculated modulus of the bituminous layers (E_1) as a function of temperature

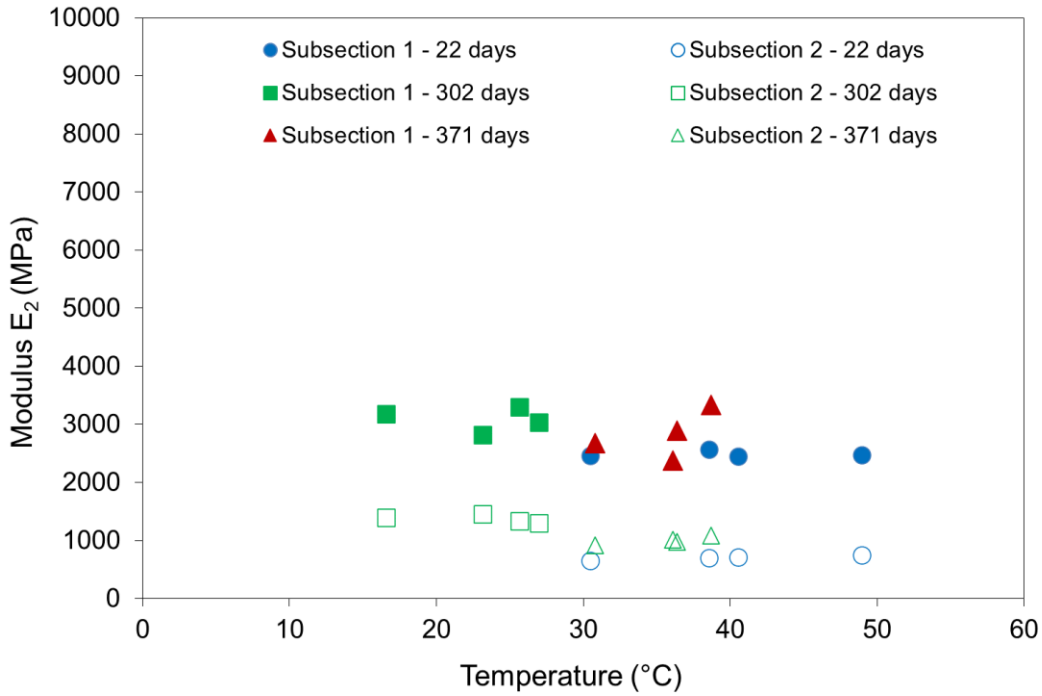

Figure 49. Back-calculated modulus of the base layer (E_2) as a function of temperature

Figure 50 compares:

- the FWD back-calculated modulus E_1 of the bituminous layers (40 mm of AC surfacing + 100 mm of CRM binder layer) measured in May and July 2021, in Subsections 1 and 2;
- the modulus of the CRM mixture measured in the laboratory using the cyclic

compression configuration (10 Hz isochronal data);

- the modulus of the AC mixture measured in the laboratory using the indirect tensile configuration (10 Hz isochronal data).

The experimental data suggests that the temperature sensitivity of E_1 sharply increased above 25 °C (measurements in July 2021) and was mainly due to the temperature sensitivity of the AC surfacing. On the other hand, during the measurements carried out in May 2021 (between 15 °C and 25 °C) the temperature had a limited effect (less than 10%) on the E_1 values.

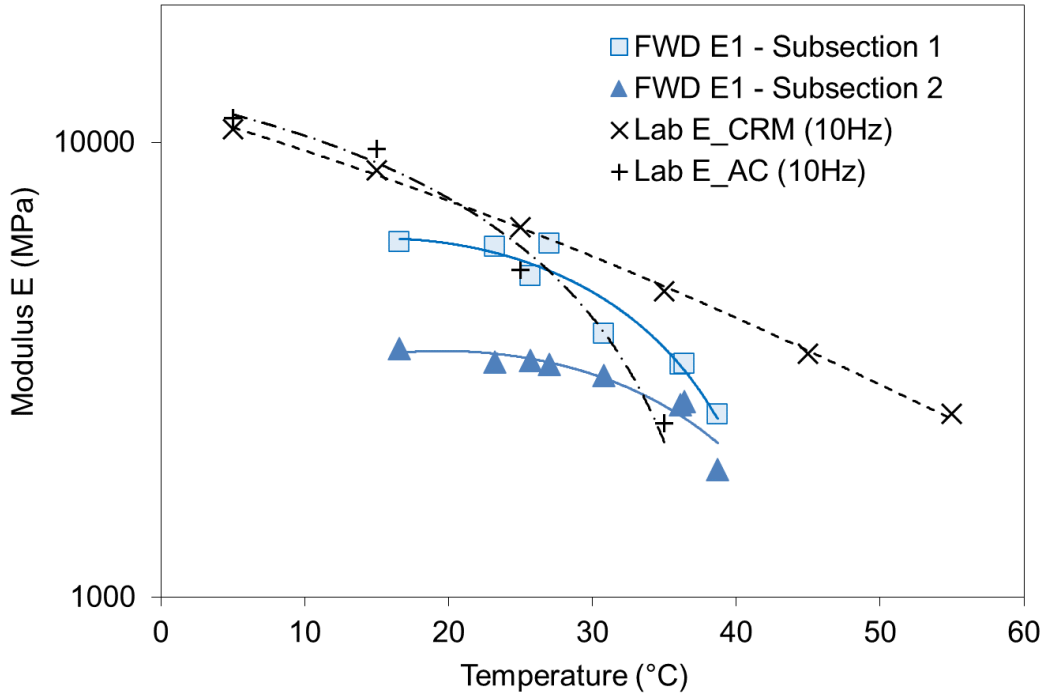

Figure 50. Comparison between back-calculated moduli and moduli obtained with laboratory specimens

Figure 51 compares the values of the back-calculated modulus E_1 of the bituminous layers (40 mm of AC surfacing + 100 mm of CRM binder layer) measured after 22 and 371 days of curing. An increase in stiffness, possibly due to the effect of curing on the CRM binder layer, is visible, but not as high as expected, especially compared to similar experiences (Godenzoni et al., 2018). Probably, the high temperatures that occurred during the first 22 days after construction (the average temperature during this period was 34,6 °C) led to a sort of “accelerated curing” and therefore the increase in stiffness in the following curing year was limited.

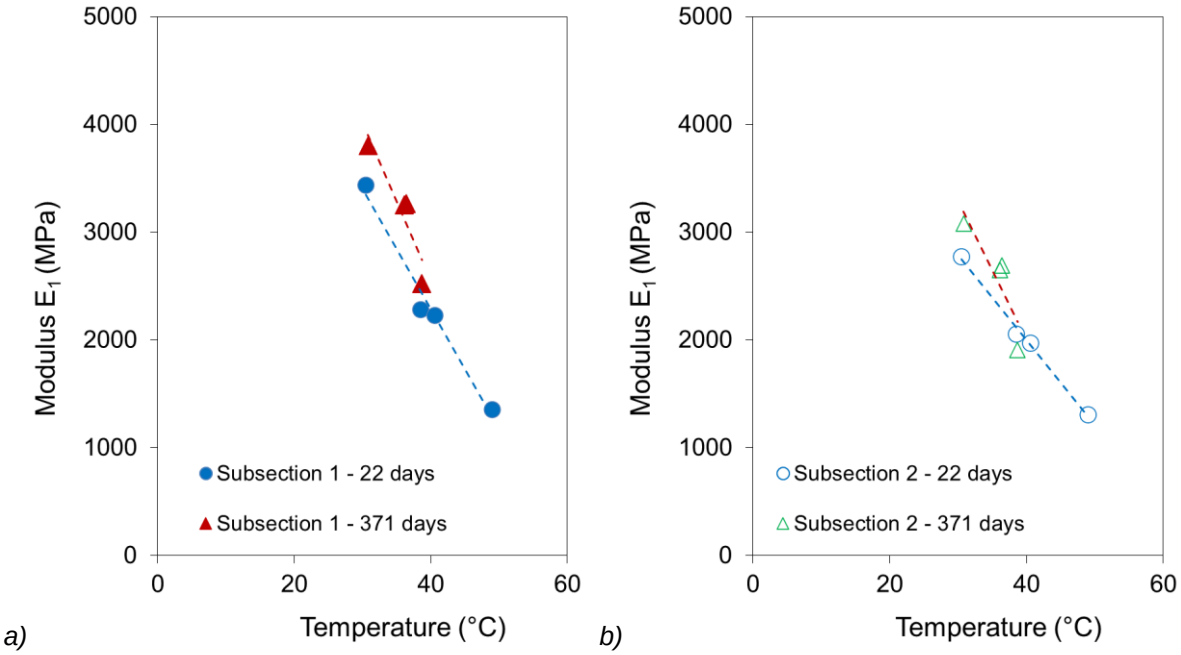

Figure 51. Effect of 1 year curing on the value of E_1: a) Subsection 1, b) Subsection 2

In summary, the FWD testing campaign allowed monitoring the evolution of the pavement response during the first curing year. The four testing repetitions performed during the same day, coupled to the readings of the temperature sensors, allowed observing how the hour-by-hour temperature fluctuations affected the surface deflections and the back-calculated moduli of the pavement layers. The magnitude of such an effect was clearly higher with respect to the curing effect during the first year. This suggests that, in those site-specific temperature and moisture conditions, the curing process was almost completed after three weeks

6 Summary and conclusions

A pavement section incorporating a CRM layer was built in the Republic of San Marino as part of the annual road maintenance of the State-owned enterprise for public works, AASLP. As part of the CRABforOERE project, temperature and moisture sensors were installed within the CRM binder layer to assist in the short-term monitoring of the pavement. In addition, laboratory and field tests were carried out to characterise the physical and mechanical properties of the CRM layer, and their evolution during the first year of service life.

The structural design of the pavement was carried out by AASLP. The resulting pavement thickness follows the trend linked to the traffic level found for other European pavements containing CRM layers investigated within the Work Package 2 and is comparable to those obtained using the national pavement design procedures analysed within the Work Package 5.

The mix design of the CRM mixture was also carried out by AASLP, following the local construction specifications. In terms of bitumen emulsion and cement dosages the composition of the CRM mixture was characterized by intermediate values among those found in the Work Package 2, with a residual bitumen-to-cement ratio B/C = 1,33.

The construction of the pavement section started on the 6th July 2020 with the milling of the existing pavement, continued the 7th of July with the construction of the CRM layer and was completed on the 8th of July when the AC wearing course was laid. The pavement was opened to traffic on the 9th July 2020, It is important to remark that, following the local construction specifications the CRM layer was sealed between two bituminous interlayers (a prime coat at the bottom and a tack coat on the top). Six moisture and temperature sensors were installed within the CRM layer during its construction. The sensors were connected to a datalogger installed close to the pavement margin. The logger transmits the measured data to a remote storage server from which they are available using a web-based service.

During construction of the pavement, the CRM mixture was sampled and compacted on site using a gyratory compactor. The compacted specimens were used to evaluate the ITS (for the mixture acceptance) and to monitor the evolution of water loss and stiffness.

During the first year of service life, besides the sensor's measurements, the structural properties of the pavement were monitored by performing three FWD test campaign 22 days, 302 days and 371 days after construction. During the first two campaigns, a total of twelve cores were extracted from the pavement. The back-calculation procedure allowed obtaining the combined stiffness modulus of the surface layer (AC surfacing + CRM binder layer).

The following conclusions can be drawn from the activities described within this report:

- After 3 days of curing at 40°C, the ITS at 25 °C of the CRM mixture was 0,60 MPa and its stiffness modulus was 4172 MPa, well above the specification limits of 0,40 MPa and 3000 MPa, respectively.
- The compaction energy specified by the construction specifications (100 gyrations) overestimated the actual compaction energy applied in the field. Consequently, the cores extracted from the pavement had higher voids and lower stiffness with respect to the laboratory-compacted specimens. However, considering the difference in voids level, the stiffness evolution due to curing was similar to those of the laboratory specimens cured at 25 °C.
- The stiffness of the AC wearing course and the CRM binder layer at 25 °C were comparable. The stiffness measured on the CRM gyratory specimens were higher, because of their lower air voids. The AC mixture also showed a higher temperature sensitivity with respect to the CRM mixture.
- The monthly average of the daily average temperature of the CRM layer ranged from 4,5 °C (January 2021) to 34,9 °C (August 2021). The monthly average of the daily

maximum temperature exceeded 50 °C in the summer months (from June to August), whereas the monthly average of the daily minimum temperature fell slightly below 0 °C only in January and February 2021. These were almost optimal conditions for the development of the material properties.

- The water content of the CRM layer remained almost constant (about 4%) until March 2021, and then slightly increased. This behaviour can be explained considering that the upper and lower surfaces of the layer were sealed using bituminous coats and that, in the long-term, the moisture of the pavement must reach an equilibrium with the surrounding soil. These curing conditions could be simulated in the laboratory by sealing the specimens using, for examples, plastic bags.
- The voids of the extracted cores, the FWD surface deflections and the back-calculated stiffness moduli showed that the overall quality of CRM layer was affected by the stiffness of the underlying base layer during construction. A better quality (lower void, higher stiffness) was obtained when the CRM layer was placed above a new cement-treated base.
- The effect of temperature on the stiffness of the surface layers was characterised by performing FWD tests at different times during the same measurement day. At high temperatures (above 25°C) the temperature-dependence of the modulus was evident and mainly due to the AC wearing course. At intermediate temperatures (15 – 25 °C) the temperature-related variation of the modulus was less than 10%. Thus, in similar conditions, a correction of the layer modulus to consider the temperature effect is not recommended.
- Comparing the FWD measurements (in the same temperature range) performed 22 days and 371 days after construction, the stiffness of the surface layer had a limited increase (less than 10 %). We may conclude that the curing process was almost completed after three weeks, thanks to the high temperatures registered in that period. In the long-term, we may expect a gradual increase of the stiffening effect due to the bitumen aging, however this interesting issue is outside of the scope of the present research that was focused on the short-term behaviour.
- The pavement section was opened to regular traffic less that two days after the construction of the CRM layer and, after one year, it doesn't show any distress.

References

Azienda Autonoma per i Lavori di Stato. (2020). *Capitolato Speciale d'Appalto per la Manutenzione Straordinaria per Opere Stradali*.

Bjurström, H., Kalman, B., Mollenhauer, K., Winter, M., Graziani, A., Mignini, C., Giancontieri, G., Lo Presti, D., & Gaudefroy, V. (2020). *Deliverable D2 – Compendium of CR performance in different climatic zones and critical review of the impact of mixture composition on performance*.

Cardone, F., Grilli, A., Bocci, M., & Graziani, A. (2015). Curing and temperature sensitivity of cement–bitumen treated materials. *International Journal of Pavement Engineering*, *16*(10), 868–880, https://doi.org/10,1080/10298436.2014.966710

Doyle, T. A., McNally, C., Gibney, A., & Tabaković, A. (2013). Developing maturity methods for the assessment of cold-mix bituminous materials. In *Construction and Building Materials* (Vol. 38, pp. 524–529). https://doi.org/10,1016/j.conbuildmat.2012.09.008

Ferrotti, G., Grilli, A., Mignini, C., & Graziani, A. (2020). *Comparing the Field and Laboratory Curing Behaviour of Cold Recycled Asphalt Mixtures for Binder Courses*. 12–14. https://doi.org/10,3390/ma13214697

Ferry, J. D. (1980). Viscoelastic properties of polymers. In *Viscoelastic properties of polymers*. https://doi.org/10,1149/1.2428174

Gergesova, M., Zupančič, B., Saprunov, I., & Emri, I. (2011). The closed form t-T-P shifting (CFS) algorithm. *Journal of Rheology*, *55*(1), 1–16. https://doi.org/10,1122/1.3503529

Godenzoni, C., Graziani, A., Bocci, M., Grilli, A., & Bocci, E. (2017). Instrumented test section for analyzing the curing process of cold-recycled mixtures. *Bearing Capacity of Roads, Railways and Airfields - Proceedings of the 10th International Conference on the Bearing Capacity of Roads, Railways and Airfields, BCRRA 2017*, 1275–1282. https://doi.org/10,1201/9781315100333-184

Godenzoni, Carlotta, Graziani, A., Bocci, E., & Bocci, M. (2018). The evolution of the mechanical behaviour of cold recycled mixtures stabilised with cement and bitumen: field and laboratory study. *Road Materials and Pavement Design*, *19*(4), 856–877. https://doi.org/10,1080/14680629.2017.1279073

Graziani, A., Godenzoni, C., Cardone, F., & Bocci, M. (2016). Effect of curing on the physical and mechanical properties of cold-recycled bituminous mixtures. *Materials and Design*, *95*, 358–369. https://doi.org/10,1016/j.matdes.2016.01.094

Graziani, A., Iafelice, C., Raschia, S., Perraton, D., & Carter, A. (2018). A procedure for characterizing the curing process of cold recycled bitumen emulsion mixtures. *Construction and Building Materials*, *173*, 754–762. https://doi.org/10,1016/j.conbuildmat.2018.04.091

Graziani, A., Mignini, C., Bocci, E., & Bocci, M. (2020). Complex Modulus Testing and Rheological Modeling of Cold-Recycled Mixtures. *Journal of Testing and Evaluation*, *48*(1), 20180905. https://doi.org/10,1520/JTE20180905

Kim, Y., Im, S., & Lee, H. D. (2011). Impacts of curing time and moisture content on engineering properties of cold in-place recycling mixtures using foamed or emulsified asphalt. *Journal of Materials in Civil Engineering*, *23*(5), 542–553. https://doi.org/10,1061/(ASCE)MT.1943-5533.0000209

Kim, Y. R. (2009). *Modeling of Asphalt Concrete* (M.-H. Education (ed.)).

Mangiafico, S., Di Benedetto, H., Sauzéat, C., Olard, F., Pouget, S., & Planque, L. (2016). Effect of colloidal structure of bituminous binder blends on linear viscoelastic behaviour

of mixtures containing Reclaimed Asphalt Pavement. *Materials and Design*, *111*, 126–139. https://doi.org/10,1016/j.matdes.2016.07.124

Meter Group. (2021). *Advanced soil moisture sensing*.

Mignini, C., Cardone, F., & Graziani, A. (2018). Experimental study of bitumen emulsion–cement mortars: mechanical behaviour and relation to mixtures. *Materials and Structures/Materiaux et Constructions*, *51*(6). https://doi.org/10,1617/s11527-018-1276-y

Miljković, M., & Radenberg, M. (2014). Fracture behaviour of bitumen emulsion mortar mixtures. *Construction and Building Materials*, *62*, 126–134. https://doi.org/10,1016/j.conbuildmat.2014.03.034

Mollenhauer, K., Winter, M., Graziani, A., Mignini, C., Bjurström, H., Kalman, B., Hornych, P., Gaudefroy, V., Lo Presti, D., & Giancontieri, G. (2020). *Deliverable D5 – International pavement designs with cold recycled material. Proposal of pavement design procedure including structure catalogue and identification of failure modes for MEPD*.

Olard, F., & Di Benedetto, H. (2003). General “2S2P1D” Model and Relation Between the Linear Viscoelastic Behaviours of Bituminous Binders and Mixes. *Road Materials and Pavement Design*, *4*(2), 185–224. https://doi.org/10,1080/14680629.2003.9689946

Pouliot, N., Marchand, J., & Pigeon, M. (2003). Hydration mechanisms, microstructure, and mechanical properties of mortars prepared with mixed binder cement slurry-asphalt emulsion. *Journal of Materials in Civil Engineering*, *15*(1), 54–59. https://doi.org/10,1061/(ASCE)0899-1561(2003)15:1(54)

Raschia, S., Perraton, D., Di Benedetto, H., Lamothe, S., Graziani, A., & Carter, A. (2021). Visco-Elasto-Plastic Characterization In The Small Strain Domain Of Cement-Bitumen Treated Materials Produced At Low Temperatures. *Journal of Materials in Civil Engineering*, *33*(4), 04021039. https://doi.org/10,1061/(ASCE)MT.1943-5533.0003653.

Woods, A., Kim, Y., & Lee, H. (2012). Determining Timing of Overlay on Cold In-Place Recycling Layer: Development of New Tool Based on Moisture Loss Index and in Situ Stiffness. *Transportation Research Record*, *2306*(1), 52–61.

Annex A: Construction Specifications

This Annex reports the material requirements extracted from the AASLP construction specifications.

- **Asphalt concrete for wearing course (AC)**
  - Table A1. Coarse aggregate characteristics (D ≤ 45 mm; d ≥ 2 mm)
  - Table A2. SBS-modified bitumen characteristics
  - Table A3. Grading envelope and bitumen content range of the asphalt concrete for wearing course
  - Table A4. Volumetric and mechanical requirements of the asphalt concrete for wearing course
- **Cold recycled mixture for binder course (CRM)**
  - Table A5. Modified bitumen emulsion for cold in plant recycling
  - Table A6. Grading envelope of the cold recycled blend for binder course (CRM)
  - Table A7. Composition and mechanical requirements of the asphalt concrete for wearing course
- **Cement treated recycled materials for base course (CTRM)**
  - Table A8. Grading envelope of the cement treated materials for base course
  - Table A9. Volumetric and mechanical requirements of the asphalt concrete for base course

Asphalt concrete for wearing course (AC)

Table A1. Coarse aggregate characteristics (D ≤ 45 mm; d ≥ 2 mm)

Parameter	Standard	Unit	Requirement	Class EN 13043
Resistance to fragmentation	EN 1097-2	[%]	≤ 20	LA_{20}
Percentage of crushed and broken surfaces	EN 933-5	[%]	100	$C_{100/0}$
Passing at 0,063 mm	EN 933-1	[%]	≤ 2	f_2
Resistance to freezing and thawing	EN 1367-1	[%]	≤ 1	F_1
Flakiness index	EN 933-3	[%]	≤ 15	FI_{15}
Shape index	EN 933-4	[%]	≤ 15	SI_{15}
Polished stone value	EN 1097-8	[-]	≥ 50	PSV_{50}
Water absorption	EN 1097-6	[%]	≤ 2	$WA_{24}2$

Table A2. SBS-modified bitumen characteristics

Bitumen designation EN 14023			**PmB 45/80-70**	
Parameter	**Standard**	**Unit**	**Requirement**	**Class**
Needle penetration at 25°C	EN 1426	[× 0,1 mm]	45 - 80	4
Softening point	EN 1427	[°C]	≥ 70	4
Fraass breaking point	EN 12593	[°C]	≤ - 12	6
Dynamic viscosity at 180°C	EN 13302	[mPa · s]	50 - 200	-
Elastic recovery at 25° C	EN 13398	[%]	≥ 80	2
Storage stability (Δ pen)	EN 133399	[× 0,1 mm]	9	2
Storage stability (Δ R&B)	EN 133399	[°C]	5	2
Resistance to hardening RTFOT	EN 12607-1			
Change in mass	EN 12607-1	[%]	≤ 0,5	3
Retained penetration at 25°C	EN 1426	[%]	≥ 60	7
Change in ring and ball softening point	EN 1427	[°C]	≤ 8	2

Table A3. *Grading envelope and bitumen content range of the asphalt concrete for wearing course*

Asphalt concrete designation	**AC12**
Sieve size [mm]	**Passing material [%]**
20	100
12,5	90 - 100
8	72 - 84
4	44 - 55
2	26 - 36
0,5	14 - 20
0,25	10 - 15
0,063	6.0 – 10,0
Bitumen content	
Bitumen content by mix weight [%]	4.7 – 5.8
Bitumen content by aggregate weight [%]	4.9 – 6.2
Bitumen content values have to be corrected by the factor: $a = 2.650/\rho_a$. Where ρ_a is the particle density [in Mg/m^3] following the procedure EN 1097-6.	

Table A4. Volumetric and mechanical requirements of the asphalt concrete for wearing course

Compaction method			
Parameter	**Unit**	**Standard**	**Requirement**
External angle	[°]	SHRP Designation M-002	1.25 ± 0,02
Speed of rotation	[revolution/min]	EN 12697-31	30
Consolidation pressure	[kPa]	EN 12697-31	600
Mould diameter	[mm]	EN 12697-31	100
Compaction temperature	[°C]	EN 12697-35	Operative temperature ± 10
Volumetric and mechanical properties			
Parameter	**Unit**	**Standard**	**Requirement**
V_m at 10 revolutions (N_1)	[%]	EN 12697-8	11 - 15
V_m at 100 revolutions (N_2)	[%]	EN 12697-8	3 - 6
VMA at 100 revolutions (N_2)	[%]	EN 12697-8	> 12
VFB at 100 revolutions (N_2)	[%]	EN 12697-8	65 - 80
V_m at 180 revolutions (N_3)	[%]	EN 12697-8	> 2
Indirect tensile strength 25°C at N_2 (*ITS*)	[N/mm^2]	EN 12697-23	0,95 – 1.80
Water sensitivity (*ITSR*)	[%]	EN 12697-12	≥ 90

Cold recycled mixture for binder course (CRM)

Table A5. Modified bitumen emulsion for cold in plant recycling

Modified bitumen emulsion				
Parameter	**Standard**	**Unit**	**Requirement**	**Class EN 13808**
Polarity	EN 1430	-	Positive	2
Bitumen content	EN 1428	[%]	60 ± 2	
Settling tendency at 7 days	EN 12847	[%]	≤ 10	3
Breaking value	EN 13075-1	-	> 150	5 or higher
Mixing stability with cement	EN 12848	[g]	< 2	10
Residual bitumen				
Needle penetration at 25°C	EN1426	[0,1 × mm]	< 100	3
Softening point	EN1427	[°C]	> 55	2
Cohesion at 10°C	EN 13589 EN 13703	J/cm^2	≥ 2	6
Elastic recovery	EN 13398	[%]	> 50	3

Table A6. Grading envelope of the cold recycled blend for binder course (CRM)

Asphalt concrete class	**AC20**
Sieve size [mm]	**Passing material [%]**
31.5	100
20	90 - 100
10	50 - 80
4	30 - 55
2	20 - 40
0,5	10 - 25
0,063	3.0 – 8.0

Table A7. Composition and mechanical requirements of the asphalt concrete for wearing course

Compaction method			
Parameter	**Unit**	**Standard**	**Requirement**
External angle	[°]	SHRP Designation M-002	1.25 ± 0,02
Speed of rotation	[revolutions/min]	EN 12697-31	30
Consolidation pressure	[kPa]	EN 12697-31	600
Energy	[revolutions]	EN 12697-31	100
Mould diameter	[mm]	EN 12697-31	150
Mould type	-	-	closed
Wet sample	[g]	-	2800
Maximum size	[mm]	-	20
Optimum water content			
Cement content	[% by aggregate weight]	2	maximum dry density and leaking water < 0,5%
Water content	[% by aggregate weight]	3, 4, 5, 6	
Optimum binders content			
Water content	[% by aggregate weight]	optimum	ITS ≥ 0,40 MPa; ITSR ≥ 80 %; ITSM ≥ 3000 MPa
Cement content[1]	[% by aggregate weight]	1.5; 2.0 e 2.5	
Emulsion content[1]	[% by aggregate weight]	4.0; 4.5 e 5.0	

[1] only the combinations that allow a bitumen/cement ratio > 1

Cement treated materials for base course (CTRM)

Table A8. Grading envelope of the cement treated materials for base course

Sieve size [mm]	Passing material [%]
40	100
31.5	85 - 100
20	65 - 94
10	44 – 78
2	18 - 50
0,5	8 - 30
0,25	6 - 22
0,063	3.0 – 11.0
CBR index after 4-day soaking (EN 13286-47)	> 50
Vertical swelling after 4-day soaking (EN 13286-47)	0

Table A9. Volumetric and mechanical requirements of the asphalt concrete for base course

Compaction method			
Parameter	**Unit**	**Standard**	**Requirements**
Energy Proctor	[MJ/m^3]	EN 13286-2	2.7 (modified)
Mould diameter	[mm]	EN 13286-2	150
Layers	[n]	EN 13286-2	5
Thickness	[mm]	EN 13286-2	120 (optimum water and R_{it}) 180 CBR mould (R_c)
Blow per layer	[n]	EN 13286-2	56 (optimum water and R_{it}) 85 (R_c)
Optimum water content			
Cement content	[% by aggregate weight]	4	Dry maximum density $\rho_{d,max}$
Water content	[% by aggregate weight]	4, 5, 6 e 7	
Optimum cement content			
Water content	[% by aggregate weight]	optimum	$R_{it} \geq 0{,}25$ N/mm^2; R_c = 2.5 - 5.0 N/mm^2
Cement content	[% by aggregate weight]	3, 4, 5	

Annex B: Materials information documents

E.M.S. S.r.l.

Dichiarazione di prestazione Reg. UE 305/11 e Reg. Del. UE 574/14: N. 02/2

1. Codice identificativo unico del prodotto: **Sabbia fine**
2. Uso previsto: **produzione di calcestruzzo; produzione di malte; produzione di miscele bituminose.**
3. Il Fabbricante, ai sensi dell'Art. 11 par. 5: **E.M.S. Srl**, via Berlinguer, 14 – 48124 Ravenna (RA) Tel 0544/401060 e Fax0544/401655. Impianto di produzione: Ca' Bianca sito in Località Fosso ghiaia – 48125 Ravenna (RA).
4. Sistema di valutazione e verifica della costanza della prestazione dei prodotti tipo: **2+**
5. Norma armonizzata: **EN 12620:2002+a1:2008 - EN 13139:2003 - EN 13043:2004**
   Organismo notificato: **0476 KIWA CERMET ITALIA SPA**
6. Prestazioni dichiarate:

CE Produttore: **E.M.S. Srl** - via Berlinguer 14 48124 Ravenna (RA) Impianto: **Ca' Bianca** sito in Località Fosso ghiaia – 48125 Ravenna (RA).	Ddt n° 1681/B data 04/05/18	Dichiaraz. Prestaz. N. 02/2 Anno prima marcatura: 06 Organismo: 0476. Certificato N. 0476-CPD-43190		
Codice identificativo e nome del prodotto	02/2	Sabbia fine		
Origine: **Ca' Bianca - Località Fosso ghiaia (RA)**	Descrizione prodotto:	Aggregato "fine" di sabbia naturale alluvionale parzialmente frantumata silico-carbonatica		
Norma di riferimento:		EN 12620:2002+ a1:2008	EN 13043:2004	EN 13139:2003
Granulometria EN 933-1 - designazione, categoria, tolleranza:	d/D: 0/2	G_F 85 /--	G_F 85 / G_{TC} 20	--/--
Granulometria tipica		Ø (mm): NPD %: NPD		
Classificazione UNI 10006	Categoria	NPD		
Indice di plasticità UNI 10006	Categoria	NPD		
Indice di appiattimento EN 933-3	Categoria (FI_x)	--		
Indice di forma EN 933-4	Categoria (SI_x)	--		
Contenuto di fini 933-1	Categoria (f_x)	f3		Cat. 1
Equivalente in sabbia EN 933-8	Cat/Valore (SE)	≥80%		
Blu di metilene EN 933-9	Categoria (MB)	MB ≤ 1,2	MB_F ≤ 10	MB ≤ 2
Contenuto di conchiglie EN 933-7	Categoria (SC_x)	--		
Percentuale di superfici frantumate EN 933-5	Categoria (C_x)	--		
Spigolosità dell'aggregato fine EN 933-6	Categoria ($E_{cs}X$)	--	NPD	--
Resistenza alla frammentazione EN 1097-2	Categoria (LA_x)	--		
Resistenza all'urto EN 1097-2	Categoria (SZ_x)	--		
Resistenza all'usura dell'aggregato grosso EN 1097-1	Categoria (M_{DE})	--		
Resistenza alla levigabilità dell'aggr. grosso EN 1097-8	Categoria (PSV_x)	--		
Resistenza all'abrasione superficiale EN 1097-8	Categoria (AAV_x)	--		
Resistenza all'abras. da pneumatici chiodati EN 1097-9	Categoria (A_N)	--		
Massa volumica apparente EN1097-6	Valore (ra) Mg/m^3	NPD		
Massa volumica dei granuli pre-essicati EN1097-6	Valore (rrd) Mg/m^3	NPD		
Massa volumica dei granuli a SSA EN1097-6	Valore (rssd) Mg/m^3	2,64		
Massa volumica in mucchio EN1097-3	Valore (rb) Mg/m^3	1,56		
Assorbimento di acqua EN1097-6	Cat/Valore (WA_x)	1,0		
Resistenza al gelo/disgelo EN 1367-1	Categoria (F_x)	--		
Degradabilità al solfato di magnesio EN 1367-2	Categoria (MS_x)	--		
Resistenza allo shock termico EN 1367-5	Valore (V_{LA} o V_{SZ})	--		
Affinità degli aggr. grossi ai leganti bitum. EN 12697-11	Valore	--		
"Sonnenbrand" del basalto EN 1367-3	Categoria (SB_{SZ} o SB_{LA})	--		
Humus (presa ed indurimento) EN 1744-1 (15.1)	Passa/non passa	Assenti	--	Assenti
Contaminanti leggeri EN 1744-1 (14.2)	Categoria (m_{LPC})	≤0,5%	--	
Stabilità di volume (Disintegr. Silic. Dicalcico) EN 1744-1 (19.1)	Passa/non passa	NPD	--	
Reattività alcali-silice (Prova accelerata) EN 8520-22	Valore	< 0,10%	--	< 0,10%
Cloruri EN 1744-1 (7)	Valore	< 0,03%	--	< 0,03%
Solfati solubili in acido EN 1744-1 (12)	Categoria (AS_x)	0,2	--	0,2
Solfati solubili in acqua EN 1744-1 (10)	Categoria (SS_x)	--		
Zolfo totale EN 1744-1 (11)	Passa/non passa	< 1%	--	< 1%
Contenuto di carbonato dei fini EN 196-2	Valore	33 %	--	
Emissione di radioattività (solo per materiali per edifici)	\	Inferiore ai limiti di legge		
Rilascio di metalli pesanti	\			
Rilascio di idrocarburi policromatici	\			
Rilascio di altre sostanze pericolose	\			

Note: NPD: Nessuna Prestazione Determinata; --:Requisito non applicabile al tipo di materiale o alla norma

Le prestazioni del prodotto sopra identificato è conforme all'insieme delle prestazioni dichiarate. La presente dichiarazione di responsabilità viene emessa, in conformità al regolamento (UE) n 305/2011, sotto la sola responsabilità del fabbricante sopra identificato

Firmato a nome e per conto di **E.M.S. Srl**

Ravenna, li 24/05/2017 il Legale Rappresentante: **Enrico Riva:** .....

All 4-1 – rev12/01/2015

1 di 1

Valli Zabban
DAL 1928
TECNOLOGIE STRADALI

SCHEDA TECNICA

RIGEVAL LX

Sito produttivo	Stabilimento di Bologna Stabilimento di Perugia	Via del Traghetto, 42 – 40100 Bologna Via della Valtiera, 101 – 06135 Collestrada
Designazione	***C60BP10***	
Descrizione del prodotto	Emulsione di bitume distillato e lattice SBR per conglomerati bituminosi riciclati a freddo	

Caratteristiche dell'emulsione	Metodo	U.d.M.	Prestazione min	Prestazione max	Classe
Contenuto di legante	UNI EN 1428	%	**60**		6
Contenuto di acqua	UNI EN 1428	%		**40**	6
Grado di acidità pH	UNI EN 12850		**2,0**	**4,0**	
Stabilità alla miscelazione con il cemento	UNI EN 12848	%		**2**	10
Sedimentazione a 7 giorni	UNI EN 12847	%		**10**	3
Viscosità a 40°C (tempo di efflusso tazza 2 mm)	UNI EN 12846	sec	**15**	**70**	3
Caratteristiche del legante recuperato tramite evaporazione (UNI EN 13074)					
Consistenza alla temperatura intermedia di esercizio Penetrazione a 25°C	UNI EN 1426	dmm	**50**	**70**	3
Consistenza alle temperature elevate di esercizio Punto di rammollimento P.A.	UNI EN 1427	°C	**55**		2
Fragilità alle basse temperature Punto di rottura Fraass	UNI EN 12593	°C	**-10**		5
Recupero di deformazione Ritorno elastico a 25°C	UNI EN 13398	%	**55**		5

Condizioni operative

- Il prodotto deve essere messo in opera a temperature comprese tra 40 e 60°C.
- Lo stoccaggio deve avvenire a temperature comprese tra 10 e 70°C. Attenzione: teme il gelo..
- Evitare riscaldamenti diretti con fluidi caldi aventi temperature superiori a 100°C.
- In caso di stoccaggio prolungato senza movimentazione, si raccomanda di miscelare il prodotto per rimuovere l'eventuale sedimento. Non agitare l'emulsione con agitatori a pale.
- Una volta all'anno è consigliabile la pulizia del serbatoio di stoccaggio

Le caratteristiche dichiarate nella presente scheda sono garantite e sono rilevabili, su campioni omogenei di prodotto prelevati in contraddittorio alla consegna secondo le vigenti norme, in particolare la UNI EN 58 e la UNI EN 12594.

Rev.1 – 09/20

Buzzi Unicem

Cementeria di Monselice s.p.a.

DICHIARAZIONE DI PRESTAZIONE
No. 0970-DoP-0195/CE/0202
Ai sensi del REGOLAMENTO DELEGATO (UE) n°574/2014 del 21 febbraio 2014

1. Codice di identificazione unico del prodotto-tipo:
   Cemento portland al calcare EN 197-1 – CEM II/A-LL 32,5 R
2. Usi previsti:
   Preparazione di calcestruzzo, malta, malta per iniezione o altre miscele per costruzione e fabbricazione di prodotti da costruzione, ect.
3. Fabbricante:
   CEMENTERIA DI MONSELICE S.p.A. – Riviera A. Mussato. 97 – 35139 Padova – ITALIA
4. Mandatario:
   Non applicabile
5. Sistema di VVCP: (Valutazione e Verifica della Costanza della Prestazione)
   Sistema 1+
6. a Norma armonizzata:
   UNI EN 197-1:2011

   Organismi notificati:
   ITC CNR, notificato con il n° 0970, ha effettuato la determinazione di prodotto-tipo sulla base delle prove (compreso il campionamento), l'ispezione iniziale dello stabilimento e del controllo di produzione della fabbrica, la sorveglianza, la valutazione e la verifica continue del controllo di produzione di fabbrica, e le prove di verifica di tipo dei campioni prelevati prima della immissione sul mercato del prodotto sotto il sistema 1+ e ha rilasciato il relativo certificato.
7. Prestazioni dichiarate

Caratteristiche essenziali	Prestazione
Costituenti e composizione del cemento comune	CEM II/A-LL
Resistenza a compressione (normalizzata e iniziale)	32,5 R
Tempo di presa	*Passa*
Stabilità - Espansione - Contenuto di $3O_3$	 *Passa* *Passa*
Contenuto di cloruro	*Passa*

8. Documentazione tecnica appropriata e/o documentazione tecnica specifica:
   Non applicabile

La prestazione del prodotto sopra identificato è conforme all'insieme delle prestazioni dichiarate. La presente dichiarazione di prestazione viene emessa, in conformità al Regolamento (UE) n. 305/2011, sotto la sola responsabilità del fabbricante sopra identificato.

Firmato a nome e per conto del fabbricante da:

Salvatore Lisi – Consigliere con poteri

Monselice, li 27 novembre 2017

Revisione 3

Annex C: Calibration of the moisture sensors

Introduction

The THEROS 12 sensors come with calibration equations to convert the raw electrical measurement into the VWC. These calibrations are valid for mineral soil types but are not validated for CRM mixtures that contain a certain volume of bitumen. Therefore, part of this project was devoted to determining “ad-hoc” calibration curves in the laboratory using Proctor-like specimens of CRM mortar.

The TEROS 12 sensor uses three stainless steel needles (Figure 13) for measuring the VWC and the temperature. The sensor was designed to be installed simply by pushing the needles inside the uncompacted soil. Unfortunately, this procedure is not applicable with compacted CRM mixtures that offer a very high resistance to the penetration of the needles due their high density and to the presence of coarse aggregates. To solve this problem, parallelepiped-shaped wood tablets with 3 nails placed in the needles position were used in the field installation (Section 3.2). This procedure was not applicable in the laboratory where Proctor-like specimens were used. In the laboratory the plan was to drill three holes in the compacted CRM mixture specimens for installing the sensors. However, this procedure was unsuccessful because the coarse aggregates did not allow the preparation of clean and straight holes. Therefore, CRM mortars specimens were used instead of CRM mixture specimens.

The following section provide the details on the compositions of the CRM mortars, the specimens’ preparation, the installation of the sensors, the measurement of the VWC and the development of the calibration curves.

Materials

The calibration was carried out on CRM mortars obtained by mixing fine RA aggregate (passing to the 2 mm sieve), natural sand, filler, and water. Bitumen emulsion and cement where not used to avoid an evolutive behaviour of the mortar and obtain specimen with a constant water content. The volumetric composition of the mortar was designed so that it had the save volume of bitumen as the CRM mixture used in the field (11%) (Figure C1).

RA aggregate, collected at the same plant of production of the CRM mixture, was sieved in the laboratory using the 2 mm sieve. The mortar aggregate blend consisted of 56% RA 0/2, 39% natural sand and 5% filler (by dry aggregate mass).

The mortars were prepared using three water dosages by aggregate mass: 3%, 5% and 7% and considering two compaction energy values, Standard Proctor and Modified Proctor. A total of 6 specimens were produced.

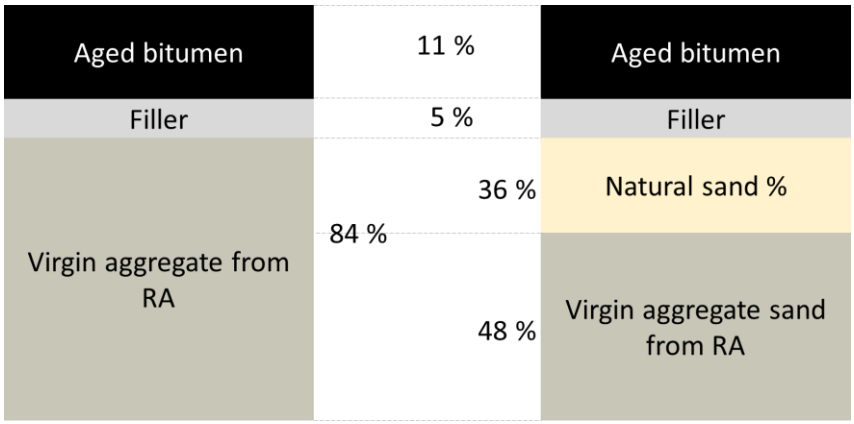

Figure C1. Volumetric composition of the CRM mixture used in test section (left) and of the mortar used for the calibration of the sensors (right)

Preparation of the specimens

The six specimens were produced using the following procedure:

1. Mixing of the aggregate blend and the pre-fixed amount of water (Figure C2a);
2. Sealing in a plastic bag of the wet aggregate blend for at least 12 hours;
3. Proctor compaction inside customised PVC moulds with diameter of 100 mm and height of 120 mm (Figure C2b-c);
4. Creation of the holes for the needles of the sensor by means of a drill (Figure C2d and e);
5. Installation of the sensors (Figure C2f);
6. Sealing of the specimens inside plastic bags to avoid water evaporation (Figure C2f);
7. Measurement of the VWC content and temperature on sealed specimens (Figure C3).

As shown in Figure C3, each sensor was installed in a different specimen for one day. After the 24 hours, sensors were removed and reinstalled in a specimen with a different water content. In this way, each sensor measured all the pre-fixed water dosages at least once. During the measurement the specimens were placed in the laboratory at ambient temperature. At the end of the measurement the specimens were broken, and their actual water content was measured.

Figure C2. Preparation of the mortar specimens: a) mixing, b) Proctor compaction, c) specimen compacted, d) creation of the needles allocations, e) specimen ready for the installation of the sensor, f) installation of the sensor

Figure C3. Measurement of the VWC and temperature of the laboratory mortar specimens

Results

Figure C4 shows an example of the measurements recorded by sensor 1 during the calibration activities. The air temperature and the mortar temperature were very similar. The highest difference was observed in the first hours after the placing of the sensor and may be due to an increase in the mortar temperature due to the drilling operation. The fluctuations in the measured temperature are due to the temperature variation between day and night. The mortar temperature ranged between 23 °C and 26 °C, while the air temperature ranged between 22.8 °C and 26.1 °C (Figure C4a). The measured VWC (Figure C4b) was constant in each day and changed when the sensor was removed and reinstalled in a specimen with a different water content. The sensors required a short interval before the stabilisation of the reading. After that, they were able to measure the differences in the water contents of the specimens.

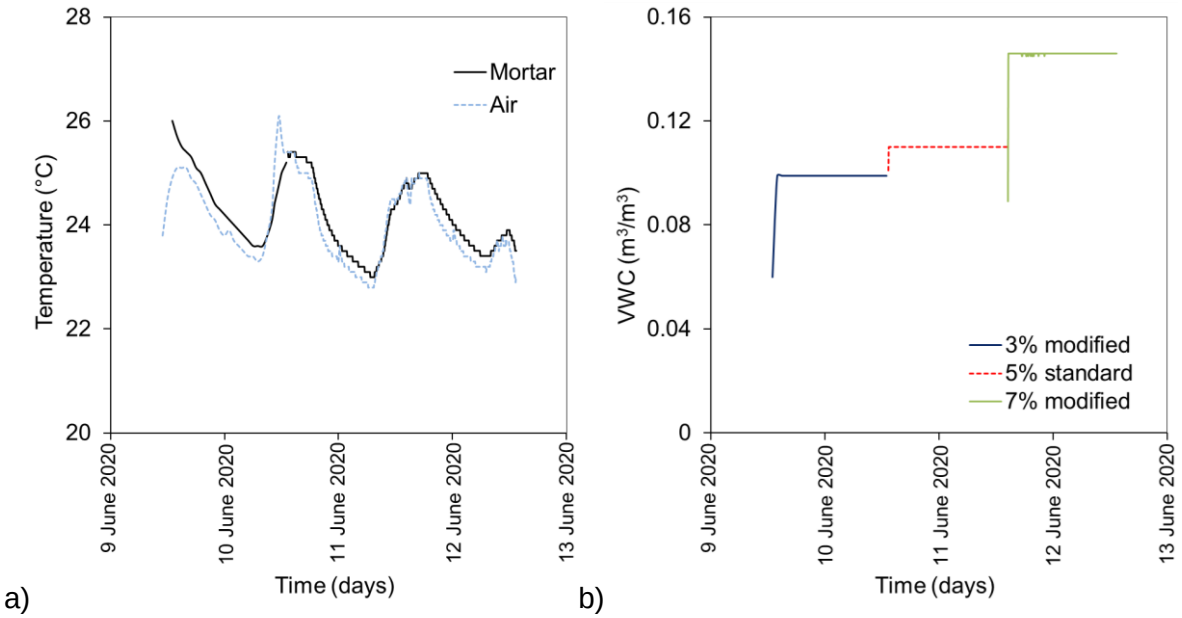

Figure C4. Temperature and VWC measured by sensor 1

Calibration curves

Figure C5 reports the calibration curves needed to convert the VWC reading of the sensors, based on the default calibration curve, into the VWC and GWC of CRM.

Figure C5a relates the VWC reading of the sensors (VWC_{CRM}) and the measured VWC of the CRM specimens (VWC_{CRM}). As can be observed there are 6 VWC levels on the y-axis, corresponding to the 3 gravimetric water contents and the 2 compaction energies. In each level we have the measurement of 3 sensors ($VWC_{Sensors}$). A relationship linking $VWC_{sensors}$ and VWC_{CRM} was obtained:

$$VWC_{CRM} = 0{,}0156\, e^{15.364 \cdot VWC_{sensors}}$$

Combining the values of VWC_{CRM} and the bulk density of the specimens (ρ_b), the GWC of the CRM was obtained using the equation reported in Figure C5b.

$$GWC_{CRM} = \frac{VWC_{CRM}}{\rho_b}$$

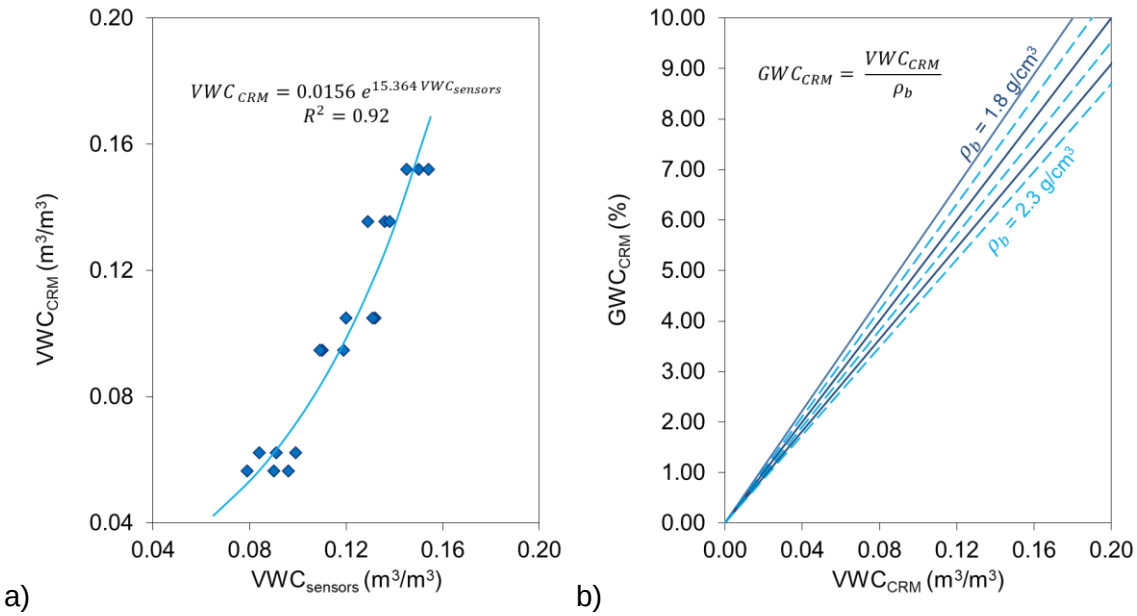

Figure C5. Sensors calibration curves: relationships to obtain a) the VWC of the CRM from VWC measured by the sensors b) the GWC of the CRM from its VWC

Annex D: FWD results

This annex reports, for each FWD measurement day:

- the measured pavement deflections normalized to the vertical load of 80 kN;
- the deflection indices (central deflection, SCI, BDI, BCI) for each measurement day;
- the deflection basins;
- the back-calculated layers' moduli.

Four measurement runs where carried out in each measurement day. In the following tables, for the sake of convenience, measurement points are identified with different kilometric progressives among the different runs.

Measurement day: 29/07/2020

Chainage	Load	Deflections (normalized to 80 kN)							
		DF1 0,0 m	DF2 0,2 m	DF3 0,3 m	DF4 0,6 m	DF5 0,9 m	DF6 1,2 m	DF7 1,5 m	DF8 1,8 m
km	kN	µm	µm	µm	µm	µm	µm	µm	µm
1,000	79,80	419	334	292	195	138	103	83	66
1,020	79,10	593	504	453	318	220	154	112	85
1,032	77,26	439	366	335	257	193	145	111	86
1,045	79,17	660	544	484	331	226	154	110	81
1,058	78,96	493	415	376	281	208	154	119	93
1,078	79,73	400	315	276	186	128	91	68	54
1,098	80,16	532	417	352	204	118	74	56	46
1,113	79,31	931	717	598	336	188	108	75	61
1,128	79,52	1042	759	602	300	172	119	92	75
1,143	79,31	679	513	430	253	157	101	71	54
1,158	79,59	598	462	397	250	162	106	72	50
1,165	79,45	682	514	435	260	156	95	60	40
2,000	77,75	443	351	304	204	143	106	83	67
2,020	77,05	623	543	492	335	227	158	115	88
2,032	79,24	558	460	421	314	229	167	126	95
2,045	76,20	721	591	525	361	241	162	115	85
2,058	79,24	588	482	440	318	226	162	123	98
2,078	79,95	417	318	269	169	112	79	61	49
2,098	76,91	577	441	370	220	129	81	60	49
2,113	76,69	929	728	620	374	210	119	81	67
2,128	79,31	963	730	601	314	178	124	96	79
2,143	79,80	710	539	451	265	159	101	68	52
2,158	79,10	722	518	444	274	169	108	72	51
2,165	79,45	766	569	470	267	156	92	58	40
3,000	78,74	443	345	299	196	137	101	81	65
3,020	76,76	691	581	521	354	240	165	120	91
3,032	79,52	554	451	413	312	227	165	125	95
3,045	78,89	745	616	543	360	233	152	107	81
3,058	79,31	617	511	464	335	236	169	127	99
3,078	79,66	435	326	276	175	115	81	62	50
3,098	80,02	565	437	366	211	122	76	57	47
3,113	79,52	951	727	608	343	189	109	77	65
3,128	79,38	1193	822	638	303	178	124	96	80
3,143	80,09	708	536	450	265	157	99	68	52
3,158	79,17	768	543	450	265	166	107	71	49
3,165	76,98	780	570	478	275	158	93	59	39
4,000	79,17	519	385	335	218	151	111	88	70
4,020	75,92	764	624	558	381	257	174	126	95
4,032	78,81	585	460	426	318	231	169	127	98
4,045	78,18	890	714	631	409	259	168	119	88
4,058	77,90	703	554	504	359	248	175	132	101
4,078	78,89	517	405	353	235	156	107	80	63
4,098	78,89	635	472	394	219	119	75	58	47
4,113	77,90	1080	856	745	419	211	117	84	72
4,128	79,10	1227	833	649	326	192	130	101	82
4,143	78,81	839	603	512	307	181	113	78	60
4,158	79,38	738	538	461	280	172	109	74	52
4,165	76,55	845	599	497	287	162	95	60	41

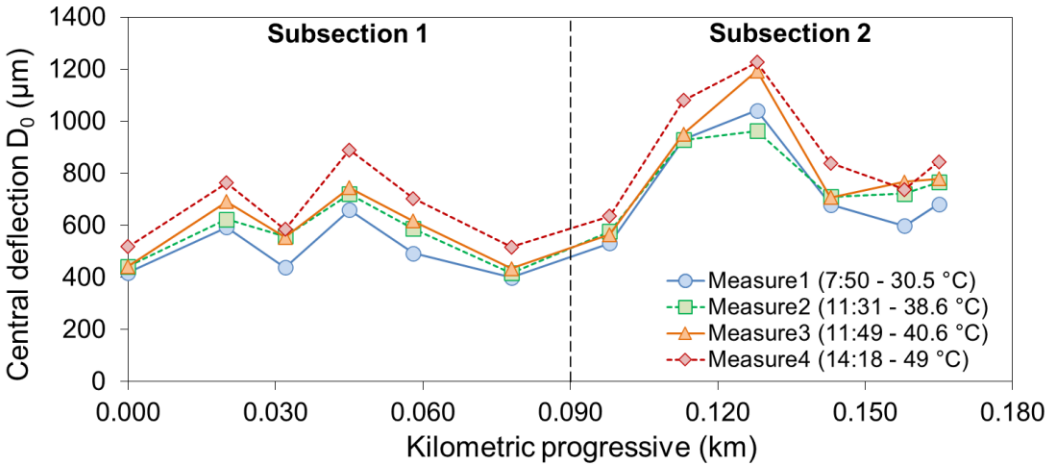
Subsection 1
Subsection 2
Central deflection D_0 (µm)
1400
1200
1000
800
600
400
200
0
0.000
0.030
0.060
0.090
0.120
0.150
0.180
Kilometric progressive (km)
Measure1 (7:50 - 30.5 °C)
Measure2 (11:31 - 38.6 °C)
Measure3 (11:49 - 40.6 °C)
Measure4 (14:18 - 49 °C)

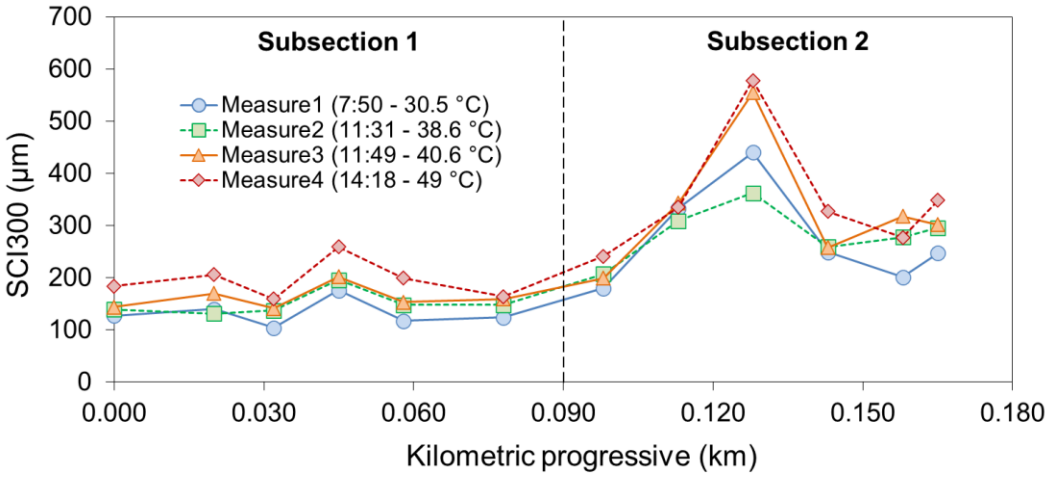
Subsection 1
Subsection 2
SCI300 (µm)
700
600
500
400
300
200
100
0
0.000
0.030
0.060
0.090
0.120
0.150
0.180
Kilometric progressive (km)
Measure1 (7:50 - 30.5 °C)
Measure2 (11:31 - 38.6 °C)
Measure3 (11:49 - 40.6 °C)
Measure4 (14:18 - 49 °C)

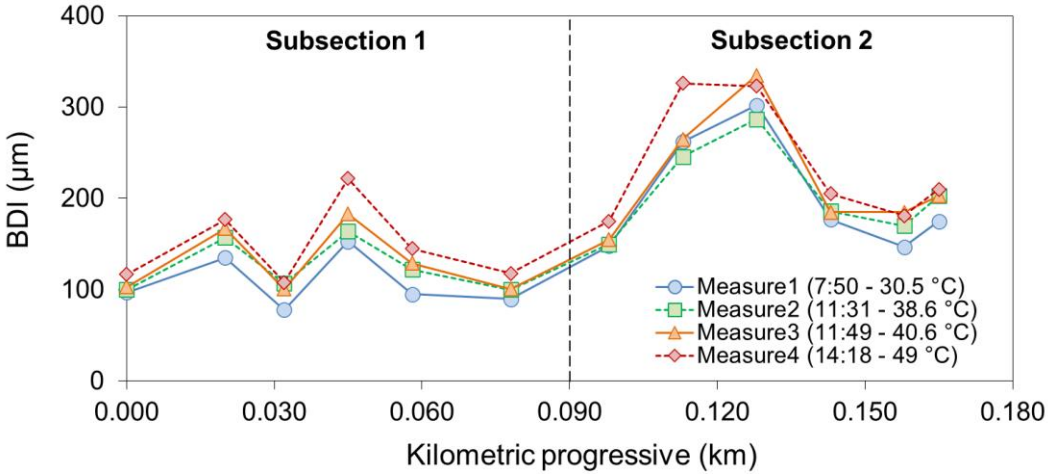
Subsection 1
Subsection 2
BDI (µm)
400
300
200
100
0
0.000
0.030
0.060
0.090
0.120
0.150
0.180
Kilometric progressive (km)
Measure1 (7:50 - 30.5 °C)
Measure2 (11:31 - 38.6 °C)
Measure3 (11:49 - 40.6 °C)
Measure4 (14:18 - 49 °C)

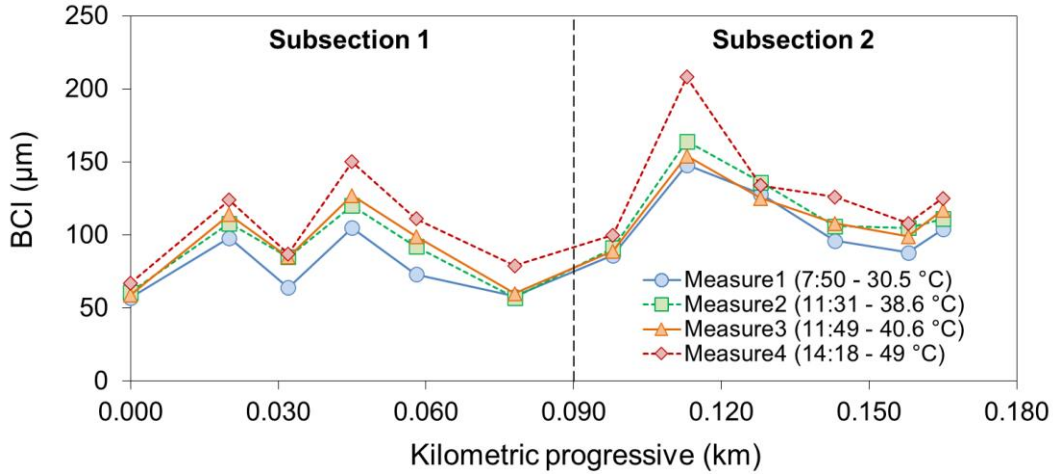
Subsection 1
Subsection 2
BCI (µm)
250
200
150
100
50
0
0.000
0.030
0.060
0.090
0.120
0.150
0.180
Kilometric progressive (km)
Measure1 (7:50 - 30.5 °C)
Measure2 (11:31 - 38.6 °C)
Measure3 (11:49 - 40.6 °C)
Measure4 (14:18 - 49 °C)

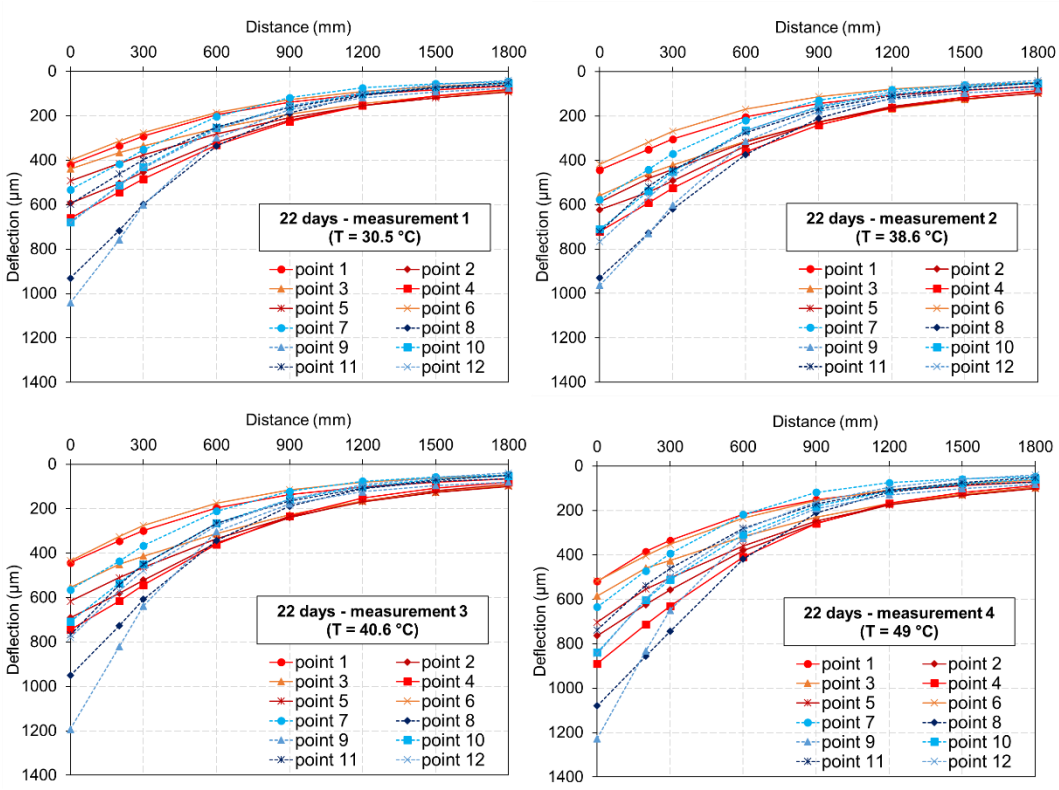
Distance (mm)
0
300
600
900
1200
1500
1800
Deflection (µm)
0
200
400
600
800
1000
1200
1400
22 days - measurement 1
(T = 30.5 °C)
22 days - measurement 2
(T = 38.6 °C)
22 days - measurement 3
(T = 40.6 °C)
22 days - measurement 4
(T = 49 °C)
point 1
point 2
point 3
point 4
point 5
point 6
point 7
point 8
point 9
point 10
point 11
point 12

Chainage km	Time	Elastic modulus			Thickness		Lack of Fit %
		Layer 1 MPa	Layer 2 MPa	Layer 3 MPa	Layer 1 mm	Layer 2 mm	
1,000	07:50	3251	2098	202	140	150	2,3
1,020	07:51	3082	2054	82	140	150	3,1
1,032	07:53	3800	3516	133	140	150	4,2
1,045	07:55	2842	2222	56	140	150	2,1
1,058	07:56	3825	2607	106	140	150	3,8
1,078	07:57	3811	2205	162	140	150	2,8
1,098	08:00	3374	797	112	140	150	3,0
1,113	08:02	2201	395	50	140	150	3,8
1,128	08:03	2113	126	93	140	150	2,5
1,143	08:04	2925	578	73	140	150	3,8
1,158	08:05	3911	975	71	140	150	4,2
1,165	08:06	2102	971	62	140	150	6,2
2,000	11:31	2432	1952	219	140	150	3,7
2,020	11:33	2420	2628	55	140	150	2,2
2,032	11:33	2426	3393	88	140	150	2,9
2,045	11:34	1703	2335	46	140	150	1,7
2,058	11:36	2249	3031	77	140	150	1,8
2,078	11:37	2426	2032	175	140	150	2,5
2,098	11:38	2525	914	101	140	150	2,5
2,113	11:39	2000	425	52	140	150	5,5
2,128	11:39	2000	186	96	140	150	3,5
2,143	11:40	2140	692	69	140	150	3,8
2,158	11:41	1948	968	67	140	150	4,9
2,165	11:42	1700	979	49	140	150	4,0
3,000	11:49	2426	2010	189	140	150	3,2
3,020	11:50	2401	2086	60	140	150	1,2
3,032	11:51	2426	3399	80	140	150	3,3
3,045	11:52	1786	2077	43	140	150	3,4
3,058	11:53	2100	2984	72	140	150	1,0
3,078	11:54	2224	2050	186	140	150	2,2
3,098	11:54	2518	967	99	140	150	2,7
3,113	11:55	1900	387	53	140	150	4,9
3,128	11:56	1600	120	95	140	150	3,3
3,143	11:57	2276	821	63	140	150	2,3
3,158	11:58	1802	950	65	140	150	5,3
3,165	11:58	1700	979	45	140	150	4,4
4,000	14:18	1600	2000	174	140	150	1,9
4,020	14:20	1274	2202	52	140	150	1,1
4,032	14:22	1478	3405	79	140	150	2,5
4,045	14:23	1001	2200	28	140	150	5,9
4,058	14:23	1102	2802	58	140	150	1,5
4,078	14:24	1650	2141	127	140	150	3,3
4,098	14:25	1582	981	94	140	150	4,0
4,113	14:26	1589	501	35	140	150	8,8
4,128	14:28	1000	199	83	140	150	2,2
4,143	14:29	1259	781	66	140	150	4,3
4,158	14:30	1292	981	73	140	150	5,9
4,165	14:30	1100	981	52	140	150	5,1

Measurement day: 05/05/2021

Chainage	Load	Deflections (normalized to 80 kN)							
		DF1 0,0 m	DF2 0,2 m	DF3 0,3 m	DF4 0,6 m	DF5 0,9 m	DF6 1,2 m	DF7 1,5 m	DF8 1,8 m
km	kN	µm	µm	µm	µm	µm	µm	µm	µm
1,000	75,78	301	257	229	164	119	89	71	57
1,020	74,57	426	363	324	228	157	114	88	70
1,032	75,28	326	291	269	210	161	125	96	75
1,045	75,07	386	338	313	241	179	137	103	82
1,058	75,00	351	309	285	220	164	123	93	73
1,078	74,79	404	326	284	184	114	73	50	39
1,098	74,71	455	364	308	186	112	74	53	44
1,113	74,86	537	405	326	189	118	82	62	52
1,128	74,36	749	543	428	226	134	95	73	64
1,143	74,79	495	408	358	237	151	99	68	53
1,158	74,71	429	354	314	211	138	93	62	44
1,165	74,50	507	412	353	229	145	92	62	45
2,000	75,14	307	258	230	163	117	89	70	57
2,020	74,43	432	372	336	237	173	128	90	70
2,032	74,50	364	327	302	235	177	134	100	79
2,045	74,79	400	347	319	245	183	140	104	83
2,058	74,29	364	318	291	223	165	123	95	72
2,078	74,43	360	289	252	167	106	72	52	41
2,098	74,15	496	388	323	192	111	73	54	44
2,113	74,15	548	411	341	201	125	88	71	56
2,128	73,87	745	554	446	246	147	105	80	65
2,143	73,94	516	433	380	245	151	96	62	44
2,158	73,94	464	374	327	221	141	90	61	44
2,165	73,58	521	425	368	239	146	89	57	41
3,000	73,65	314	264	236	168	120	91	73	60
3,020	73,37	427	368	334	238	174	131	94	73
3,032	73,87	366	330	306	242	182	137	106	80
3,045	73,87	429	375	343	261	193	145	107	84
3,058	73,94	360	319	295	226	168	126	96	75
3,078	74,08	346	284	249	167	110	76	54	42
3,098	73,73	449	361	305	185	112	75	56	46
3,113	73,37	510	393	321	189	120	86	66	55
3,128	73,44	775	562	454	244	145	104	80	65
3,143	73,30	528	436	381	248	155	100	66	49
3,158	73,30	489	391	340	224	143	93	62	43
3,165	73,30	512	420	366	238	146	89	57	42
4,000	74,08	340	288	257	181	129	96	76	60
4,020	73,73	456	390	348	242	170	125	87	70
4,032	74,29	347	315	294	234	178	136	104	80
4,045	73,87	440	382	355	268	197	147	108	85
4,058	73,87	374	328	301	230	169	126	95	75
4,078	74,01	347	285	250	170	112	76	55	43
4,098	73,58	496	387	325	193	112	73	55	44
4,113	73,44	553	409	337	196	123	88	67	56
4,128	72,95	766	559	446	244	147	105	81	65
4,143	73,58	527	443	387	253	155	98	65	46
4,158	73,73	478	387	335	219	139	91	61	41
4,165	73,51	526	432	376	241	147	89	58	42

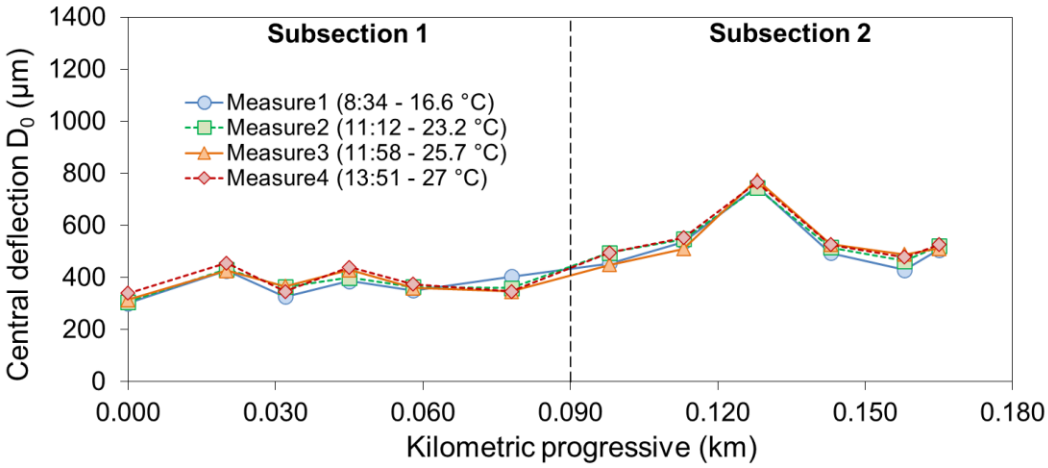
Subsection 1
Subsection 2
Measure1 (8:34 - 16.6 °C)
Measure2 (11:12 - 23.2 °C)
Measure3 (11:58 - 25.7 °C)
Measure4 (13:51 - 27 °C)
Central deflection D0 (µm)
1400
1200
1000
800
600
400
200
0
0.000
0.030
0.060
0.090
0.120
0.150
0.180
Kilometric progressive (km)

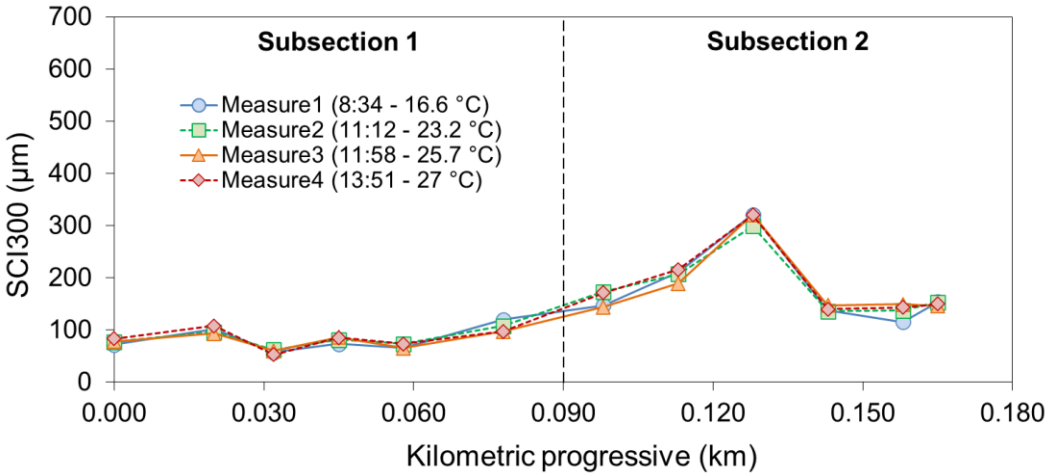
Subsection 1
Subsection 2
Measure1 (8:34 - 16.6 °C)
Measure2 (11:12 - 23.2 °C)
Measure3 (11:58 - 25.7 °C)
Measure4 (13:51 - 27 °C)
SCI300 (µm)
700
600
500
400
300
200
100
0
0.000
0.030
0.060
0.090
0.120
0.150
0.180
Kilometric progressive (km)

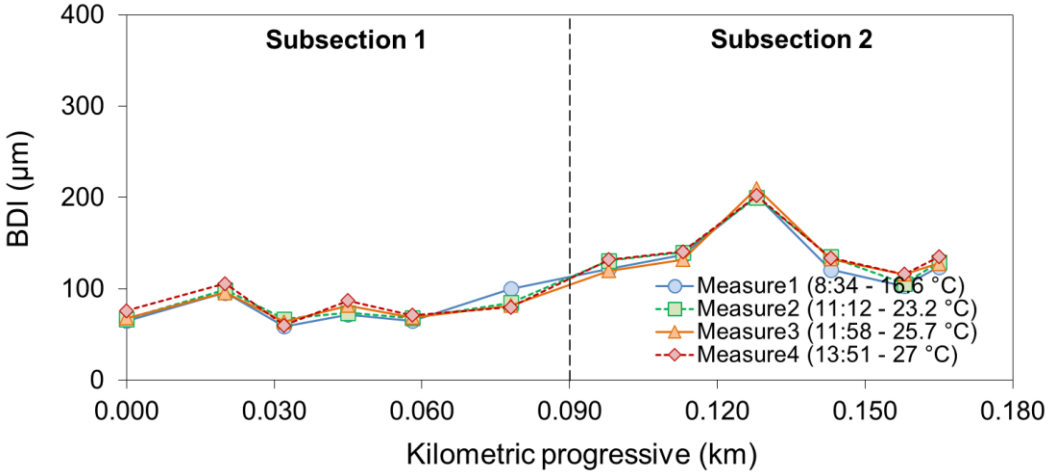
Subsection 1
Subsection 2
Measure1 (8:34 - 16.6 °C)
Measure2 (11:12 - 23.2 °C)
Measure3 (11:58 - 25.7 °C)
Measure4 (13:51 - 27 °C)
BDI (µm)
400
300
200
100
0
0.000
0.030
0.060
0.090
0.120
0.150
0.180
Kilometric progressive (km)

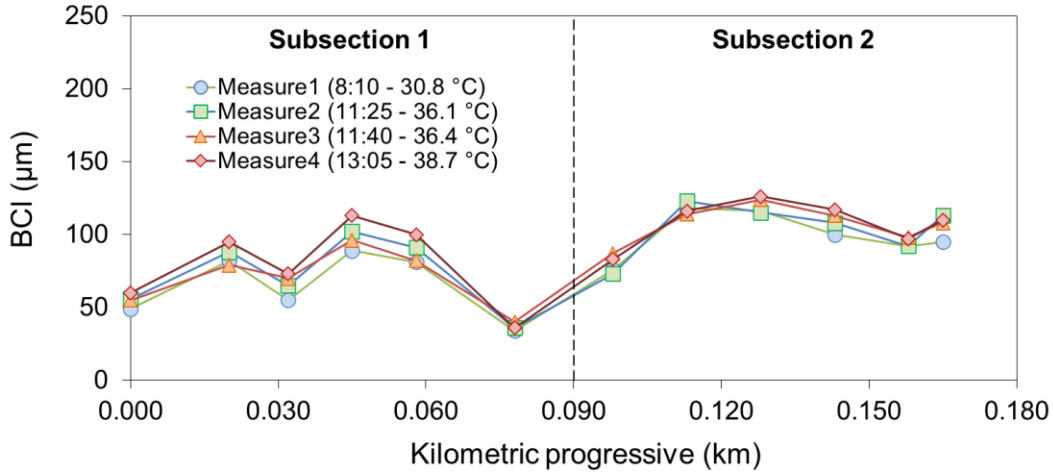
Subsection 1
Subsection 2
Measure1 (8:10 - 30.8 °C)
Measure2 (11:25 - 36.1 °C)
Measure3 (11:40 - 36.4 °C)
Measure4 (13:05 - 38.7 °C)
BCI (µm)
Kilometric progressive (km)

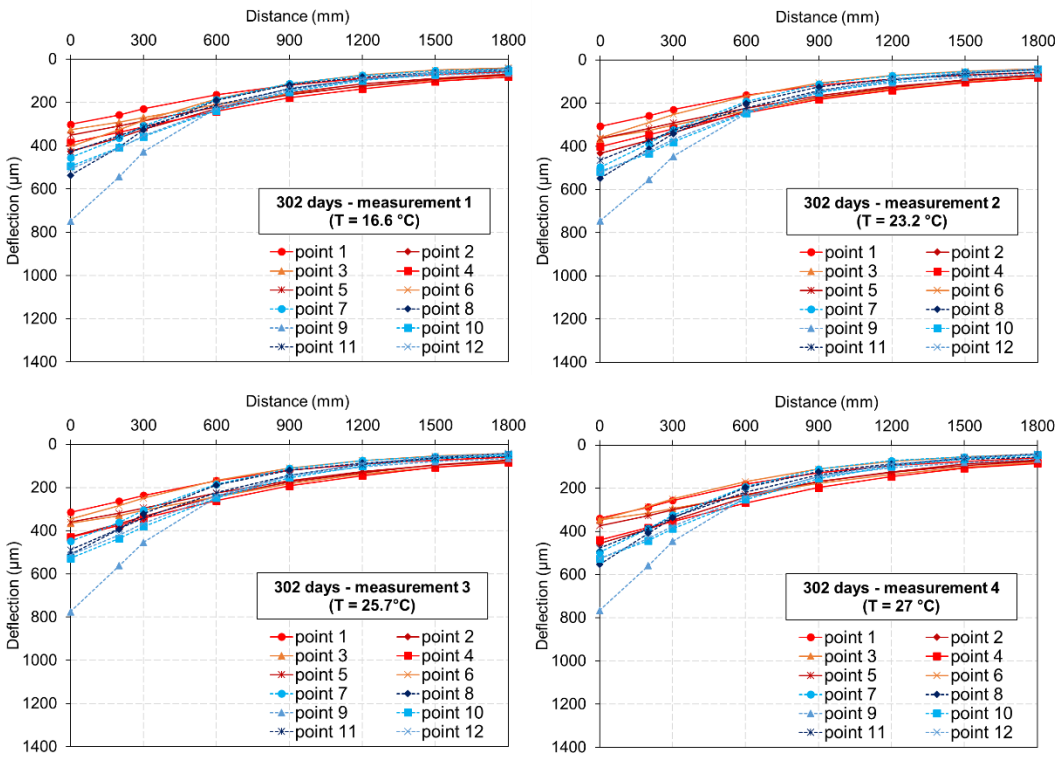
Distance (mm)
Deflection (µm)
302 days - measurement 1 (T = 16.6 °C)
302 days - measurement 2 (T = 23.2 °C)
302 days - measurement 3 (T = 25.7°C)
302 days - measurement 4 (T = 27 °C)
point 1
point 2
point 3
point 4
point 5
point 6
point 7
point 8
point 9
point 10
point 11
point 12

Chainage km	Time	Elastic modulus			Thickness		Lack of Fit %
		Layer 1 MPa	Layer 2 MPa	Layer 3 MPa	Layer 1 mm	Layer 2 mm	
1,000	08:34	6789	3032	228	140	150	1,4
1,020	08:35	4640	2274	138	140	150	1,8
1,032	08:36	6861	3910	190	140	150	4,5
1,045	08:37	6713	3881	114	140	150	2,7
1,058	08:38	6679	3915	151	140	150	3,4
1,078	08:39	4504	1957	105	140	150	2,2
1,098	08:40	4523	838	127	140	150	2,1
1,113	08:41	2426	803	159	140	150	1,8
1,128	08:42	1724	416	123	140	150	3,0
1,143	08:43	2730	2716	80	140	150	1,4
1,158	08:44	5623	1969	84	140	150	3,1
1,165	08:45	4130	1548	71	140	150	2,3
2,000	11:12	6198	2350	263	140	150	2,5
2,020	11:13	5978	2518	106	140	150	3,3
2,032	11:14	6261	3442	157	140	150	4,5
2,045	11:14	5761	3631	133	140	150	3,2
2,058	11:15	5868	3385	149	140	150	3,9
2,078	11:16	5318	1544	164	140	150	3,3
2,098	11:17	3325	904	129	140	150	2,9
2,113	11:18	1965	1320	137	140	150	1,9
2,128	11:19	1674	554	113	140	150	1,6
2,143	11:20	4710	1591	56	140	150	1,7
2,158	11:21	3381	2922	73	140	150	2,2
2,165	11:22	4659	1393	60	140	150	2,3
3,000	11:58	5459	2702	254	140	150	2,2
3,020	11:59	4559	3089	119	140	150	3,3
3,032	12:00	5830	3859	152	140	150	5,0
3,045	12:01	4956	3558	118	140	150	3,3
3,058	12:02	4881	3858	156	140	150	4,3
3,078	12:03	4819	2681	150	140	150	2,6
3,098	12:04	4669	788	138	140	150	2,0
3,113	12:06	2855	815	167	140	150	1,3
3,128	12:06	1591	489	114	140	150	1,6
3,143	12:07	3408	1810	68	140	150	1,8
3,158	12:08	4128	1908	73	140	150	3,5
3,165	12:09	3256	2137	62	140	150	2,4
4,000	13:51	5982	2806	202	140	150	2,3
4,020	13:52	4493	2448	106	140	150	2,8
4,032	13:53	7948	3820	138	140	150	4,4
4,045	13:54	5715	3355	90	140	150	2,9
4,058	13:55	5885	3655	140	140	150	3,4
4,078	13:56	5979	2035	153	140	150	3,1
4,098	13:56	3244	971	120	140	150	2,1
4,113	13:57	1996	987	155	140	150	1,3
4,128	13:58	1650	479	118	140	150	1,2
4,143	13:59	4016	1855	57	140	150	1,3
4,158	14:00	4628	1936	68	140	150	3,6
4,165	14:01	3946	1530	61	140	150	1,9

Measurement day: 13/07/2021

Chainage km	Load kN	Deflections (normalized to 80 kN)							
		DF1 0,0 m µm	DF2 0,2 m µm	DF3 0,3 m µm	DF4 0,6 m µm	DF5 0,9 m µm	DF6 1,2 m µm	DF7 1,5 m µm	DF8 1,8 m µm
1,000	74,22	322	287	251	171	122	92	71	57
1,020	73,09	489	410	370	264	182	135	104	82
1,032	74,22	340	327	307	247	192	150	115	88
1,045	74,15	517	483	436	314	225	166	125	98
1,058	73,44	506	432	396	296	215	160	119	94
1,078	74,15	241	199	172	116	82	65	53	44
1,098	74,29	466	385	325	200	124	85	63	52
1,113	73,30	759	617	503	285	167	115	88	73
1,128	74,01	830	624	514	287	171	118	94	78
1,143	73,80	616	510	429	259	159	102	68	51
1,158	74,15	545	451	384	246	154	102	66	46
1,165	73,73	592	485	406	248	153	99	63	44
2,000	74,71	372	315	277	185	129	97	76	61
2,020	73,80	509	438	399	281	193	140	106	84
2,032	75,00	375	362	337	269	204	156	117	89
2,045	74,36	570	531	479	341	239	176	130	99
2,058	74,29	507	461	422	311	220	162	120	95
2,078	74,22	265	213	181	121	85	66	54	45
2,098	74,57	458	385	322	197	124	85	63	52
2,113	74,29	821	651	529	283	160	108	83	69
2,128	74,43	812	638	513	283	168	120	90	73
2,143	73,94	615	526	441	274	166	104	68	52
2,158	74,08	634	477	401	249	157	102	66	46
2,165	73,30	610	511	446	287	174	103	63	43
3,000	74,29	326	301	265	181	126	94	74	57
3,020	74,15	466	440	400	285	206	152	112	85
3,032	74,29	398	387	365	286	216	162	121	92
3,045	73,58	582	517	466	330	234	172	127	98
3,058	73,94	485	443	397	289	207	151	112	87
3,078	74,08	261	221	192	132	92	68	51	40
3,098	74,15	482	422	356	214	127	87	66	56
3,113	73,87	741	577	480	282	168	115	88	74
3,128	73,23	941	715	573	292	168	120	93	76
3,143	74,15	588	514	450	286	173	104	69	52
3,158	73,94	585	486	414	260	162	99	63	43
3,165	72,24	641	497	423	254	146	88	56	41
4,000	74,50	343	333	291	193	133	100	77	63
4,020	73,65	535	480	432	301	206	152	113	85
4,032	74,71	408	397	376	294	221	166	123	93
4,045	73,80	652	564	510	358	245	177	128	101
4,058	74,08	540	483	441	320	220	159	116	91
4,078	74,50	255	205	174	118	82	65	52	43
4,098	74,15	508	417	348	209	126	85	64	53
4,113	73,44	842	664	540	280	164	114	88	73
4,128	73,87	936	689	551	299	173	124	96	81
4,143	73,51	654	547	467	289	172	104	68	53
4,158	74,01	632	497	411	254	157	104	67	46
4,165	73,30	679	543	452	266	156	94	60	43

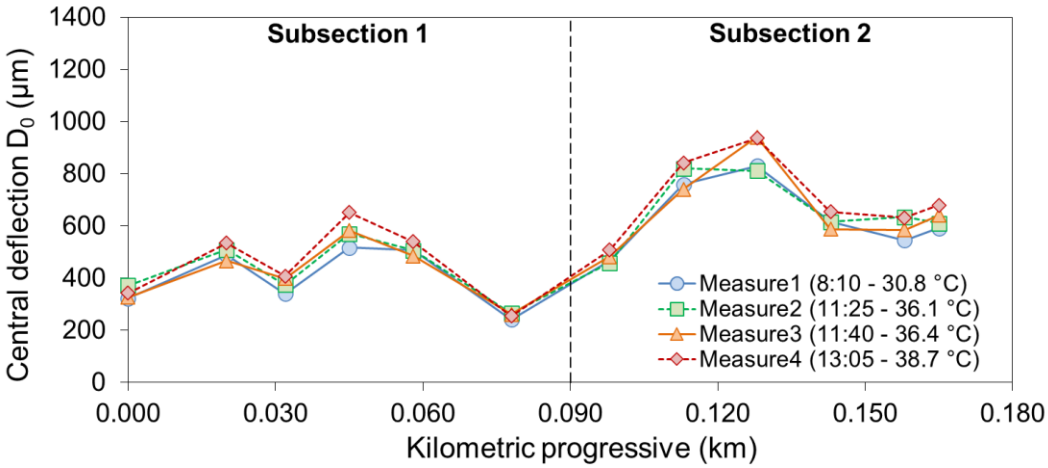
Subsection 1
Subsection 2
Central deflection D_0 (µm)
1400
1200
1000
800
600
400
200
0
0.000
0.030
0.060
0.090
0.120
0.150
0.180
Kilometric progressive (km)
Measure1 (8:10 - 30.8 °C)
Measure2 (11:25 - 36.1 °C)
Measure3 (11:40 - 36.4 °C)
Measure4 (13:05 - 38.7 °C)

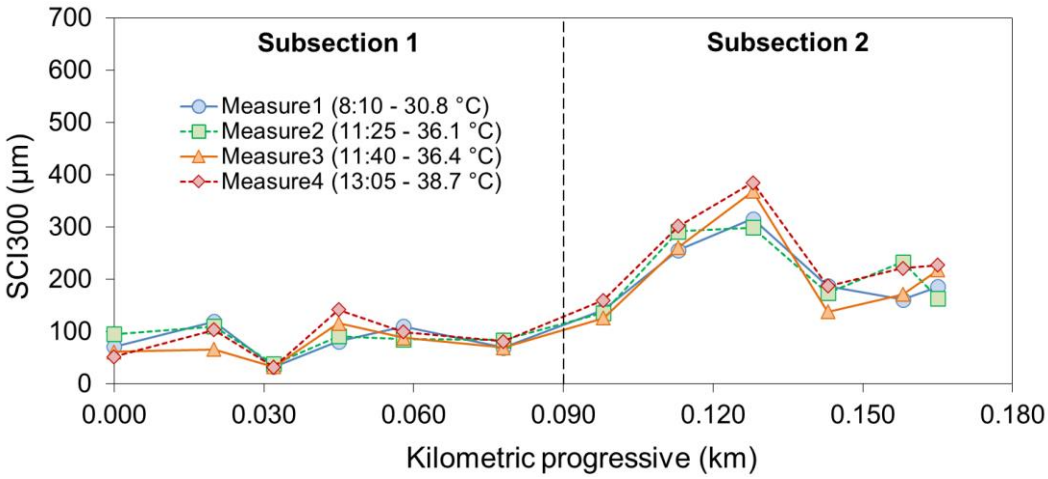
Subsection 1
Subsection 2
SCI300 (µm)
700
600
500
400
300
200
100
0
0.000
0.030
0.060
0.090
0.120
0.150
0.180
Kilometric progressive (km)
Measure1 (8:10 - 30.8 °C)
Measure2 (11:25 - 36.1 °C)
Measure3 (11:40 - 36.4 °C)
Measure4 (13:05 - 38.7 °C)

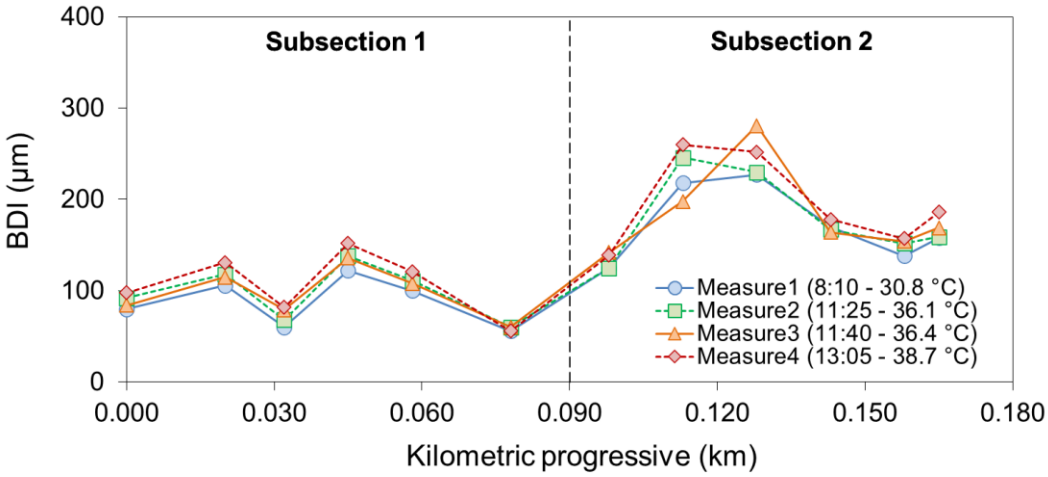
Subsection 1
Subsection 2
BDI (µm)
400
300
200
100
0
0.000
0.030
0.060
0.090
0.120
0.150
0.180
Kilometric progressive (km)
Measure1 (8:10 - 30.8 °C)
Measure2 (11:25 - 36.1 °C)
Measure3 (11:40 - 36.4 °C)
Measure4 (13:05 - 38.7 °C)

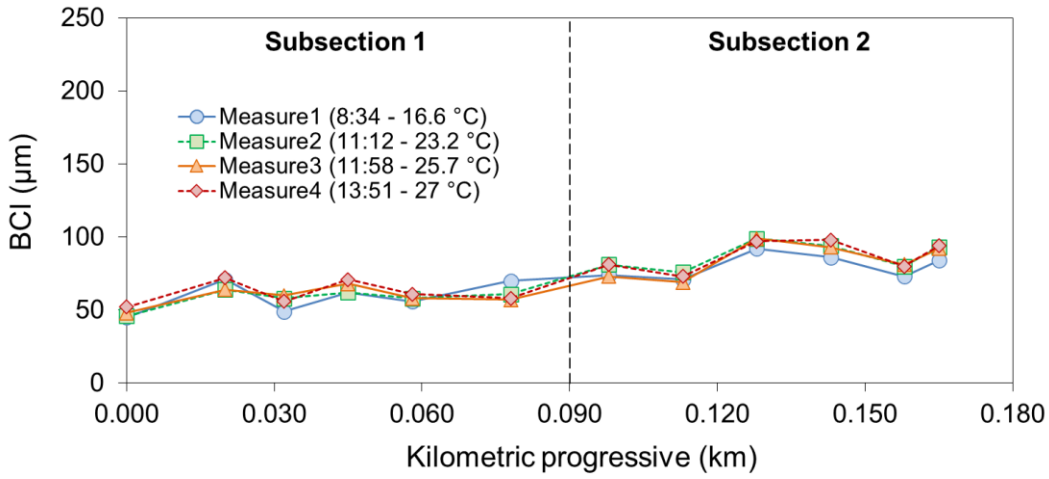
Subsection 1
Subsection 2
Measure1 (8:34 - 16.6 °C)
Measure2 (11:12 - 23.2 °C)
Measure3 (11:58 - 25.7 °C)
Measure4 (13:51 - 27 °C)
BCI (µm)
Kilometric progressive (km)

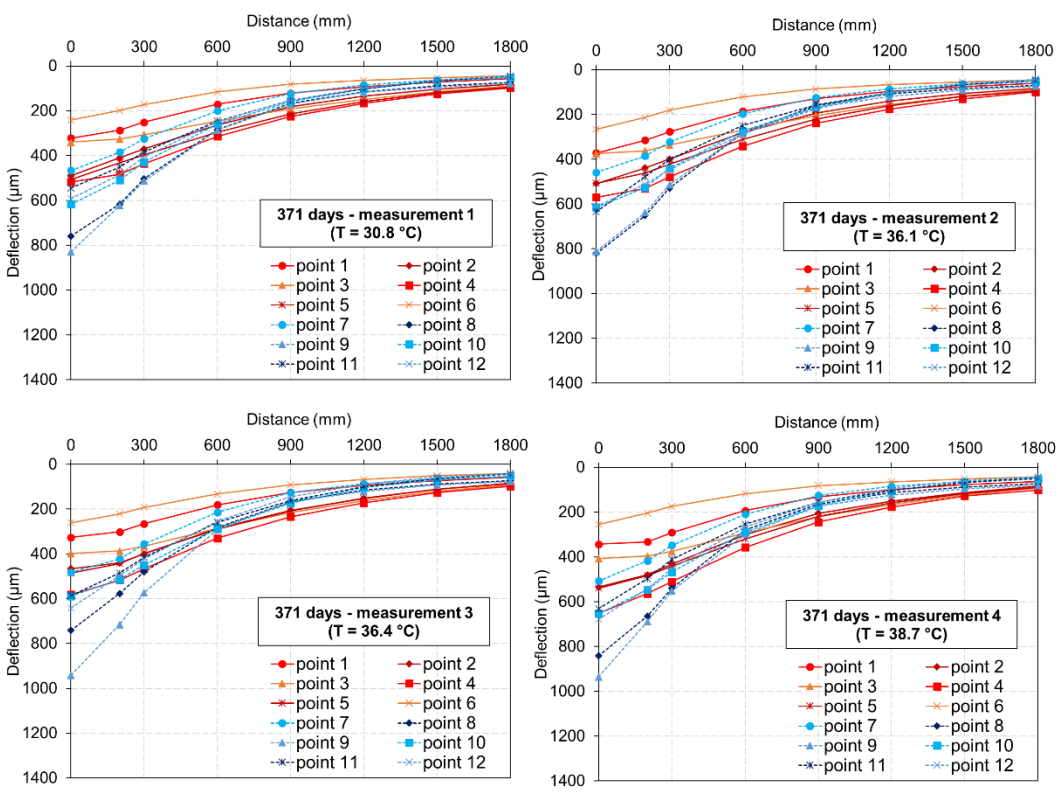
Distance (mm)
Deflection (µm)
371 days - measurement 1 (T = 30.8 °C)
371 days - measurement 2 (T = 36.1 °C)
371 days - measurement 3 (T = 36.4 °C)
371 days - measurement 4 (T = 38.7 °C)
point 1
point 2
point 3
point 4
point 5
point 6
point 7
point 8
point 9
point 10
point 11
point 12

Chainage km	Time	Elastic modulus			Thickness		Lack of Fit %
		Layer 1 MPa	Layer 2 MPa	Layer 3 MPa	Layer 1 mm	Layer 2 mm	
1,000	08:10	3550	2980	211	140	150	4,8
1,020	08:11	3300	2054	139	140	150	3,0
1,032	08:11	4800	3780	204	140	150	7,9
1,045	08:12	3453	2023	115	140	150	4,9
1,058	08:13	3925	2363	120	140	150	3,9
1,078	08:14	3811	2879	449	140	150	3,4
1,098	08:16	3574	1426	114	140	150	1,6
1,113	08:16	2974	336	86	140	150	2,4
1,128	08:17	2157	314	107	140	150	2,5
1,143	08:18	2974	980	62	140	150	2,6
1,158	08:19	3995	1290	62	140	150	3,7
1,165	08:20	2800	1150	63	140	150	4,1
2,000	11:25	2999	1998	213	140	150	4,1
2,020	11:27	2989	1999	107	140	150	3,6
2,032	11:27	3889	2999	167	140	150	9,0
2,045	11:28	2589	2297	94	140	150	4,9
2,058	11:29	3873	2398	108	140	150	4,4
2,078	11:30	3173	2596	456	140	150	3,1
2,098	11:31	2893	1448	135	140	150	2,2
2,113	11:32	2552	273	87	140	150	2,9
2,128	11:33	2119	358	100	140	150	2,0
2,143	11:33	3721	809	60	140	150	2,5
2,158	11:34	1413	1923	64	140	150	3,6
2,165	11:35	3196	1238	49	140	150	4,4
3,000	11:40	3580	2899	194	140	150	5,3
3,020	11:41	3780	2772	109	140	150	5,1
3,032	11:42	3394	2542	161	140	150	10,0
3,045	11:42	2494	2042	99	140	150	4,4
3,058	11:43	3025	2842	117	140	150	4,8
3,078	11:44	3325	4232	280	140	150	4,4
3,098	11:45	2957	1234	122	140	150	4,1
3,113	11:46	2871	292	112	140	150	3,1
3,128	11:46	2015	210	93	140	150	2,3
3,143	11:47	2798	1185	63	140	150	4,5
3,158	11:48	2922	1995	48	140	150	2,7
3,165	11:49	2587	970	61	140	150	3,3
4,000	13:05	2599	3250	201	140	150	6,1
4,020	13:07	2489	2226	108	140	150	4,9
4,032	13:08	3189	3933	133	140	150	8,1
4,045	13:08	2052	2028	85	140	150	3,7
4,058	13:09	2711	1940	115	140	150	6,0
4,078	13:10	2111	6619	246	140	150	4,3
4,098	13:11	1915	1932	110	140	150	2,7
4,113	13:12	1810	353	87	140	150	2,9
4,128	13:13	1469	363	92	140	150	3,3
4,143	13:14	2176	1403	54	140	150	2,5
4,158	13:14	2085	1371	68	140	150	4,8
4,165	13:15	1998	1055	58	140	150	3,8